السيرة الذاتية

الاسم الرباعي:- سهى موسى خورشيد رشيد الاوسي

العنوان:- بغداد –الدورة- محلة 830-زقاق 7-دار 21

الهاتف:- 07902260931

البريد الالكتروني:- suhamouse@yahoo.com

عنوان الاطروحة:

Optical system design improvement for IR homing head

تأريخ المناقشة : 25/9/ 2006

المشرفين: الدكتور احمد كمال احمد , الدكتور حسن حمادي ,الدكتور صباح محمود جمعه

السيرة الذاتية

الاسم الرباعي:- سهى موسى خورشيد رشيد الاوسي

العنوان:- بغداد –الدورة- محلة 830-زقاق 7-دار 21

الهاتف:- 07902260931

البريد الالكتروني:- suhamouse@yahoo.com

عنوان الاطروحة:

Optical system design improvement for IR homing head

تأريخ المناقشة : 25/9/ 2006

المشرفين: الدكتور احمد كمال احمد , الدكتور حسن حمادي ,الدكتور صباح محمود جمعه

REFERENCES

AverY, D. G, Goodwin. D. W, and Rennie. A .E (1957)
Journal. Sci. Inst. V34, pp 394.

Baker, K. (1983)
Design requirements for a passive infrared homing head
Advanced Infrared Detectors and System, pp 24-26.

Boutry, G. A (1961)
Instrumental Optics
Bell and Bain,LTD

Breckenridge, R.W (1975)
Cryogenics cooler for IR system
SPIE, V14(1), PP 57-62.

Chao, Z.W and Chu,J.I (1988)
Opt. Eng. V27(6), 440.

Chung, W. J. , Yoo, J. R., Kim, Y. S., and Heo, J. [1997]
Mechanism of the blue up-conversion in Tm^{3+} /Nd^{3+}
dopted calcium aluminate glass
J. Am. Ceram. Soc, V80, pp 1485-1490

Davidson, M.W (2006)
Transfer Function
The Florida State University, 32310.

Ditteon, R. (1998)
Modern geometrical optics
John Wiley & Sons, Canada.

Dowski, E.R, Jr. , Thomas, C.W and Cracht, J.V (1995)
Extended depth of field through wavefront coding
Applied Optics, V34,N11, pp 1859-1866.

Dubner, H. (1959)
Optical design for infrared missile seeker
IRE,V1, pp 1537-1539.

Due Pre, F.K and Daniels, A. (1973)
Miniature refrigerator for electronic devices
Cryogenics.

Fisher, D.W, Lefteich, R.F, and YateS, H.W (1966)
Survey of IR trackers
Applied Optics, V5(4),pp 507.

Froelich, A. J. (1980)
A low-cost infrared seeker (LCIRS) for terminal homing
SPIE, Infrared System V256, pp 37-45.

Fukui, Y. (2003)
Modulation Transfer Function
http:// faculty-web.at.nwu.edu/med/fukui/faweb.html

Fundamental Optics (2004)
http://www.mellesgriot.com

Gaussorgues, G.L (1984)
Thermographie infrarouge
TEC and DOC.

Genoud, R. H. (1959)
Infrared search- system range performance
IRE,V1, pp 1581-1585.

Goodman, J.W (1996)
Introduction to Fourier Optics, 2nd edition
McGraw-Hill company, INC.

Herr, K.C, and Hughes, J.L (1973)
Mariner Mars 1969 Infrared spectrometer gas delivery system and Joule-Thomson cryostate
Cryogenics.

Houston, J. D. and Carswell, A. I. (1978)
Four-component polarization measure lidar atmospheric scattering
Appl. Optics, V17, pp 298-311.

Hudson, R. D. (1969)
Infrared system engineering
John Wiley & Sons, United States of America.

Horn, S.B (1980)
Cryogenics cooling options forward looking infrared FLIR
SPIE Proceeding, V245, pp 101-107.

Howard, J.M (2001)
Optical design using computer graphics
Applied Optics, V40, N19.

Larmore, L. S. (1959)
Range equation for passive infrared devices
IRE. V1,pp 1590-1595.

Longhurst, R.S (1967)
Geometrical and Physical optics, 2nd edition.
Jarrold and Sons, LTD, Great Britain.

Mclean, W. E. (2004)
Optical designs
http:// www. optical document . com

Meissinger, H.F. (1959)
Simulation of infrared system
IRE, V1, 1586-1589.

Michel, E., and Razeghi, M. (1998)
Opto-Electronics
Review, V6(1), pp 11-23.

Mohammed, H. H. and Mustafa, F. I. (2000)
Optical design of Igla missile homing head (report, Al-Razi State Company), Iraqi Military Industrialization Corporation (MIC).

Nichols, D.W.,et al (1959)
Millitary applications of IR techniques
Proceeding of the IRE, V13, pp 1161.

Nussbaum, A. (1998)
Optical system design
Prentice-Hall, INC.

Optikos corporation (1999)
How to measure MTF
Review 20, N 4-04-001.

Scott, R. M. (1959)
Optics for infrared system
IRE, V1, 1956-1960.

Shannon, R. R. (1997)
The art and science of optical design
Cambridge University Press, United States of America.

Smith, W. J. (1966)
Modern optical engineering
McGraw-Hill, United States of America.

Spot-optics (2006)
http:// www.spot- optics . com
P.I 03616810283, Italy.

Starkiewics, J. (1948)
Nature, V12, pp 1481.

Vnderhill, E.A. (1947)
German application of infrared
Proce. Natl. Electronics conf.V3,pp 248.

Walstrom, P.L. (1988)
Joule-Thomson effect and internal convection heat transfer in turbulent He II flow
Cryogenics, V28.

Weast, R. C. , Astle, M. J., and Bayer, W. H. (1984-1985)
Handbook of chemistry and physics, 65th ed.
CRC.

Weisstein, E.W. (1999)
Convolution
CRC Press LLC.

Williams, C. S. and Becklund, O. A. (1972)
Optics
John Wiley & Sons, United States of America.

Williams, C. S. and Becklund, O. A. (1989)
Introduction to optical transfer function
John Wiley & Sons, Canada.

Wilman, H. (1948)
Proceeding Physics Society 60(2),pp 117.

Woods, R.L. ,Saunders,J.E., and Micheal, .J.A. (1993)
Concentric-design rigid bifocal lenses PartI
Journal of British Contact lens Association, V16,N1,pp 25-36

Wyant, J.C. ,and Creath, K. (1992)
Applied optics and optical engineering, Chapter 1
Academic press, INC

Yoo,G. (2005)
Aberration theory
University of Rochester.

Zajac,H. (1974)
Optics
Addison-Wesley, INC.

Chapter Five

CONCLUSIONS AND SUGGESTIONS FOR FUTURE WORK

Chapter Contents

5. CONCLUSIONS AND FUTURE WORK

5.1 Conclusions

It appears that it is possible to put forward the high performance requirements of the optical system for an infrared homing head whose most sensitive element for achieving a high quality image is the dome. From the present investigation one may draw the following conclusions:

a. The size of the spot projected on the detector by the optical system of the homing head can be as small as $10.5\mu m$ which is far below the side of the squared detector $900\mu m$. The spot size is found to depend on two important parameters, namely the wavelength of the IR radiation and the focal number of the whole system. The spot size is directly proportional to the wavelength. In the presence of aberrations the spot size decreases exponentially with the focal number. In the case of the diffraction limited system the spot size varies linearly with the focal number.

b. A target at a range of about 7.5 *km* can be detected by the dome configuration when the atmosphere is clear. The range is directly proportional to the detectivity and inversely proportional to the temperature of the detector. As one may expect its value improves with the improvement of weather conditions. Furthermore, the value of the detection range is highly affected by the IR radiation wavelength; it increases with the increase of wavelength. It has been deduced from the present work that from the practical point of view where the spot quality and MTF curve have been taken into account, a detection range of about 7.5 *km* can be achieved under clear weather conditions using the $4\mu m$

wavelength of IR radiation.

c. The modulation transfer function is a sensitive measure concerning the spot image in the frequency domain. Furthermore, it is very sensitive to the amount of image aberrations; it decays as the aberration increases. The amount of the decay is directly proportional to the contrast of the spot image.

d. The cutoff frequency in the MTF curve varies with the resolution of the image; as the cutoff frequency increases the resolution increases. Within the vicinity of the cutoff frequency the image improves since the MTF curve approaches the ideal case.

e. The OID software that has been specifically written for the homing head optical system proved to be very useful for computing the range directly. Furthermore, with the aid of the OID software many other parameters can be computed such as the encircled energy, the field of view, and the effective focal length once the relevant equation of the parameter is known since these parameters are important for determining the range.

5.2 Suggestions for Future Work

The following topic may be suggested for future work in the field of the present investigation.

a. The suggested optical system design may be studied analytically with regard to the defocusing situations. The influence of defocusing on the performance of the system may be added to the aberration.

b. The suggested optical system design may be modified for laser homing head working, for instance in the active mode, taking into account the materials of the lenses in the system. A quadrant detector instead of the present work single detector may also be considered for tracking distant targets.

c. Further developments can be put forward with regard to the softwares considered in the present work to be applied on various types of optical systems, such as the optical design of laser transmitter and receiver employed in the wireless optical communications.

Abstract

The present work aims to design an optical system for infrared (IR) homing head. The homing head of interest works through $(3-5)\mu m$ atmospheric window, so it must have high quality characteristics. The characteristics of the optical system design include the point spread function (PSF), modulation transfer function (MTF), total spot size (Z_T)or focusing, and range (*R*). These characteristics are determined with the aid of special mathematical methods, which give the efficiency and accuracy of the adopted optical system design. The work has been performed in multi-stages; the most interest of them are namely design improvement and programming for determining the efficiency of the suggested optical system design.

The improvement stage depends originally on a standard optical system design for IR homing head. Some modifications and improvements have been imposed on this standard design to achieve a new one of high quality characteristics. These improvements include choosing the most suitable material for the firist element in the system, and optimum features for each optical element in the suggested design. An improvements stage was then followed on the radius of curvature, thickness, and diameter of the optical elements constituting the system. The improvements process was carried out by Zemax software.

The improvements stage included the implementation of specially developed software for determining the characteristics of the IR homing head since the most important; the range could not be determined directly by the Zemax software. Therefore, a multi-task software was designed by

using the Visual Basic programming language. The new software is called OID which is short for optical infrared design; it works through Windows operating system. This software is able to plot any optical design graphically, and can determine the main parameters that influence the efficiency of the optical system such as PSF, MTF, Z_T, and *R*. These parameters have been computed by special methods based on some mathematical relations.

The present work has gained some credibility when a comparison between the results of Zemax software and those of the designed OID software have been carried out, which have shown harmonic behavior, which insure succeful results. It has been found that with the aid of the proposed optical system a target at a range of about 7.50 *km* can be detected under clear weather conditions using an IR radiation of $4\,\mu m$ wavelength. Furthermore, the total spot size as small as $10.6\,\mu m$ can be projected on the detector with the lowest possible aberrations. The newly develop OID software can be employed in future on other optical system designs such as those used in the field of wireless laser communication systems.

Contents

List of Figures

List of Tables

List of Symbols

Symbol	Caption
A	Area of the jet nozzal
A_d	Area of detector
A_j	Junction area.
B	Band width
c	Speed of light ($3\times10^{8}\, m/s$)
c_1	First radiant constant
c_2	Second radiant constant
C_{040}	Spherical aberration coefficient.
C_{020}	Defocusing coefficient.
D	Distance between depth of focus and aperture.
D_d	Diameter of detector
D_o	Diameter of aperture
D^*	Detectivity
d_o	Geometrical pupil radius.
f	Effective focal length
f/no	Focal number
f_{mirror}	Focal length of mirror
f_{lens}	Focal length of lens
f_s	Spatial frequency
f_c	Cutoff frequency
G	Degree of contrast.
h	Planck's constant
I	Spectral radiant intensity
I_o	Radiant exitence of the IR radiation.
I_{max}	Maximum intensity
I_{min}	Minimum intensity
J_o	Zero order Bessel function
J_1	First order Bessel function
k	Boltzmann's constant
k_i	Power of lens
n	Refractive index
NA	Numerical aperture
p	Total power.
q	Electronic charge.
R_o	Zero-bias resistance
R_v	Visibility factor

r_1	First radius of curvature of lens
r_2	Second radius of curvature of lens
R_{max}	Maximum range
s_i	Distance between image and center of lens.
s_o	Distance between object and center of lens.
S/N	Signal-to-noise ratio
t	Thickness
T	Jet nozzal temperature (K)
T_d	Detector temperature (K)
T_{dp}	Dew point temperature (K)
W	Spectral radiant emittance
x_i	Ray height.
Z	Spot size
Z_T	Total spot size
α'	Angle of incident ray
β	Angular blur spot
β_{atm}	Total transmission coefficient
β_{aerosl}	Aersol transmissin coefficient
β_{water}	Water transmissin coefficient
$\beta_{mlecular}$	Molecular transmissin coefficient
δ	Depth of field
δ `	Depth of focus
ΔW	Aberration
ε_x	Transvers aberration
ε_z	Longtudinal aberration
η	Quantum efficency
λ	Wavelength
ρ	Optical axis
σ	Stefan's constant
τ_a	Atmoshere transmission
τ_o	Optical transmission
ϕ	Incident flux

List of Abbreviations

Abbreviation	Caption
Al_2O_3	Sapphire
$CaAl_2O_3$	Calcium aluminate glass
FM	Frequency modulation
FT	Fourier transform
FOV	Field of view
Ge	Germanium
IFOV	Instantaneous field of view
InSb	Indium antimonide
IR	Infrared
MTF	Modulation transfer function
OID	Optical infrared system design software
OPL	Optical path length
OSD	Optical system design
OTF	Optical transfer function
P	Pupil function
PSF	Point spread function
PTF	Phase transfer function

المستخلص

يهدف هذا البحث إلى تطوير التصميم البصري لمنظومة التوجيه بعيد المدى التي تعمل ضمن منطقة الأشعة تحت الحمراء (Infrared)، ولذلك يجب أن تكون ذات خصائص عالية الجودة. إن خصائص تصميم المنظومة البصرية تتضمن دالة الانتشار النقطي (PSF)، ودالة التضمين الانتقالي (MTF)، سعة البقعة الكلية أو التبئير، والمدى. هذه الخصائص حُسِبَت اعتماداً على طرائق رياضية خاصة تقوم بإعطاء الكفاءة والدقة لعمل المنظومة المتبناة. لقد تم تنفيذ العمل في عدة مراحل أهمها تطوير المنظومة (Improvement) وبرمجة حساب كفاءة التصميم البصري للمنظومة المقترحة.

إن مرحلة التطوير تعتمد أصلا على تصميم قياسي لرأس توجيه يعمل ضمن المنطقة تحت الحمراء، حيث أدخلت بعض التحويرات والتحسينات على هذا التصميم للحصول على تصميم جديد بخصائص عالية الجودة. وقد شملت التحويرات اختيار المواد البصرية الملائمة لكل عنصر في المنظومة البصرية المقترحة. واختيار الصفات البصرية الملائمة لكل عنصر. لذا فأن المرحلة التي تلتها هي مرحلة اختيار الصفات المثلى لنصف قطر التكور والسمك والقطر لمكونات المنظومة. إن اختيار الصفات والمواد البصرية المثلى في المنظومة تتضمن تغيير المواد البصرية للعنصر الأول من المنظومة، ثم تغيير الصفات البصرية لكل عنصر إلى الحد الذي يعطي أفضل النتائج وذلك اعتماداً على برنامج زيماكس (Zemax).

وتضمنت المرحلة التالية من البحث تصميم وتنفيذ برنامج خاص لحساب خصائص المنظومة البصرية الموجهة حرارياً وذلك لان برنامج زيماكس غير مهيأ لحساب العامل الأكثر أهمية في العمل وهو المدى مباشرة. إن للبرنامج المصمم والذي يحمل التسمية OID (مختصر Optical Infrared Design) عدة مهام ويعمل ضمن بيئة نظام تشغيل النوافذ (Windows). ويمكن لبرنامج OID ان يرسم اي منظومة بصرية وحساب العوامل الرئيسة التي تحدد كفاءة المنظومة البصرية المستخدمة وهي دالة الانتشار النقطي، دالة التضمين، سعة البقعة، والمدى. والعوامل الثلاثة الأولى حُسِبوا بطرائق مختلفة اعتمدت على علاقات رياضية وهندسية خاصة.

إن المقارنة بين النتائج المستخلصة من برنامج زيماكس مع تلك المستخلصة من برنامج OID تشير إلى مصداقيتها لأنها أظهرت تصرف توافقي وهذا ما يؤكد نجاح العمل. لقد وجد بالاستعانة بالمنظومة البصرية المقترحة إن هدفا على مدى 7.5كم يمكن اقتفاءه تحت ظروف جوية صافية بوساطة أشعة تحت الحمراء بطول موجي ٤ مايكرومتر. إضافة إلى ذلك فأن بقعة بقطر صغير يصل إلى 10.5 مايكرومتر يمكن تسقيطها على الكاشف بأقل زيوغ ممكن. إن البرنامج OID الجديد يمكن استعماله مستقبلا في تصاميم منظومات بصرية أخرى كتلك في مجال منظومات الاتصالات الليزرية اللاسلكية.

جمهورية العراق
وزارة التعليم العالي والبحث العلمي
جامعة النهرين
كلية العلوم

تطوير تصاميم المنظومـــــة البصرية للرؤوس الموجهـــــة حراريـــــاً

أطروحـــــة

مقدمـــــة إلـــــى كليـــــة العلـــوم في جامعـــــة النهريـــن كجـزء من متطلبـــات نيـل شهـــادة دكتوراه فلسفـــة

فـــي

الفيزيـــــاء

مـــن قبـــل

سهى موسى خورشيد رشيد الأوسي

رجب ١٤٢٧ هـ
تموز ٢٠٠٦ م

Republic of Iraq
Ministry of Higher Education and Scientific Research
Al-Nahrain University
College of Science

OPTICAL SYSTEM DESIGN IMPROVEMENT FOR IR HOMING HEAD

A Thesis
Submitted to the College of Science of Al-Nahrain University
as a Partial Fulfillment of the Requirements for the Degree of
Doctor of Philosophy
in
Physics

By

Suha Mousa Khorsheed Al-Awsi

Rajab **1427 A. H.**

July **2006 A. D.**

قال الله تعالى

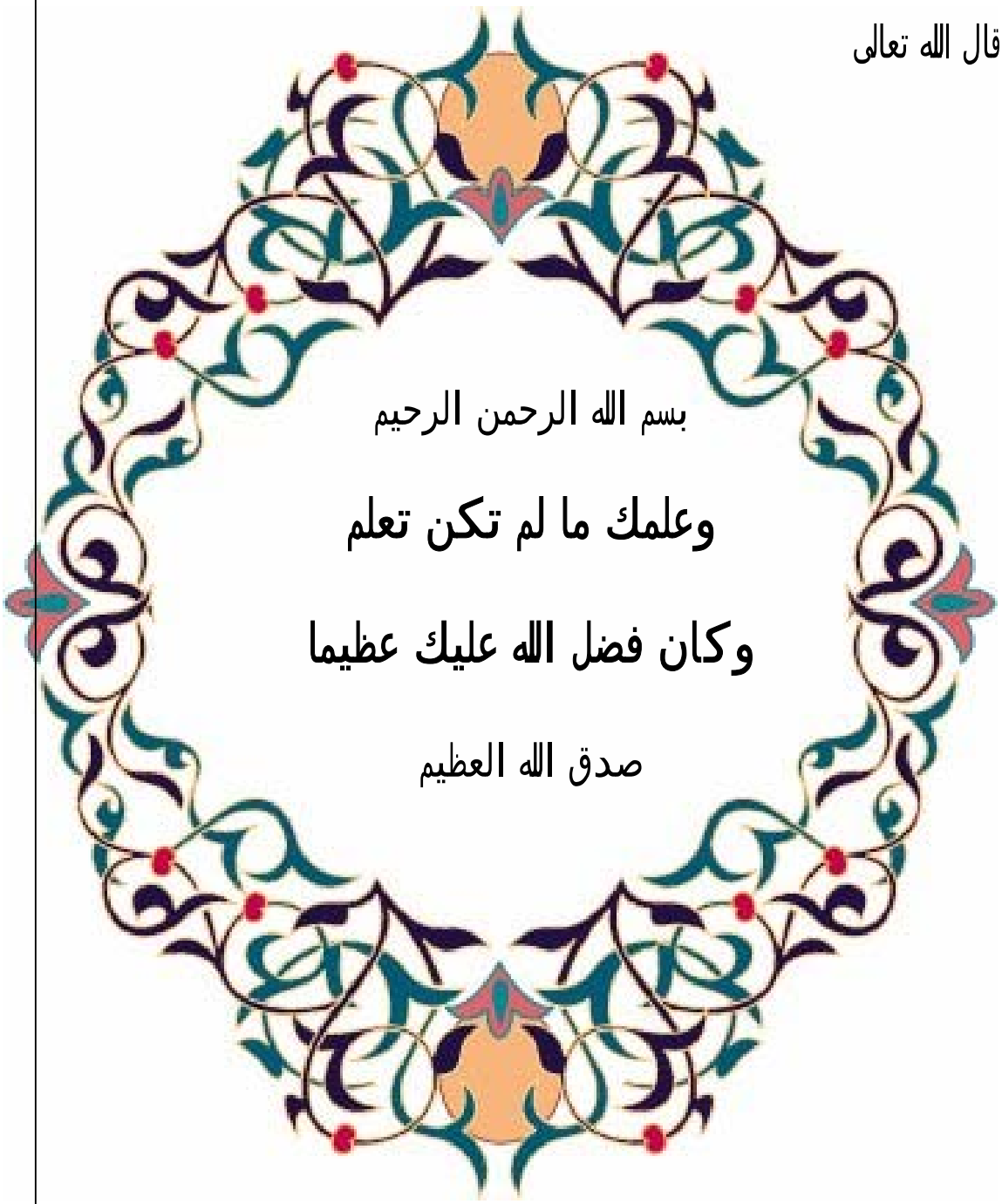

بسم الله الرحمن الرحيم

وعلمك ما لم تكن تعلم

وكان فضل الله عليك عظيما

صدق الله العظيم

سورة النساء ١١٣

Dedicated to my husband
Mohammed Al-Taei
and
my family

Certification

We certify that this thesis was prepared under our supervision at Al-Nahrain University as a partial requirement for the degree of Doctor of Philosophy in physics

Signature:
Name: *Dr. Hassan H. Mohammed*
Title: *Professor*
Address: *Ministry of Science and Technology*
Date:

Signature:
Name: *Dr. Sabah M. Juma*
Title: *Professor*
Address: *College of Science Al- Nahrain University*
Date:

Signature:
Name: *Ahmad K. Ahmad*
Title: *Assistant Professor*
Address: *College of Science Al- Nahrain University*
Date:

In the view of the recommendation, I forward this thesis for debate by the Examining Committee.

Signature:
Name: *Ahmad K. Ahmad*
Title: *Assistant Professor*
Address: *Head of Physics Department*
Date:

Examining Committee Certificate

We certify that we have read the thesis entitled "OPTICAL SYSTEM DESIGN IMPROVEMENT FOR IR HOMING HEAD" and as an examining committee, examined the student Suha Mousa Khorsheed in its contents and what is related to it, and that in our option it is adequate as standard of a thesis, with VERY GOOD standing of the degree of doctor of philosophy in physics.

Signature:
Name: Dr. Fareed F. Rasheed
(Chairman, Professor)
Date:

Signature:
Name: Dr. A. M. Suhail
(Membre, Assistant Professor)
Date:

Signature:
Name: Dr. Abdul-Hussain K. Iltaif
(Membre, Assistant Professor)
Date:

Signature:
Name: Dr. Samir K. Yassin Al-Ani
(Membre, Assistant Professor)
Date:

Signature:
Name: Dr. Adawiya J. Haider
(Membre, Assistant Professor)
Date:

Signature:
Name: Dr. Sabah M. Juma
(Supervisor, Professor)
Date:

Signature:
Name: Dr. Hassan H. Mohammed
(Supervisor, Professor)
Date:

Signature:
Name: Dr. Ahmad K. Ahmad
(Supervisor, Assistant Professor)
Date:

Signature:
Name: Dr. Laith A. A. Al-Ani
(Dean of the Collage of Science)
Date:

Acknowledgments

I would like to acknowledge my sincere thanks and appreciation to my supervisors Dr. Hassan H. Mohammed, Dr. Sabah M. Juma and Dr. Ahmad K. Ahmad for suggesting the project, assistance, encouragement, and valuable advice.

Thanks are due to the Head of Physics Department, and the staff of the Department for their kind attention.

Sincere thanks to my husband Mohammed Al-Taei, and to my family for their help and patience.

Suha

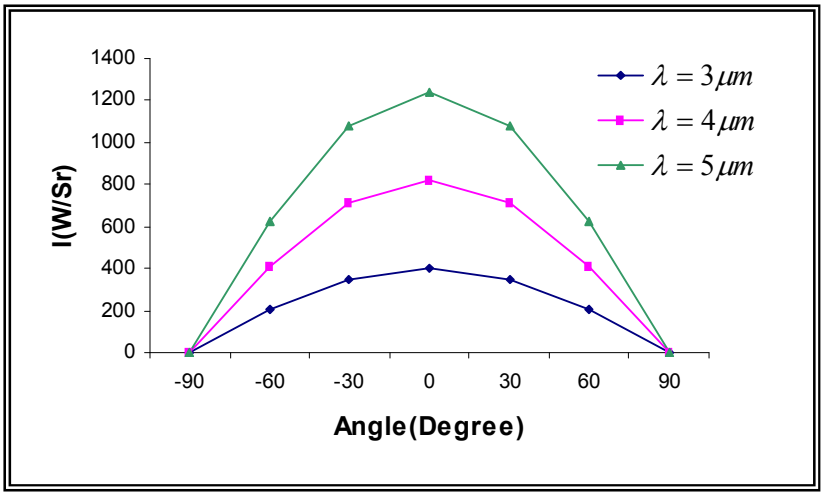

Figure 4.42 Intensity versus reception angles for different wavelengths.

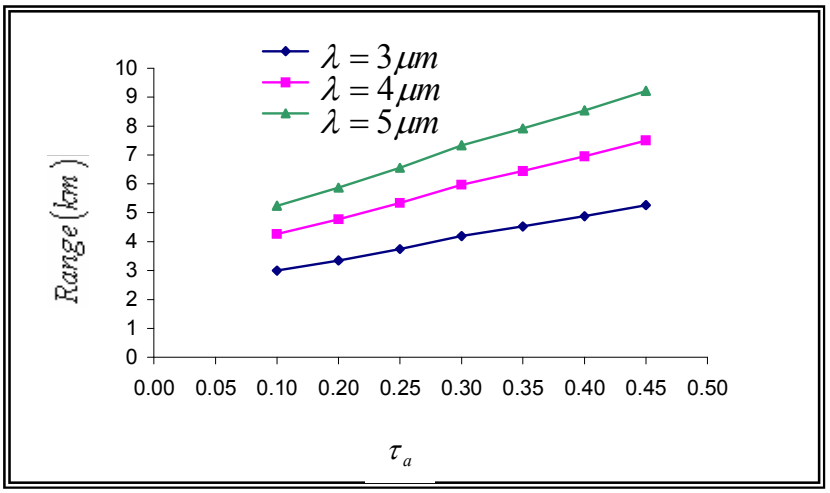

Figure 4.43: Range versus atmosphere transmission for different wavelengths.

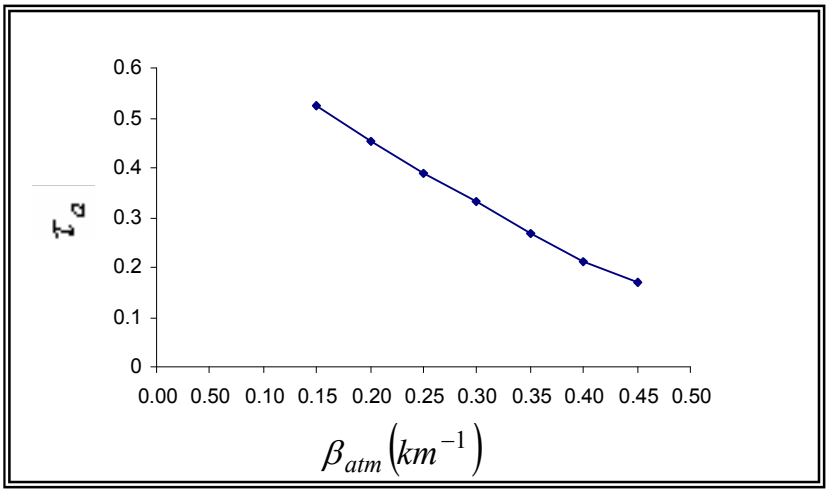

Figure 4.44: Transmission versus total transmission coefficient.

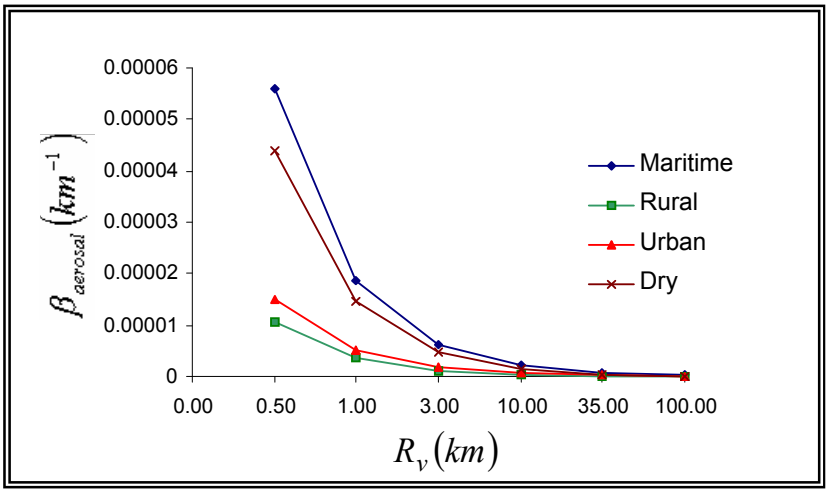

Figure 4.45: $\beta_{aerosal}$ versus visibility factor for different regions.

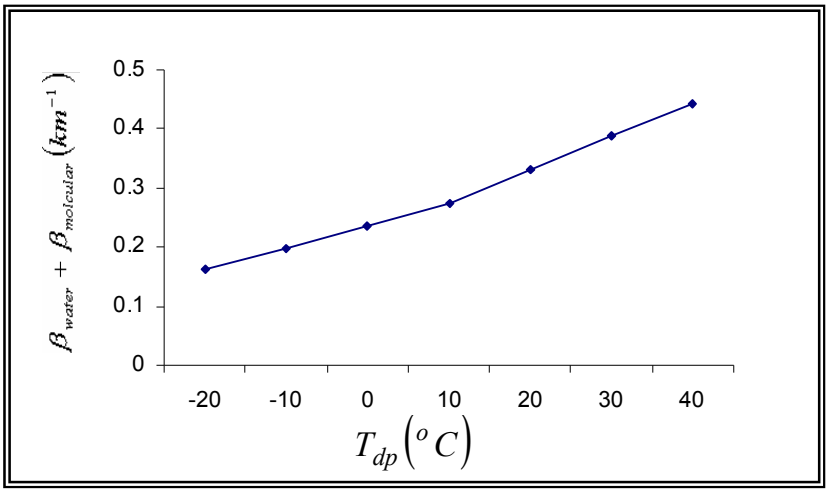

Figure 4.46: $\beta_{water} + \beta_{molcular}$ versus dew point temperature.

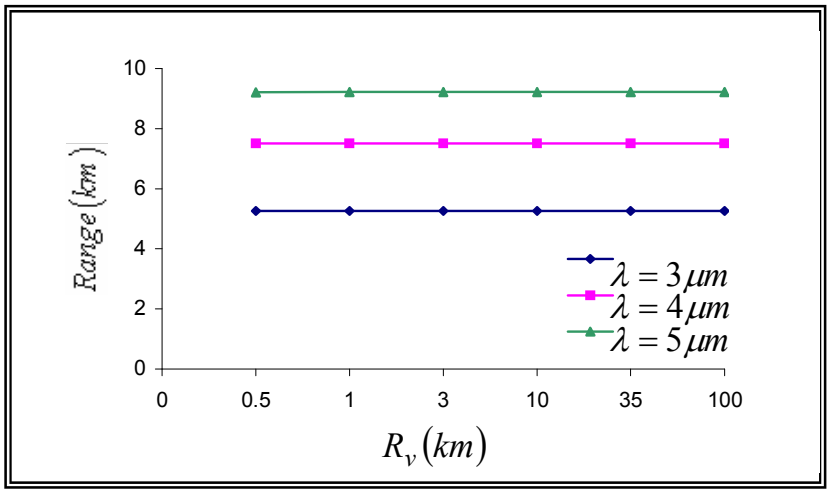

Figure 4.47: Range versus visibility factor for different wavelengths.

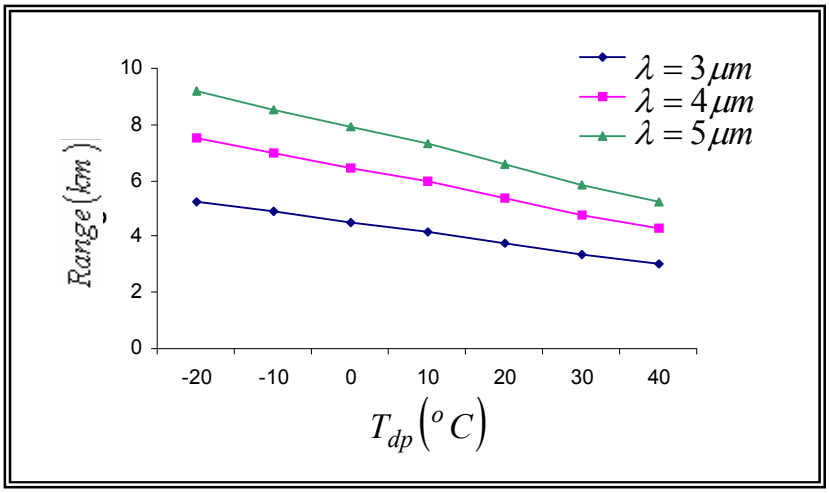

Figure 4.48: Range versus dew point temperature for different wavelengths.

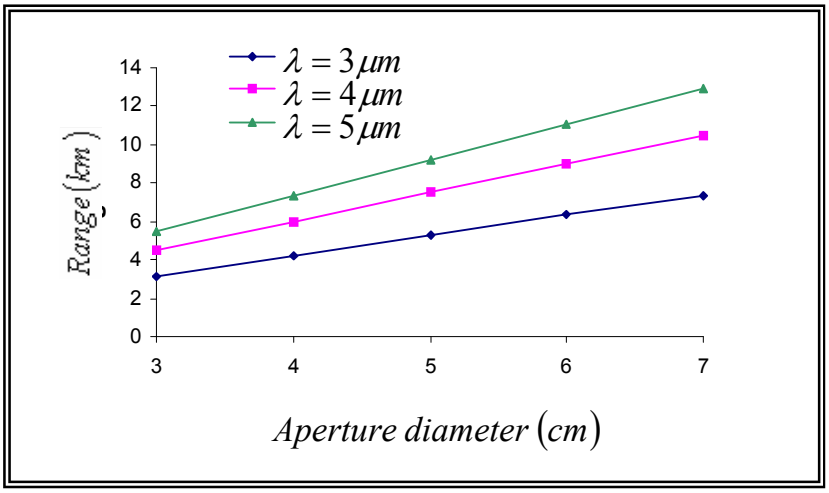

Figure 4.49: Range versus aperture for different wavelengths.

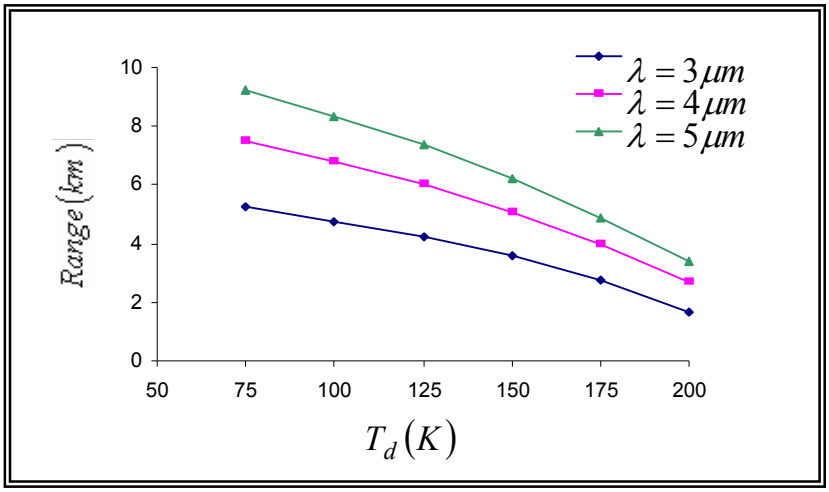

Figure 4.50: Range versus detector temperature for different wavelengths.

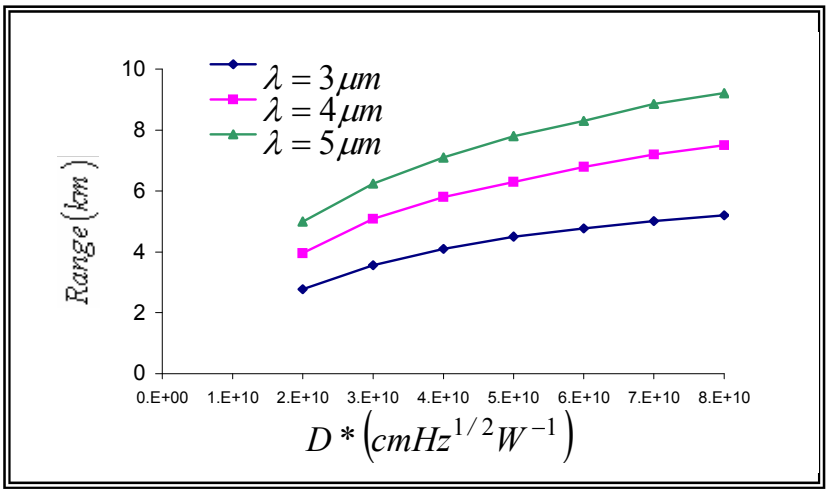

Figure 4.51: Range versus detectivity for different wavelengths.

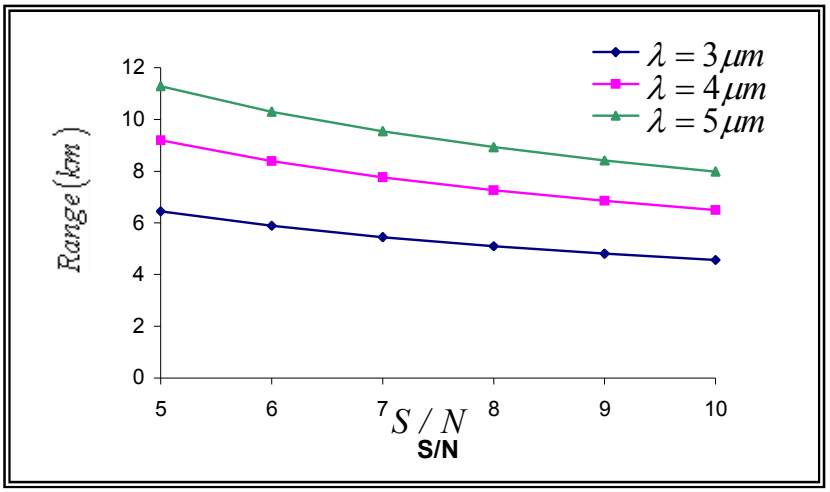

Figure 4.52: Range versus signal to noise ratio for different wavelengths.

The observation of the range curves shows logical behaviors with respect to the variation of its parameters. By noticing figure 4.41, one can see that the range is proportional with the spectral radiant intensity (*I*) of the radiation emitting from the source (target). The spectral radiant intensity takes different values for the different angles (θ) at the wavelengths of interest, thus the range in turn takes different values according to the different angles and wavelengths too. The spectral

Chapter One

INTRODUCTION

Chapter Contents

1. INTRODUCTION

1.1 Design of Optical Systems

The optical design process should be consistent with the required applications. Many applications require some specialized design and a successful optical system design requires from the designer careful consideration of the design specifications, which is the most important step in the optical design process. The ordinary design process can be broken down into the following three steps: **(a)** the choice of the type of design to be executed, that is, the number and types of elements and their general configuration, **(b)** the determination of the powers of lens, materials, thickness, and spacing of the elements. which are usually selected to control the chromatic aberrations and Petzval curvature of the system, as well as the focal length, working distance, field of view, and aperture diameter, and **(c)** the adjustment of the shapes of the various elements or components to correct the basic aberrations to the desired and optically acceptable values [**Shannon 1997**].

The optics used in an infrared (IR) homing head shows, the configuration of the optical system. The folded optical system consists of a dome, primary mirror, secondary mirror, correcting lens, focal plane (reticle), and detector [**Dubner 1959**]. Once the optical system has been specified and built the next task is to test its performance. The usual optical tests are measurement of modulation transfer function (MTF), transmission, and optical spot size. Environmental testing at elevated temperatures is also carried out in large environmental chambers.

1.2 The Homing Head System Configuration

The homing head is guided missiles follow the IR target by means a sequential control processes. These processes transforms the IR image of the target into a digital signal carried an information about the mobility direction and the position of the target. Therefore, the homing head consist of an ***eye*** that see the target (which is the optical system) and a ***brain*** (controller) that govern the homing head direction by exporting commands to the ***body*** of the homing head to track and follow the target.

The homing head system block diagram is shown in figure 1.1 include the following essential elements:

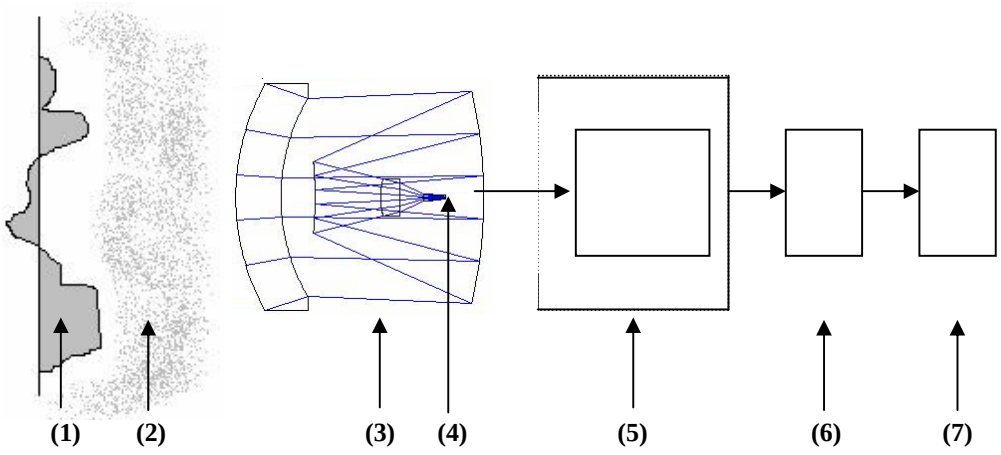

(1) IR target. **(2)** Atmospheric transmission. **(3)** Optical design. **(4)** IR detector (focal plane). **(5)** Signal conditioning electronics. **(6)** Signal processor. **(7)** Information display or storage.

Figure 1.1: Important elements of IR system described as follows [**Matra Confidential Document**]

1. The IR target, which represents in this work the emitting radiation from the aircraft jet engines.

2. The atmosphere, which represent the medium between the IR source and the tracking system.

3. The IR tracking system consists of the optoelectronic device including the optics and spatial filtering.

4. The IR detection where the conventional detector is InSb coupled with Joule-Thomson cooling system [**Walstrom 1988**].

5. Signal conditioning electronics.

6. Signal processing.

7. Error signal to be used for the angle correction for the target position with respect to the homing system and send the corrected position to the autopilot.

A reticle found in an IR seeker seperates effect of an IR target from its background and produce appropriate modulated signals that make possible a variety of the signal processes for guidence or target tracking [**Dubner 1959**].The most important element in the field of interest is the optical design since it represents the eye that by which the homing head should be seen clear and accurate image for the IR target.

1.3 The Passive Tracking and Searching Modes

IR homing heads have been widely developed and used considerably. These guiding systems are desirable in two ways. Firstly, if IR homing heads are used, the weapon delivery system can leave the immediate area or take cover when fired without being affected, as the mission will not required any further commands from the launchers in this case. Secondly, since in this case missile homing depends on the radiation produced by the virtue of the target physical temperature, then it is difficult to decoy the missile or camouflage the target to prevent it radiating.

All objects will emit some energy in the IR bands and depending on the type of target and temperature either the 3 to 5 μm or 8 to 12 μm band will usually be used. It is at these two bands that the atmosphere has two distinct windows. The longer wavelength band will give the missile some capability in bad weather and fog [**Baker 1983**].

The optics used in an IR missile-seeker results from a series of design compromises involving sensitivity, resolution and geometry. Since the optics must be part of a gimbal system and must be contained in a prescribed enclosure, the geometry problem is the most dominant. The configuration of an IR missile is as follows. The folded optical system consists of a dome, two mirrors, correcting lens, a reticle or a light chopper and detector **[Dubner 1959]**

A tactical round would accomplish a spin-up via an aerodynamic situated on the periphery of the seeker dome at the missile nose. A pair of

spin bearings allows the case holding the dome to rotate freely about the seeker longitudinal axis, causes the scan field of view to rotate across the detector elements. The detector is placed at the optical system focal plane; the elements are situated at radial intervals from the seeker's axis so as to cover the entire scan field of view in one scan interval [**Froelich 1980**].

The efficiency of the optical system design of IR homing head depends on two important modes, namely the search mode (*IFOV*, Instantaneous Field of View) and tracking mode (*FOV*, Field of View).

One of the specifications of an optical system is its field of view, that is, the angular measure of the volume of the space within which the system can respond to the presence of the target. A system designed to search for a target usually has a small instantaneous field of view that is moved systematically by optical or mechanical means so as to cover a much larger search field. The instantaneous field of view is determined by a field stop placed in the image plane. It may consist of a physical aperture, an optical modulator, or a detector. In the camera, a particularly simple example, a field of view is determined by the size of the film. A particularly convenient optical relationship states that in any optical system the object and its image subtend equal angles from their corresponding principal points [**Hudson 1969**].

The concept of the angular field of view (*FOV*) is important when the usable image size is limited. *FOV* is the angle subtended by the source producing the maximum usable image size, the *FOV* of the sensor is given by

$$FOV = 2\tan^{-1}\left[\frac{Usable\ image\ size}{Effective\ \ focal\ length}\right] \qquad (1.1)$$

According to literature, the instantaneous field of view IFOV is often determined by the size of detector; it is given by

$$IFOV = \frac{A_d}{f^2} \quad (Sr) \qquad (1.2)$$

where f is the effective focal length, and A_d is the detector's area.

$$A_d = \frac{\pi D_d^2}{4} \qquad (1.3)$$

The *FOV* of the IR homing head tracking mode is usually equal $\pm 45^o$ whereas the searching mode *IFOV* is equal to $\pm 4^o$ The *FOV* and *IFOV* are very important parameters for calculating the range of the passive guidance missile. More details on *FOV* and *IFOV* are found in the following Chapter.

1.4 Historical Review

German applications of the missile guidance appeared at the end of 1940's. They developed passive systems operating at $1-3\mu m$ window. In 1944 the Admiralty Research Laboratory in Britain and American workers developed methods of manufacturing of PbS and PbSe detectors. Starkiewicz (1948) studied the vacuum sublimation and chemical deposition for forming suitable films of PbS.

The researches concerned with the optical system design of IR homing head have received attention since the latest of 1950's. Older designs have

been improved during the last few decades. Most of the published literature has dealt with these improvements, while others have put forward new optical designs. Some publications showed an interest in the field of view (FOV), the materials of the system elements, and the aberrations of the optical system, whereas other publications studied the homing head based on the thermal radiation of the target. The following is a literature survey in the chronological order of the most important publications that are relevant to the present work.

Avery et al (1957) studied the InSb cooled p-n junction detector. This detector to be used for the missile guiding system was prepared using slice single crystal of InSb, the slice mounted in a demountable metal Dewar cooling this detector at 90*K*. Larmore (1959) solved the problem of determining the maximum range at which an IR device could detect a target. The solution required a detailed analysis of the spectral radiation of the target in addition to the absorption in the intervening spaces, and the response of the detector. Dubner (1959) found the optics used in IR missile-seeker results from a series of design compromises involving sensitivity, resolution, and geometry. Since the optical parts of the system must be contained in a prescribed enclosure, the geometry problem has been the most dominant. The optical system consisted of a dome, primary mirror, secondary mirror, correcting lens, reticle, and detector.

Genoud (1959) described the passive IR search system which consisted of a telescope with an instantaneous field of view or resolution element that scans the field in a time called frame time. He found the maximum range at which a target could be detected clearly depend on the

environmental conditions in the region of the target. Meissinger (1959) studied the IR tracking and guidance systems by means of simulation, which was often necessary to supplement the theoretical analysis. Scott (1959) described the main differences between the optics of an IR system and visible system. These differences result from the image size requirements in the two portions of the spectrum. Any optical system no matter how perfect in design or construction will be limited in its resolution by diffraction. The effect of this diffraction depends on the sizes of the optics and wavelength of radiation forming the image.

In the 1960s a little work was published on IR tracking and guidance systems. In the early of 1960's, the researches was limited in the small reliable cooling devices, thus it was became available and used for cooling the InSb detectors. Fisher (1966) solved the problem of encoding the position of IR target signal in the field of view in such a way that the homing will know which direction to move in order to bring the target to the center of the field.

Due Pre (1973) studied the physical properties of materials at low temperature (77*K*). He found that the physical properties were often significantly different from those encountered at room temperature. Later, this has open the way to new or improved optoelectronic devices that require liquid nitrogen temperature or lower. Typical application need this technology of cooling are infrared detectors. Brecknrige et al (1974) worked through the design of the miniaturized cooling system for the IR detectors used in the IR homing system. They briefly described the characteristics of the cooler, which are suitable for cooling the IR system to temperature in the

range of 4-120 *K*.

Houston and Carswell (1978) obtained information on the polarization state of the scattering depending on the atmospheric conditions. The results were presented and discussed for clear weather conditions, haze, and several cloud types. This attribution was classified and kept confidential by the military particularly in the United States of America for a time.

Froelich (1980) developed a low-cost IR seeker for man portable terminal homing heads. The minimizing of production costs emphasized on design simplicity and inexpensive manufacturing processes. Low cost IR seeker engagement parameters represent a short–range round launched over a land combat vehicle. The seeker optical system has an aerodynamically spun dome that holds a roof mirror on the inside cylindrical axis. This provides a rotary field scans. He used a coated germanium anti-solar spectral filter with a pass-band that cuts on at the wavelength of 2.3 μm.

Woods et al (1993) performed a research on systematic investigation of the effects of changes in the design of bifocal contact lenses upon visual performance. The main purpose of the optical investigations of contact lenses had been to elucidate the effect of differences in the optical design, the optical and visual results were compared and models developed to predict visual performance from the optical performance measurements of bifocal contact lenses. Optical performance was measured by using modulation transfer function (MTF) system, and the visual performance was measured with a contrast sensitivity system. Dowski et al (1995) used the improvements in the field of digital processing. They designed an optical digital system near diffraction limited imaging performance. This system is a

standard incoherent optical system modified by a phase mask with digital processing of resulting intermediate image.

Howard (2001) performed numerical calculations for ray tracing and analysis and rendering graphics for system drawings. The computer was the primary tool used for optical designing. Mclean (2004) considered the basic purpose of the optical design for helmet and head mounted device. It intended to focus small image sources to provide a specific field of view to the viewer with sufficient eye clearance for spectacles and protective masks, and sufficient size eye movement, vibration, and head/helmet slippage. These objectives achieved by series of calculations that required determining the size of element.

Liu et al (2005) proposed a new bifocal optical system used for distant object tracking. This system combines a birefringent element with a conventional glass lens. The spot image size and its variation with the axial distant controlled according to the requirement of a distant object tracker.

In private communication, H. H. Mohammed To the best of our knowledge, Ratioas upgraded the Air defense “SAM-7” (Strela-2) with new achievement, where protection against blinking jammers and flares was carried out. Protection against jammers is provided by a new design of the reticle with large opaque area, and jammers can only increase the sized from the target where target (and the jammers) is in the transmissive-to-opaque sector area. Protection against flares is based on the physical spectral differences between target and flares. When using the signals from two different spectral channels, processing them simultaneously with one

channel as tracking channel, it is possible to determine the flare position on the FOV and make the signal from it smaller than the target, so the homing head will continue track the target.

1.5 Aim of the Project

The present work aims to put forward an improved optical design for an IR homing head. The effective design parameters would be studied and analyzed. The range of the suggested optical system would be determined and investigated under various weather conditions. This range is considered with regarding the angle between the homing head and the target as well as the detector temperature, which we consider the probability of its variation during the flight of the missile towards the target. It has been intended to perform the present investigation computationally by means of well-known Zemax software and a newly suggested computer program written in Visual Basic language.

1.6 Work Objective

The following are the main steps for executing the present research objective.

1. Suggest an optical system design for IR homing based on design parameters mentioned in this chapter and improve this suggested design by choosing suitable optical materials and features for some of the constituent elements of the optical system.

2. Study the suggested system design analytically by investigating the effective parameters and their role.

3. Obtain some parameters from which one can determine the efficiency of the suggested design, such as the system range, spot size, and MTF by using Zemax software.

4. Design and implement new software specifically for the homing head purposes.

5. Determine the parameters with the aid of the new software depending on the physical equations and the significance of these parameters.

6. Compare the results obtained by Zemax software with the corresponding ones obtained by the present work software.

7. Discuss and analyze the results.

1.7 Thesis Outline

The thesis consists of five chapters; chapter one is a general introduction about the topic of the project, whereas the other four chapters deal with the optical system design of IR homing head and its parameters that determine the efficiency of the design. The following is a brief description of the last four chapters

Chapter Two Entitled "*IR Homing Head"*

This chapter is dedicated to present a description of optoelectronic components of the IR homing head and their features and how these features can be used in tracking and searching the IR homing head. The optical materials used in IR system designing and infrared detectors are considered with details. The effect of the Earth's atmosphere and visibility factor on the range of the homing head is considered in addition to the tracking and searching modes calculations.

Chapter Three Entitled "*Optical Considerations*"

This chapter includes detailed descriptions on the paraxial optics with regarding the aberrations containing in the wavefront due to the considering the third order approximation of ray tracing. The image formation model showed with its related terminologies of transfer functions. The point spread function, spot diagram, and the transfer functions were mathematically described in the three cases namely ideal, perfect, and usual.

Chapter Four Entitled "*Computational Results and Discussion*"

In this chapter, a suggested optical system design for IR homing head is considered and improved. Some effective parameters are calculated by means of Zemax software and another software OID that has been designed and implemented. The OID suits the purposes of designing IR homing head. A comparison between the results of both Zemax and OID software is

carried out. Investigation of the parameters of interest for range determinations is carried out.

<u>Chapter Five</u> Entitled "*Conclusions and Suggestions for Future Work*"

The conclusions drawn from the present investigation are stated in this chapter. The conclusions are concerned with the assessment of using Zemax and OID software. Also, this chapter presents some future work suggestions that are relevant to the field of the present investigation.

4.6 Range Evaluation

The maximum range is the maximum distance in which the homing head can detect and lock on. The range evaluation can be considered as the most important parameters for the homing head characterization the target clearly. When the target is at a distance is equal or less than the maximum range, the recognition of the target is capable and depends only on the surrounding situations, weather conditions, and ratio between the received intensity and maximum intensity emitting from the target.

Equation (2.55) of the maximum range includes all the independent or dependent parameters may be affecting the range determination. This equation is partitioning into four terms multiplied by each other, each term includes some parameters belong to defined source of the range contribution. In the following paragraph, the detail of each term evaluation is given and the percentage of the range contribution considered.

4.6.1 Target and Atmosphere Transmittance Term Calculation

This term is concern with the amount of the received radiation and its transmission, it is denoted as $\left[I\tau_a\right]^{1/2}$. This term is evaluated depending on some constants listed below according to the following steps

The area of the jet nozzle pipe A=3660cm^2, $\sigma = 5.67\times10^{-12}$ $\mathrm{Wcm^{-2}K^{-4}}$, and T=850 *K.* [**Hudson 1969]**.

1. By using equation (2.13): $\lambda_{\max} = \dfrac{2898}{T(K)} = \dfrac{2898}{850} = 3.409\ \mu\mathrm{m}$.
2. By using equation (2.14 and 2.15): $X_1 = \dfrac{\lambda_1}{\lambda_{\max}} = \dfrac{3}{3.409} = 0.889$

and $$X_2 = \frac{\lambda_2}{\lambda_{\max}} = \frac{5}{3.409} = 1.470$$

3. Referring to [**Gaussorgues 1984**] Z (0.889)=0.1723
   and Z (1.470)=0.5308
4. By equation (2.11): $w = 5.67 \times 10^{-12}(850)^4[0.5308 - 0.1723]$
   $= 2.948\, W/cm^2$
5. By equation (2.16): $I_o = \frac{2.948 \times 3660}{\pi} = 3434.46\, W/Sr$

Taking into the emissivity of the tailpipe, which is 0.85 [**Hudson 1969]**, I_o becomes $3436 \times 0.85 = 2919.3\, W/Sr$. According to Hudson and using the radiation slide rule in the $3.2 - 4.8\ \mu m$ region to find that 26.6% of the radiation flux loss in this region. Therefore, the value of the radiant exitance of the IR radiation emitted by jet engine and received by the detector I_o become $2919.3 \times 0.266 = 776.53\, W/Sr$, which is close to the true value given by Matra (760 W/Sr).

6. By using equation (2.56): The maximum I is given at zero angle as $I = I_o \cos(0) = 776.53 \times \cos(0) = 776.53\, W/Sr$.
7. From table (2.1): $\beta_{aerosonal}$ for different region can be given by R_v, and R_v given in table (2.3), while $\beta_{H_2O} + \beta_{Molecules}$ at dew point temperature –20-40 ^oC is given from table (2.2) at different path lengths.
8. By using equation (2.17) the atmosphere transmission can be calculated to be equal 0.525.
9. The numerical result of the current term is 20.194 $[W/Sr]^{1/2}$.

4.6.2 Optics Term

This term contain various factors characterize the optical part (suggested OSD) within the homing head, which is denoted as $\left[\frac{\pi}{2}(NA)D_o\tau_o\right]^{1/2}$. The following steps show how to evaluate the optics

1. By using equation (2.53): $NA = \frac{5}{2\times 2.09} = 1.1$.
2. By using equation (2.41): $(\tau_{o)system} = \frac{\sum_{i=1}^{7}(\tau_o)_i}{7} = 0.7$,

   where 7 is the number of elements.
3. The numerical result of the current term is 2.56 $(cm)^{1/2}$.

4.6.3 Detector Term

This term belongs to purely detector figures of merits, it is denoted as $\left[D^*\right]^{1/2}$. Since the calculations of D^* is monopolized and has no enough published data, a qualitative approaches is used to achieved D^* at useful range of T_d.

The detectivity depends on the temperature of the detector. For the InSb detector the detectivity D^* as a function of the detector's temperature T_d is determined by the adopted method which is based on the descriptive relationship between D^* and T_d shown in figure 4.39-a. Within the range of the detector's temperature 77-200 *K*, it is seen that D^* decreases in a linear manner with increasing T_d as shown in figure 4.39-b. Thus, in this region D^* can be achieved by using a linear interpolation method. This method which requires the knowledge of two values of D^* is describe as follows.

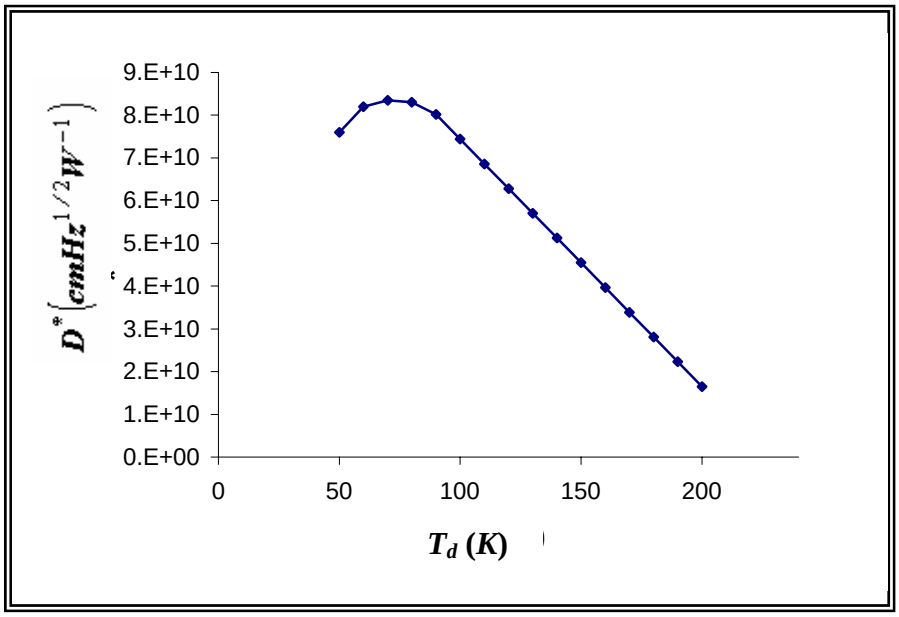

Figure 4.39-a D^* versus T_d for InSb detector.

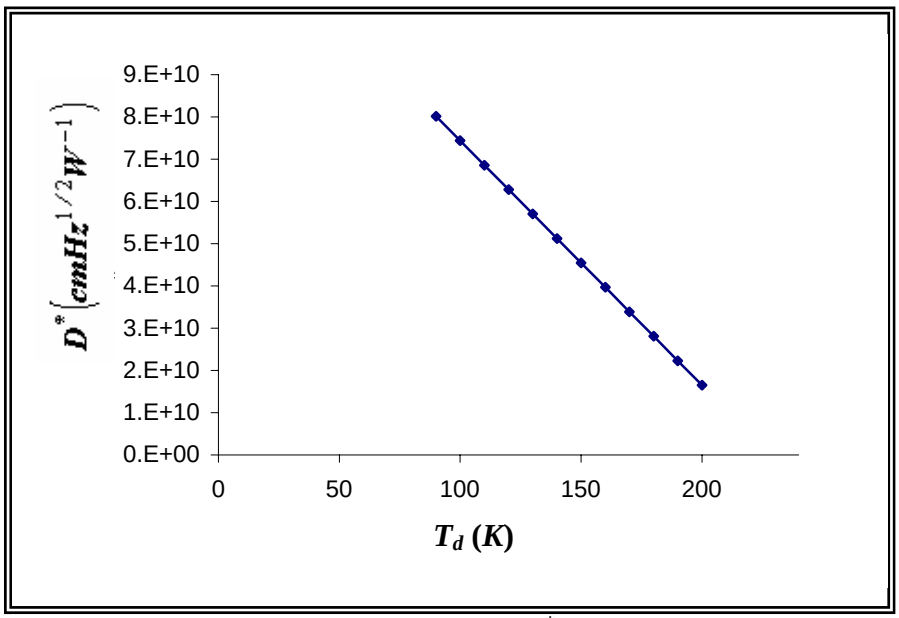

Figure 4.39-b Linear relation of D^* as a function of T_d.

Consider figure 4.39-c. The detectivity D_o^* at temperature T_{do} lies between the two given values D_1^* and D_2^* at T_{d1} and T_{d2} respectively. Thus,

$$D^* = \frac{D_1^*(T_{d2} - T_d) + D_2^*(T_d - T_{d1})}{T_{d2} - T_{d1}} \qquad (4.30)$$

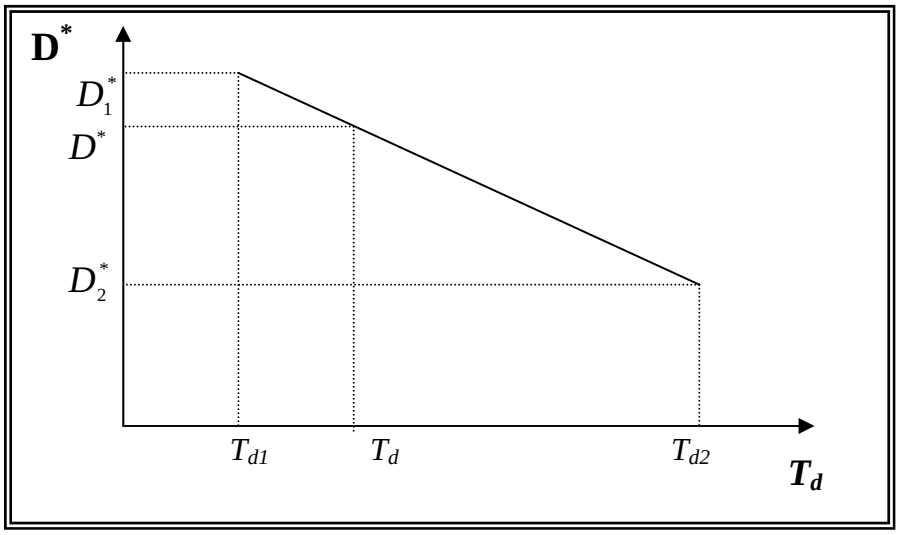

Figure 4.39-c Linear interpolation schematic.

For the present work, let $D_2^* = 9\times10^{10}\ cm.Hz^{1/2}\ W^{-1}$ at $T_{d1} = 60K$ and $D_2^* = 9\times10^{9}\ cm.Hz^{1/2}\ W^{-1}$ at $T_{d2} = 200K$. Therefore, since the detector's temperature of interest is *77 K*, one can determine the detectivity D^* as follows:

$$D^* = \frac{9\times10^{10}(200-77)+9\times10^{9}(77-60)}{200-60} = 8.01\times10^{10}\ cm.Hz^{1/2}\ W^{-1}$$

The detectivity of InSb detector at T_d=77K is $D^* = 8.01\times10^{10}\,cm.Hz^{1/2}\ W^{-1}$, thus the final numerical of the current term is 283132.9 [$cm.Hz^{1/2}\ W^{-1}$]$^{1/2}$.

4.6.4 Signal Processing Term

This term contain factor describing system and signal processing characteristics, it is denoted as $\left[\frac{1}{(IFOV\times B)^{1/2}(S/N)}\right]^{1/2}$. The following steps show how to evaluate the system characteristics and signal processing, using the data given by Hudson, *B*=200 *Hz* and *S/N* ranging from 5 to 10, thus the average value (i.e. 7.5) is considered.

1.The area of the detector is computed by equation (1.3) $A_d = \frac{\pi \times (0.09)^2}{4} = 6.36 \times 10^{-3} cm^2$, and by using equation (1.2) $IFOV = \frac{6.36 \times 10^{-3}}{(2.09)^2} = 1.45 \times 10^{-3} Sr.$ or 2.5^o

2. The final result of the signal processing term is 4.97×10^{-2} $Sr^{-1/4}Hz^{-1/4}$.

Finally, the maximum range is the production of the previously determined four terms, which is found equal to about 7.28 *km*. It should be mentioned that this value is evaluated at the range of the wavelengths 3-5 μm through natural conditions, and it is normal for the range to be greater or lower at better or worse conditions. Computation of the range depends on several effective parameters the most important one is the wavelength, where the variation of the range with the wavelength was noticeable. The computed results of the range are listed in table 4.7 using the design parameters mentioned in the paragraph (1.3).

Table 4.7: Range values verses its parameters

No.	Range effective parameters	Symbol	Determined Value (unit)	Resulted Value (unit)
1	*Max. spectral radiant intensity at 0 angle.*	*I*	*1000 W/Sr*	*776.53 W/Sr*
2	*Atmosphere transmission.*	τ_a	*0.6*	*0.525*
3	*Numerical aperture*	*NA*	*1*	*1.1*
4	*Aperture and detector diameters*	D_o, D_d	*7 cm, 0.09 cm*	*5 cm, 0.09 cm*
5	*Detectivity at 77K of InSb detector for 3-5 μm region.*	D^*	1×10^{11} $cm.Hz^{1/2}\ W^{-1}$	8.01×10^{10} $cm.Hz^{1/2}\ W^{-1}$
6	*Instantaneous field of view*	*IFOV*	$1.45 \times 10^{-3} Sr$	$1.45 \times 10^{-3} Sr$
7	*Band width*	*B*	*200 Hz*	*200 Hz*
8	*Signal to Noise ratio*	*S/N*	*5*	*7.5*

The window specified to determine the range by OID contains a table that displays the results of the important parameters appearing in the range equation. These parameters are considered at different design and environment conditions to give different values for the computed range..

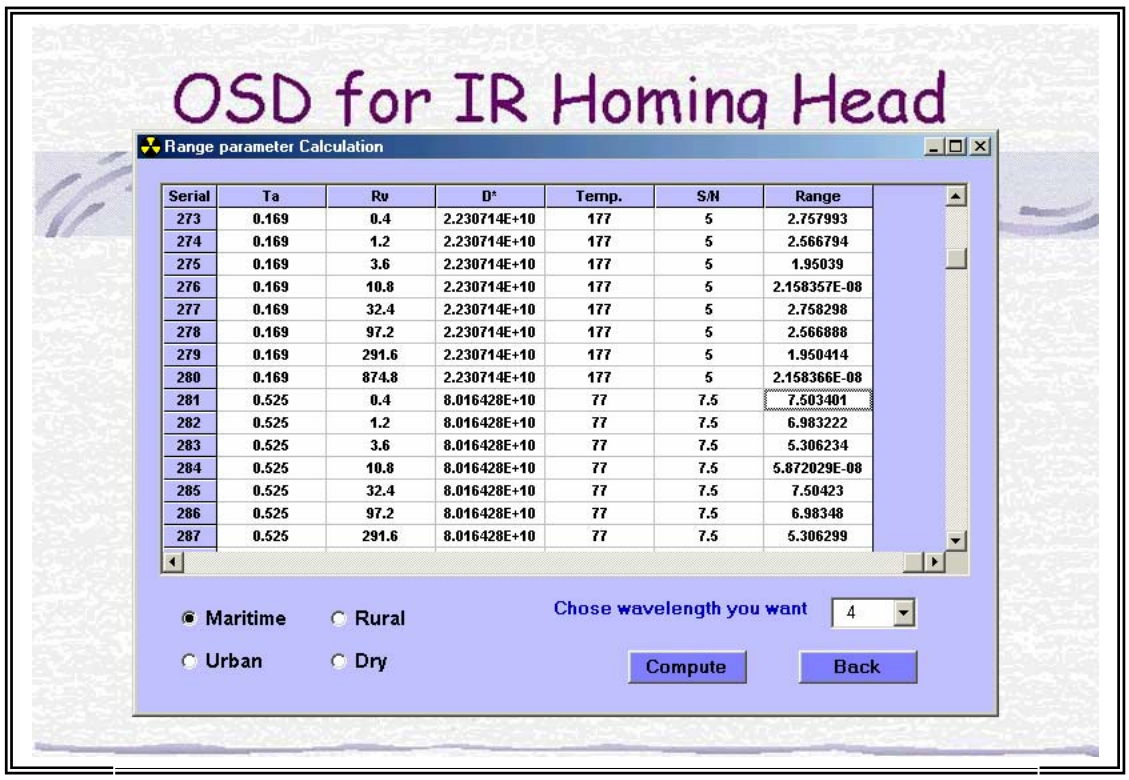

Figure 4.40: Range results by OID software.

Figure 4.40 shows the window for computing the range by OID software. It should be mentioned that two more columns do not appear in figure 4.40. These two columns are the spectral radiant intensity *I* and the wavelength λ; they can be displayed by moving a scroll bar

By observing the range values, it is found that the range is tending to be better by improving each parameter. In order to notice the range behavior with respect to the improvement of each parameter alone, the range is consider to be changed by changing each one parameter with keeping the other parameters constant at excepted values, which aid to analyze the different conditions of the range. Tables 4.8, 4.9 and 4.10the result of the range for different wavelength.

Table 4.8: Range and its related parameters for $\lambda = 3\mu m$.

I (W/Sr)	Angle	Transm.	Rv (km)	Range(km)
405.10	0	0.53	0.4	5.26
350.82	30	0.53	1.2	4.90
202.55	60	0.53	3.6	3.72
0.00	90	0.53	10.8	0.00
405.10	0	0.53	32.4	5.26
350.82	30	0.53	97.2	4.90
202.55	60	0.53	291.6	3.72
0.00	90	0.53	874.8	0.00
405.10	0	0.45	0.4	4.88
350.82	30	0.45	1.2	4.54
202.55	60	0.45	3.6	3.45
0.00	90	0.45	10.8	0.00
405.10	0	0.45	32.4	4.88
350.82	30	0.45	97.2	4.54
202.55	60	0.45	291.6	3.45
0.00	90	0.45	874.8	0.00
405.10	0	0.39	0.4	4.52
350.82	30	0.39	1.2	4.21
202.55	60	0.39	3.6	3.20
0.00	90	0.39	10.8	0.00

Table 4.9: Range and its related parameters for $\lambda = 4\mu m$.

I (W/Sr)	Angle	Transm.	Rv (km)	Range(km)
823.29	0	0.53	0.4	7.50
712.99	30	0.53	1.2	6.98
411.65	60	0.53	3.6	5.31
0.00	90	0.53	10.8	0.00
823.29	0	0.53	32.4	7.50
712.99	30	0.53	97.2	6.98
411.65	60	0.53	291.6	5.31
0.00	90	0.53	874.8	0.00
823.29	0	0.45	0.4	6.95
712.99	30	0.45	1.2	6.47
411.65	60	0.45	3.6	4.92
0.00	90	0.45	10.8	0.00
823.29	0	0.45	32.4	6.96
712.99	30	0.45	97.2	6.47
411.65	60	0.45	291.6	4.92
0.00	90	0.45	874.8	0.00
823.29	0	0.39	0.4	6.45
712.99	30	0.39	1.2	6.00
411.65	60	0.39	3.6	4.56
0.00	90	0.39	10.8	0.00

Table 4.10: Range and its related parameters for $\lambda = 5\mu m$.

I (W/Sr)	Angle	Transm.	Rv (km)	Range(km)
1241.49	0	0.53	0.4	9.21
1075.16	30	0.53	1.2	8.58
620.74	60	0.53	3.6	6.52
0.00	90	0.53	10.8	0.00
1241.49	0	0.53	32.4	9.22
1075.16	30	0.53	97.2	8.58
620.74	60	0.53	291.6	6.52
0.00	90	0.53	874.8	0.00
1241.49	0	0.45	0.4	8.54
1075.16	30	0.45	1.2	7.95
620.74	60	0.45	3.6	6.04
0.00	90	0.45	10.8	0.00
1241.49	0	0.45	32.4	8.54
1075.16	30	0.45	97.2	7.95
620.74	60	0.45	291.6	6.04
0.00	90	0.45	874.8	0.00
1241.49	0	0.39	0.4	7.91
1075.16	30	0.39	1.2	7.37
620.74	60	0.39	3.6	5.60
0.00	90	0.39	10.8	0.00

In the following a graphical picturing on the behavior of the range regarded with respect to some parameters that considered in the computation work.

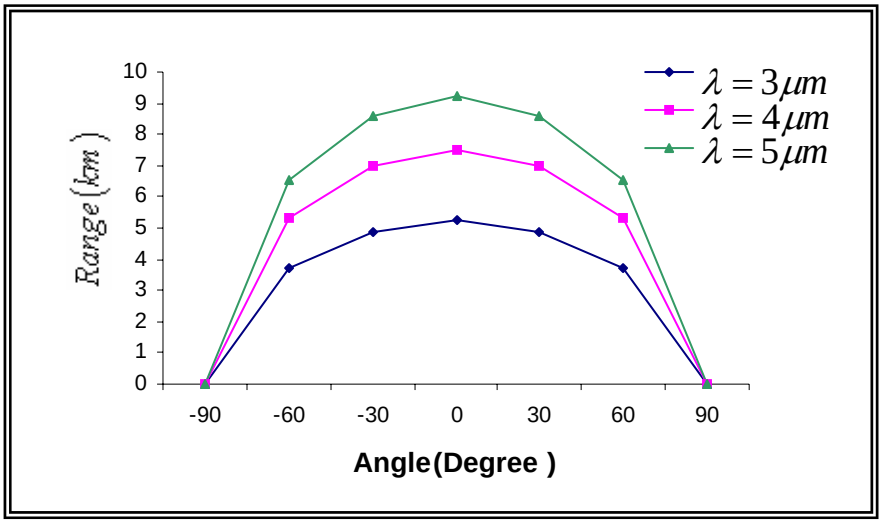

Figure 4.41: Range versus reception angle for different wavelengths.

radiant intensity is distributed depending on the angle between the face of the source and the homing head to be increased from angle 90^o into the angle zero at the right of the homing head, the angle zero is corresponding to the maximum spectral radiant intensity behavior, and then the spectral radiant intensity decreases up to lower value when angle directed towered -90^o which is the left of the homing head as shown in figure 4.42 for the wavelengths $(3,4, and\ 5)\mu$m .

The comparison between figures 4.41 and 4.42 shows that the behaviors of the range is shifted toward greater spectral radiant intensity by increasing the wavelength, the position of the peak of the range behavior at the wavelength $3\mu m$ is at spectral radiant intensity of $405.1 W/Sr$ corresponding to range of about 5.26 *km*, it was 823.3 *W*/*Sr* corresponding to a range of about 7.50 *km* at the wavelength $4\mu m$, and at $5\mu m$ wavelength the radiant intensity was about 1241.5 *W*/*Sr* corresponding to arrange of about 9.21 *km*. The qualitative description of the range behavior as function of radiant intensity refers to a nonlinear relationship between the radiant intensity and the wavelengths as shown in figure 4.42, since it causes irrespective differences between the radiant intensity behaviors for different wavelengths. This interprets the non-equal horizontal shift between the three peaks of the range behavior belong to the wavelength of interest. Whereas the irrespective differences of the radiant intensity gave also irrespective differences between the range behaviors which interprets the irrespective increasing of the peaks of the range behaviors at the wavelengths of interest.

Figure 4.43 presents the dependency of the range on the atmospheric transmission (τ_a) at the wavelengths $3, 4, and\ 5\mu m$. It noticeable that the range is increased with the increasing of atmosphere

transmission by irrespective differences at different wavelengths of interest. The divergent differences refer to the nonlinear dependency of the range on the atmosphere transmission and wavelength, whereas both atmosphere transmission and wavelength are independent on each other. It is noticeable that the τ_a adopted the values from 0.17-0.525 depending on the total transmission coefficient (β_{atm}) described in figure 4.44. The decrease exponential relationship of figure 4.44 gave maximum τ_a of about 0.525 at transmission coefficient β_{atm} equal to 0.16, while the minimum τ_a is 0.17 at β_{atm} of about 0.44. It is shown that the τ_a is sensitive for any small change at the lower transmission coefficient region, while it is not more changed at the region of higher transmission coefficients. Therefore, one can say it is necessary to calculate the β_{atm} with high accuracy, this require for both the β_{aerosl} and ($\beta_{H_2O} + \beta_{Molecules}$) to be accurately calculated.

In order to credit the accuracy, β_{aerosl} that depend on the factor of weather condition (i.e. visibility factor; R_v) is calculated depending on the type of the region (i.e. Maritime, Rural, Urban, and Dry). Figure 4.45 shows the β_{aerosl} behavior taken for different types of regions at different R_v. It is observable that β_{aerosl} has values are very different at the very bad weather condition (i.e. smaller R_v), these differences decreased step by step until they became approach to zero at the excellent weather condition (i.e. $R_v \geq 50$). In this situation, β_{aerosl} value seems to be identified at the four regions under consideration, which is resulting a range value is minimum at very bad condition and then the range is improved by improving the R_v until it was maximum at excellent condition of weather. At the excellent condition there is very little effect

for the region type on the determined range. Whereas $(\beta_{H_2O} + \beta_{Molecules})$ are depending on the dew point temperature (T_{dp}) as shown in figure 4.46. In spit of the relation between $(\beta_{H_2O} + \beta_{Molecules})$ and T_{dp} is sensitive for any change in the T_{dp}, it was active and more affect the atmosphere transmission comparing with the β_{aerosl} at the excellent weather condition. Strong effect of $(\beta_{H_2O} + \beta_{Molecules})$ on atmosphere transmission is come from the shape of the relationship between them, which is exponentially increased to yield higher values comparing with β_{aerosl}.

Therefore, it is clear that the behavior of the $(\beta_{H_2O} + \beta_{Molecules})$ at very clear weather is dominant on the behavior of β_{aerosl} when both are collected to make atmosphere transmission. Also, the atmosphere transmission depends almost on the T_{dp} greater than its dependency on the weather condition. In other words, T_{dp} (i.e. humidity) has greater effect on the atmosphere transmission from the weather condition, which is lead to make the maximum range is weakly related by the weather condition as shown in figure 4.47. But at not enough clearly weather, β_{aerosl} is strongly affecting the atmosphere transmission, whereas $(\beta_{H_2O} + \beta_{Molecules})$ are weakly affecting, and the range is depending mainly on the weather condition as shown in figure 4.47.

Figure 4.48 shows the behavior of the range at various dew point temperatures, which is opposite relationship to that of the range as a function of atmosphere transmission, where the range takes higher value at lower dew point temperature, and then it decrease by increasing the dew point temperature. The differences between the range behaviors at different wavelengths of interest are irrespective along the temperature

range of dew point. Therefore, dew point temperature has larger share than the weather condition (R_v) in the atmosphere transmission calculations, and then in the range calculations at clear weather conditions, while an inverse situation is found at not enough clearly weather conditions.

Figure 4.49 present the variation of the range with respect to aperture diameter (D_o), which represent the dependency of the range on the second term of optics since the second term consists of a set of constants besides one variable is the aperture diameter. Because of the numerical aperture (*NA*) is the ratio between the diameter of aperture and the effective focal length (constant), the range was depending on $\left[D_o^2\right]^{1/2}$ or it simplified as D_o. Therefore, the relation of the range as a function of aperture diameter is increase linearly with intercept equal to zero at all the wavelengths of interest. The range behaviors at $3, 4, \text{and } 5\ \mu\text{m}$ diverge by increasing the diameter of aperture. This proves achieving greater range for larger aperture through logical limitations.

Figures 4.50 show that the range increases as one reduces the temperature of the detector irrespective of the wavelength of the IR radiation. However, if these plots are extrapolated towards the higher temperatures, the wavelength would have very little effect on the range and the range becomes very short and undesirable. The influence of wavelength on the range is significant at low temperatures of the detector. If the detector's temperature is kept constant at a certain low value, the range increases with decreasing IR wavelength. For example, at about 77 *K,* the range increases by about 1 *km* at $\lambda = 5\ \mu m$ and it is decreases by about 1.5 *km* at $\lambda = 3\ \mu m$; a value which is considerably high and

interesting from the application point of view. The long range is achieved at low detector's temperature in the FIR region.

The range of detection increases with the detectivity at various wavelengths as shown in figure 4.51. At the $5\,\mu m$ wavelength the range increases from 5.26 *km* at $D^*= 2.23\times10^{10}$ to 9.5 *km* at $D^*= 8.01\times10^{10}$; a value of considerable importance in the detection of target. At any specific value of the detectivity, the range increases with the increase of the wavelength of the IR radiation. In addition, the gradient of the plots increases as the wavelength increases.

If one hope for a range of about (9.21 *km*) at $\lambda=5\,\mu m$ it may be deduced from the plots of the figures 4.50 and 4.51 that the parameters T_d, and D^* should have the values (77 *K*, and 8.01×10^{10} $cm.Hz^{1/2}\,W^{-1}$) respectively.

Figure 4.52 shows the behavior of the range with respect to the signal to noise ratio (*S/N*). Since the fourth term in the range equation consists of a set of constants except *S/N* is variable according to an external conditions. Figure 4.52 describes the variation of the range with the variation of the fourth term totally. It is noticeable that lower *S/N* of about 5 make the range adopted higher value, but the value of *S/N*<5 lead to reduce the range irrespectively and make the image appear blur, which is useless for the purpose of tracking. Whereas highest *S/N* of about 10 gave lower range, but the image is clear detailed. It shown that the behavior of the range contain sharp decay at lower region of *S/N*, while it does not more changed at higher *S/N*. The differences between range behavior and wavelengths 3, 4, and 5 μm are irrespective along the range of *S/N*. The average ratio of *S/N* is 7.5, at this situation the noise is called

"white noise". The range at the natural ratio is 7.5 *km* for MIR, while it raised up to 8.92 *km* by decreasing the *S/N* to be just 5 and it descend up to 6.31 km by increasing *S/N* to be 10. Furthermore, lower *S/N* is greatly affecting the range that seems to be sensitive to any change in the *S/N*, while in the white noise region the *S/N* gave inactive differences in the range.

4.8 Results Analyses

The parameters that need to be discussed in detail in the present work are the PSF, MTF, spot diagram and its size, and the range. These parameters concern the optical system under consideration that have been investigated with the aid of Zemax and OID software. The proposed OID software has the advantage of computing the detection range directly which cannot be performed by the Zemax software at the present time.

The results of PSF, MTF, spot diagram, and spot size extracted by OID were adopting the same behavior at all the proposed methods. Also, they were identifying the behavior of Zemax results. The identification of the results behavior reflects the success of applying different methods to compute the effective parameters. Figure 4.53 summarized the results of the effective parameters that analyzed with more details in the following.

PSF results show insignificant amplitude with respect to the variation of the wavelengths. PSF of $4\,\mu m$ wavelength has maximum amplitude with less spread and its behavior similar to that of the perfect PSF, while PSFs of other wavelength differ by its less amplitude and surrounding rings. Maximum amplitude expresses the high energy that illuminates the image, whereas narrow width of PSF brings out the sharpness of the image. As a result, the image consisting of greatly

variation of gray levels, which means that the contrast of the image is high.

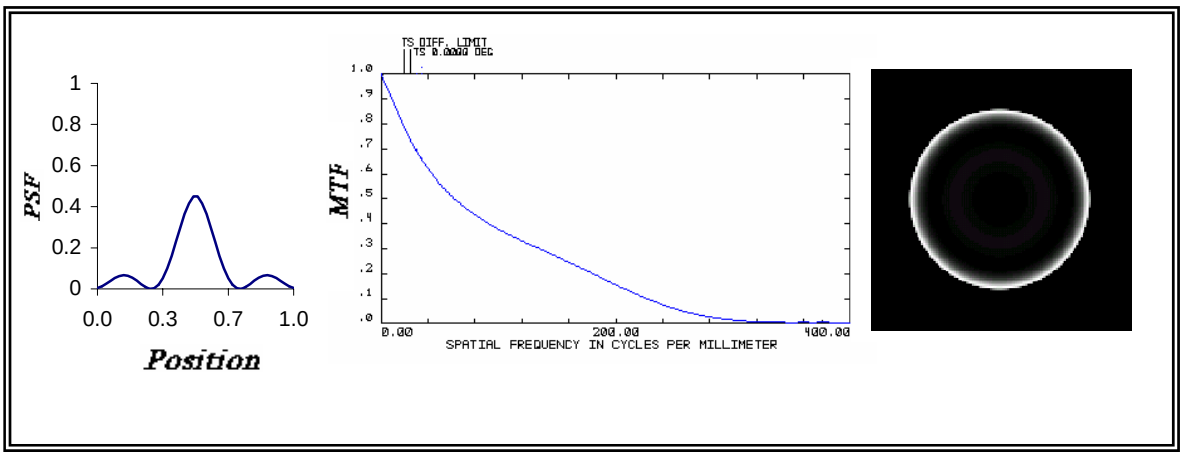

Figure 4.53-a The PSF, MTF, and spot image for $\lambda = 3\mu m$

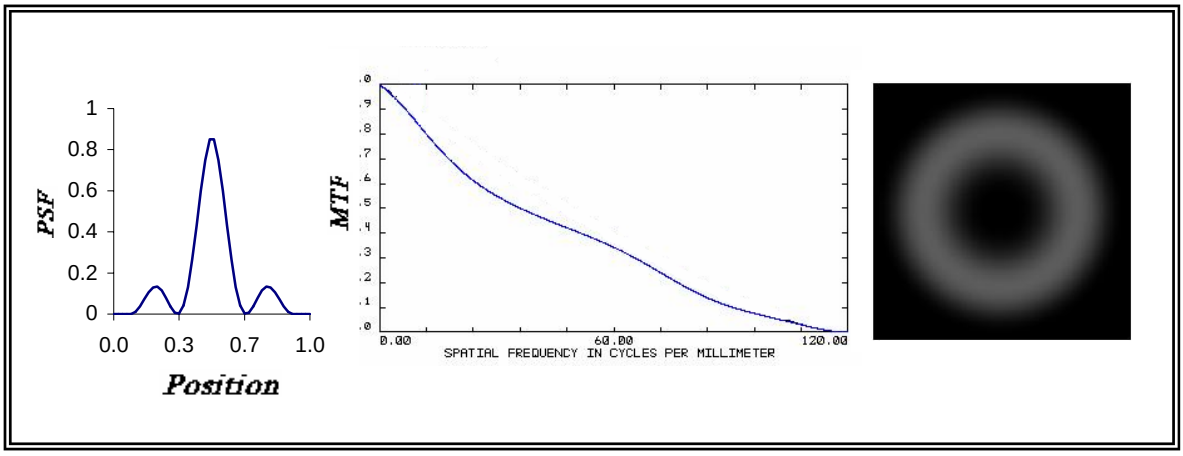

Figure 4.53-b The PSF, MTF, and spot image for $\lambda = 4\mu m$.

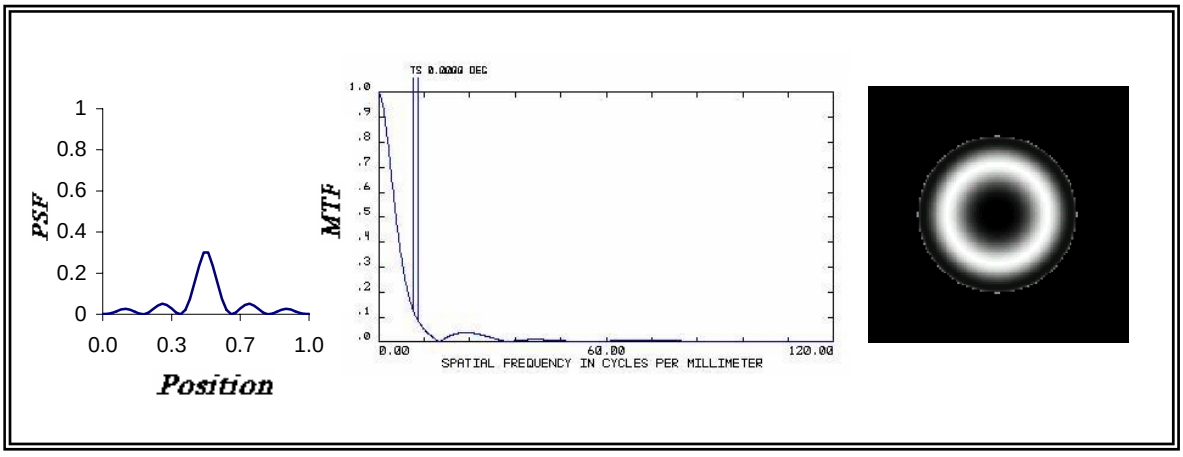

Figure 4.53-c The PSF, MTF, and Spot image for $\lambda = 5\mu m$.

The MTF curve is a considerable measure of the image resolution in the frequency domain. It reveals the presence of aberration in the image when it is compared with the perfect MTF curve. The perfect MTF curve obtained by the Zemax software possess the same behavior of that obtained by OID software. At the $5\mu m$ wavelength of the IR radiation the MTF curve is the worse since it contains a sharp decay with some ripples that appears by increasing the frequency, that means less amount of the high frequency information pass as illustrated in figure 4.53-a. At $\lambda = 4\mu m$ the MTF curve is smooth and close to the diffraction limit as shown in figure 4.53-b. This result is the most favourable for the purpose of tracking and detection, besides the wavelength $\lambda = 4\mu m$ is closed to the peak response of the InSb detector used in IR homing. At $\lambda = 3\mu m$ the MTF curve is smooth and decay slowly to be far away from the perfect case in comparison with the MTF of 4 μm as shown in figure 4.53-c.

The MTF curves computed by the OID and Zemax softwares compared with the perfect MTF for $\lambda = 4\mu m$ reveal the aberration produced by the optical system which is perceptible in the two figures. At high frequencies the aberration is highly reduced since the MTF curve of the suggested optical system approaches the perfect one and thus the spot image will be of high resolution. However, within the spatial frequency of range, which is specific for the present work design, one may suggest that the MTF curve is not far away from the perfect one. This result would give credibility to the suggested optical system design for the homing head.

The results of the spot shape at the IR radiation wavelengths of 3, 4, and 5 show that the spot image quality at $4\mu m$ wavelength is more

favourable than that at 3 or 5 μm since it has less number of bright rings around it. A large number of bright rings indicate the presence of high diffraction and distortion of the spot.

The spot image formed by the optical system has several characteristics. The size of the spot and the radiation wavelength are proportional to each other. Furthermore, an increase in the focal number of the system decreases the spot size; the two parameters being exponentially related to each other. The quality of the spot image is found to be in its best state at the $4\mu m$ region where the aberrations are insignificant. At other IR regions the spot is distorted and contains on one or more bright rings. At the $4\mu m$ wavelength of the IR radiation, the spot size is found to be $10.5\mu m$ by the Zemax software and 10.6 or 10.8 μm by the OID software; the values are same or very close to each other. This result confirm the accuracy of the OID software when compared to the standard Zemax software.

As one would expect the results of the range have shown that it is directly proportional to the detectivity (D^*), atmosphere transmission (τ_a), and aperture diameter (D_o). The detectivity related with the improvement of detector's specifications. Atmosphere transmission means that the detection range of the optical system increases at the clear weather conditions. The diameter of aperture determine the amount of illumination in the consisted image, the larger aperture received most rays which make the image has more contrast and indicates the target lie at the viewing range. The increasing relationship between the range and spectral radiant intensity (I) suggests that variations in I would lead to insignificant changes in the detection range.

In the IR radiation region between the wavelength 3 and 5 μm, the range is proportional to the wavelength such behavior gives the system engineer a good picture with regard to the selection of a detector particularly when the maximum range is the major task of the IR homing head. It is found that under the most favourable weather conditions a range of about 5.26 *km* can be achieved at $\lambda = 3\mu m$ as shown in figure 4.54. As indicated in the figure the range increases to about 7.50 *km* at $\lambda = 4\mu m$ and to about 9.21 *km* at $\lambda = 5\mu m$ which is the cut-off the InSb detector. Thus the highest possible detection range that can be achieved by the optical system of the homing head with the aid of the OID software is about 9.21 *km* under excellent weather conditions. The computed 7.50 *km* detection range at $\lambda = 4\mu m$ is very close to the value of 7-8 *km* which has been determined experimentally by the Iraqi group experiment carried out in 2000. The experiment, which has been carried out at Tammoz air base was a test for real evaluation of a developed infrared detection and tracking system for the detection and tracking range evaluation using the aircraft MIG 25 jet engine with after burner [**Mohammed and Mustafa 2000**].

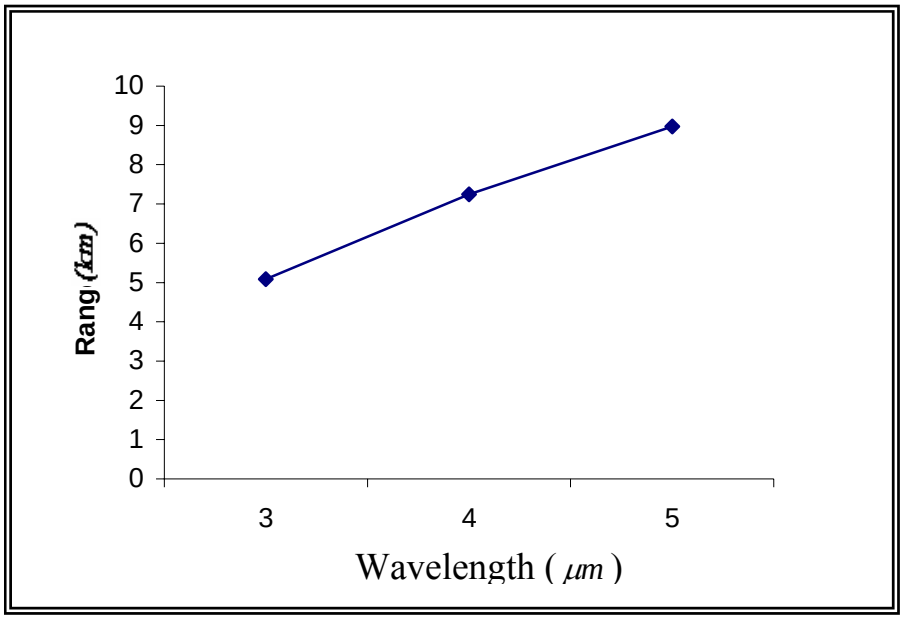

Figure 4.54: Range versus wavelength.

Therefore, due to the above arguments one would choose the wavelength $\lambda = 4\mu m$ within the middle IR region as an excellent compromise with regard to the PSF, MTF, and spot quality, and the range. As mentioned before this wavelength represents the maximum response of the available detectors working within the range 3-5 μm of the infrared region.

Chapter Three

OPTICAL CONSIDERATIONS

Chapter Contents

3. OPTICAL CONSIDERATIONS

3.1 Introduction

Optical design is the process of finding the description of individual elements and their arrangement in the desired optical system. The descriptions provide the information as specifications necessary to manufacture the system. The designer starts with an idea for a needed system that will solve specific imaging problems. The required image implies certain imaging characteristics that have been specified using such terms as resolving power, acutance, modulation transfer function (MTF), permissible distortion, field of view, focal number (*f*/no) or numerical aperture, encircle energy, and range of color. Also to be met are the physical requirements such as size of package, size of image, and the object-image distance [**Williams and Becklund 1972**].

In the early days of an optical design, the designer could usually assemble a system from available, or easily shaped, elements and could detect by visual examination some of the imperfections of the image. Nowadays, the designer assumes a system by listing a set of initial construction parameters as a first guess in describing the desired system. For each element the parameters, typically, are the index of refraction and dispersion of the material, the diameter and thickness of the element, and curvatures of the two surfaces. The separation and order of the elements are also part of the design [**Williams and Becklund 1972**].

3.2 Reflecting System

A part from complete absence of chromatic aberration, a mirror has certain advantage over a lens. The formula describing refraction at a single surface can be converted into corresponding formula for reflecting by putting $n' = -n$. Consequently, one would expect some of the aberration of a reflecting surface to be less than those of a refracting surface under similar condition. In the outer zones of the aperture are related by a mount proportional to ρ^4 so that the spherical aberration of the mirror is corrected [**Longhurst 1967**].

The paraxial ray, which relates conjugate object and image point to the physical parameters of a spherical mirror, can be derived rather easily as shown in figure 3.1. Since $sin\theta_i = \theta_r$, the angle *SAP* is bisected by *CA*, which therefore divided the side *SP* of triangle *SAP* into segments proportional to remaining two sides [**Zajac 1974**].

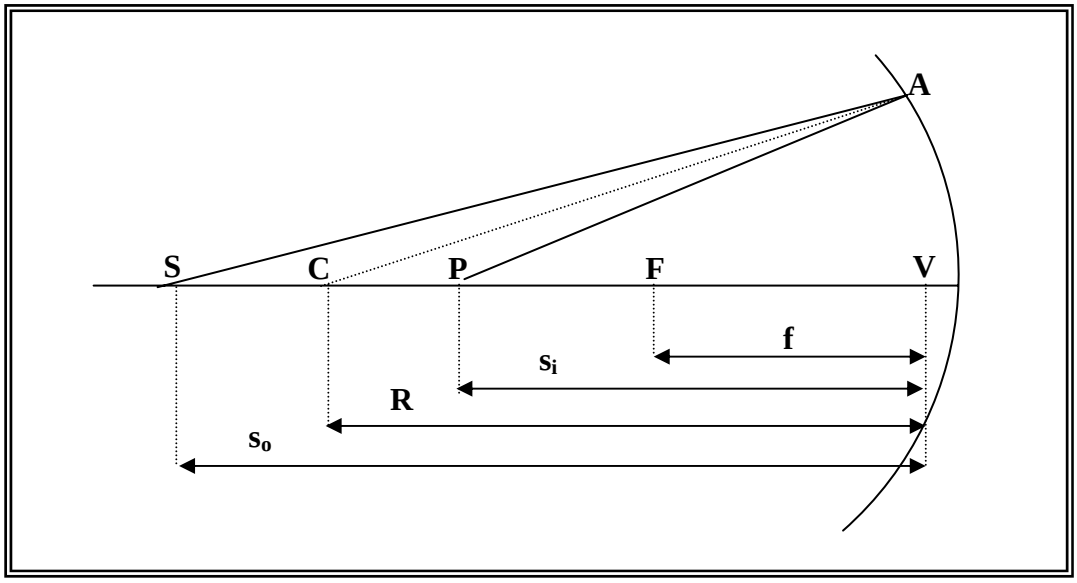

Figure 3.1: Physical parameters of paraxial ray.

$$\frac{SC}{SA} = \frac{CP}{PA} \tag{3.1}$$

Furthermore,

$$SC = s_o - |R| \quad \text{and} \quad CP = |R| - s_i \tag{3.2}$$

where s_o and s_i are on the left and therefore positive. If we use the same sign convention for R as we did when we dealt with refraction, it will be negative because C is to the left of V i.e. the surface is concave. Thus

$$|R| = -R \tag{3.3}$$

and

$$SC = s_o + R \quad \text{while} \quad CP = -(s_i + R) \tag{3.4}$$

In the paraxial region $SA \approx s_o$, $PA \approx s_i$ and equation (3.1) becomes

$$\frac{s_o + R}{s_o} = -\frac{s_i + R}{s_i} \tag{3.5}$$

$$\frac{1}{s_o} + \frac{1}{s_i} = -\frac{2}{R} \tag{3.6}$$

which is often referred to as mirror formula. It is equally applicable to concave ($R < 0$) or convex ($R > 0$) mirrors. The primary or object focus is defined by:

$$\lim_{s_i \to \infty} s_o = f_o \tag{3.7}$$

While the secondary or image focus correspond to

$$\lim_{s_o \to \infty} s_i = f_i \tag{3.8}$$

Consequently, from equation (3.6) one can get:

$$\frac{1}{f_o} + \frac{1}{\infty} = \frac{1}{\infty} + \frac{1}{f_i} = -\frac{2}{R} \tag{3.9}$$

so, $f_o = f_I = -R/2$. Thus, dropping the subscripts on the focal length, we have

$$\frac{1}{s_o} + \frac{1}{s_i} = \frac{1}{f} \tag{3.10}$$

The Cassegrainian system shown in figure 3.2 uses a convex secondary mirror placed inside the prime focus, it redirects the rays to the

primary mirror to a new focus [**Hudson 1969**]. The cassegrainian system utilized a convex hyperbola secondary mirror to increase the effective focal length. It functions as if the primary wave of the same aperture but had a larger focal length or radius of curvature.

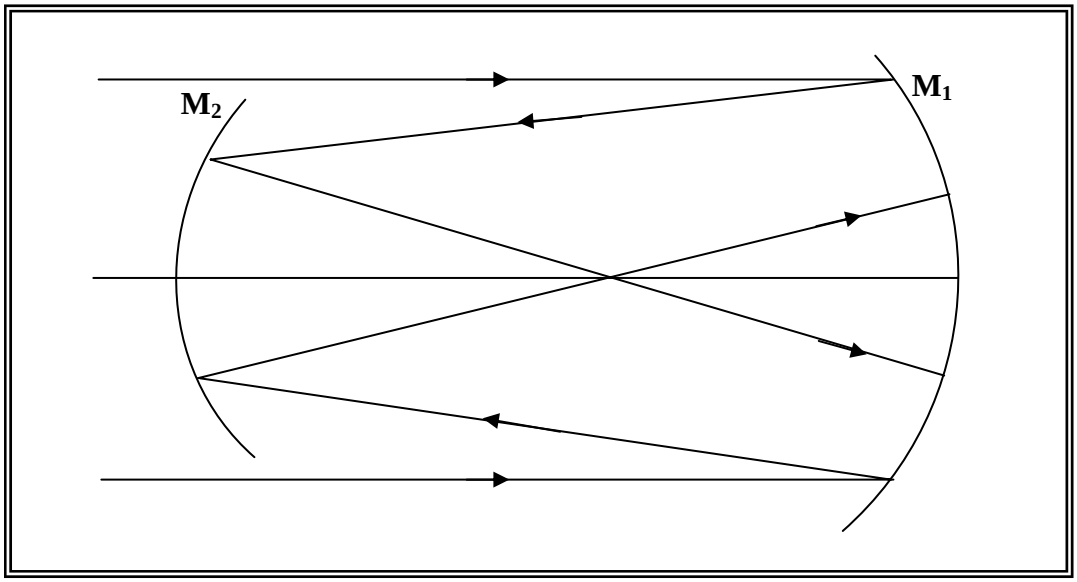

Figure 3.2: Cassegrainian mirrors.

3.3 Paraxial Ray Tracing

Assume a ray of light leaving an object point and striking the lens, the ray refracted at the first surface, translated to the second surface, and then refracted at the second surface as shown in figure 3.3. The behavior of the ray can be described quantitatively in the following ways:

First refraction

At point P_1, if all the angles are small then Snell's law is activated. The Snell's law angles are not convenient. One can eliminate them using the following identities

$$\theta_1 = \alpha_1 + \phi \text{, and } \theta_1^{'} = \alpha_1^{'} + \phi \qquad (3.11)$$

where α_1 is the angle that the incident ray makes with the axis OZ, α_2 is the corresponding angle for the refracted ray, and ϕ is the angle that the radius r_1 of the lens surface makes at the center of curvature C.

$$\sin\phi = \frac{x_1}{r_1} \tag{3.12}$$

but the paraxial approximation can be used to simplify equation (3.12) as follows

$$\phi = \frac{x_1}{r_1} \tag{3.13}$$

substituting equation (3.11) and (3.13) into Snall's law the result can be written as

$$n_1'\alpha_1' = \frac{n_1 - n_1'}{r_1} x_1 + n_1\alpha_1 \tag{3.14}$$

$$n_1'\alpha_1' = n_1\alpha_1 - x_1 k_1 \tag{3.15}$$

and $$x_1 = x_1' \tag{3.16}$$

where the constant k_1 is called the refracting power of the first surface and is defend as

$$k_1 = \frac{n_1' - n_1}{r_1} \tag{3.17}$$

equation (3.17) may also written as

$$k_1 = c_1(n_1' - n_1) \tag{3.18}$$

Translation

When the ray is travels from the first surface into second one. As it goes from P_1 to P_2, its distance from the axis becomes

$$x_2 = x_1' + t_1' \tan\alpha_1' \tag{3.19}$$

by using the paraxial approximation for small angles

$$x_2 = x_1' + t_1'\alpha_1' \tag{3.20}$$

where t_1' is the distance between the lens vertices V_1 and V_2 .(lens thickness).

$$\alpha_2 = \alpha_1' \tag{3.21}$$

equations (3.20) and (3.21) give the location and slope of the ray that strikes second surface after a refraction and translation.

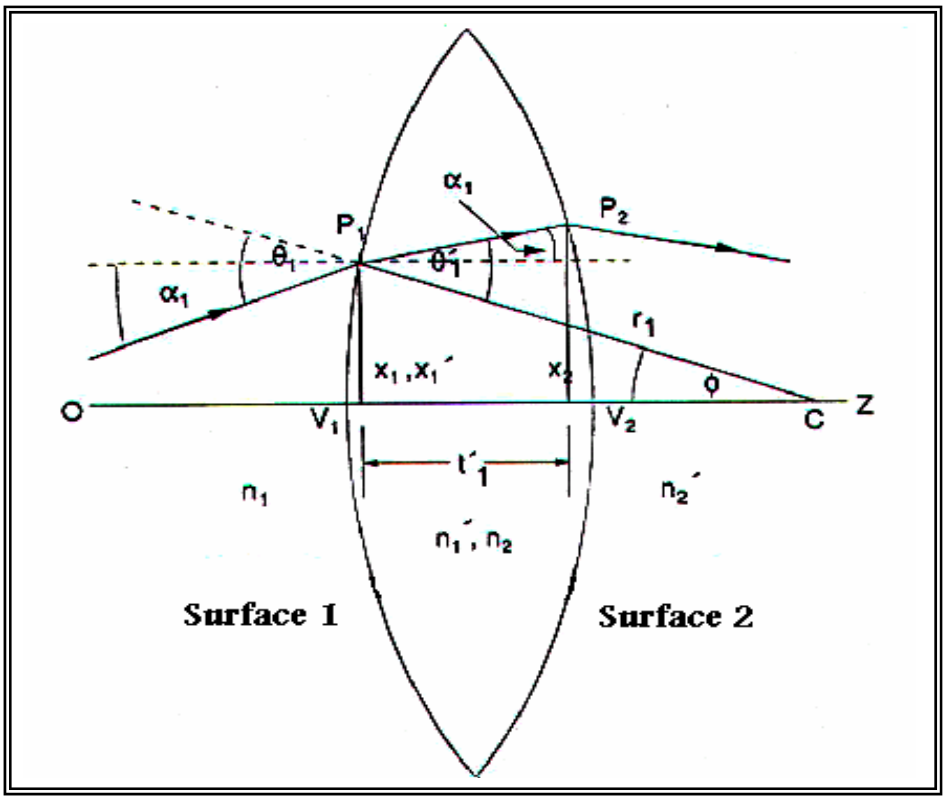

Figure 3.3: Ray tracing through a lens.

Second refraction

To continue the ray trace at this surface, another refraction equation are introduced by expressing k_2 in terms of two indices at this surface and the radius

$$n_2'\alpha_2' = n_1'\alpha_2 - x_2 k_2 \qquad (3.22)$$

and $$x_2' = x_2 \qquad (3.23)$$

This process can obviously be applied to any number of refracting or reflection surfaces within the limits of the paraxial approximation for a symmetrical optical system with an arbitrary number of components [**Nussbaum 1998**].

3.4 Optical Path Length (OPL)

The Fermat's principle states that "The path actually taken by ray ingoing from any point to another is the shortest optical path length" as shown in figure 3.4.

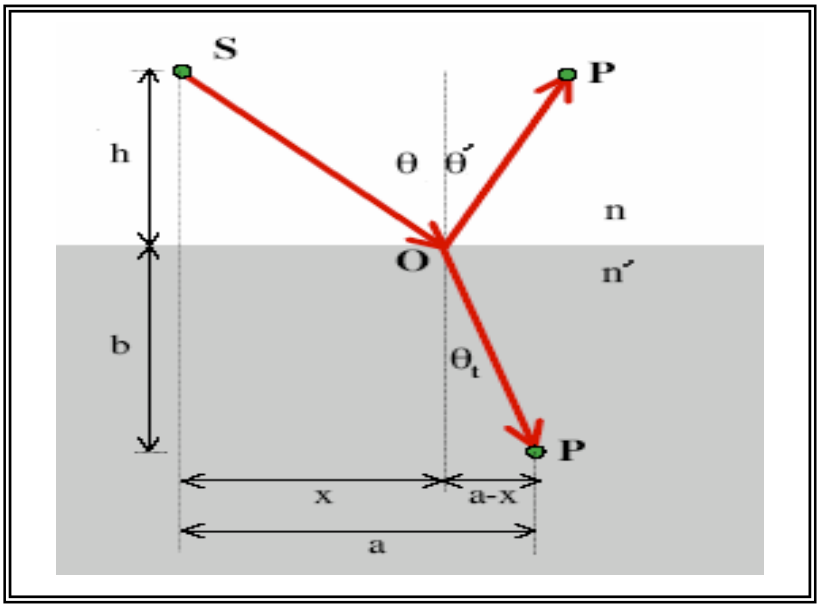

Figure 3.4: Fermat's principle.

Therefore, the optical path length OPL is given as

$$OPL = n.\overline{SO} + n'.\overline{OP} \tag{3.24}$$

$$= n.\sqrt{h^2 + x^2} + n'.\sqrt{b^2 + (a-x)^2} \tag{3.25}$$

minimize OPL has $\frac{dOPL}{dx} = 0$

then $$n.\frac{x}{\sqrt{h^2 + x^2}} + n'.\frac{-(a-x)}{\sqrt{b^2 + (a-x)^2}} = 0 \tag{3.26}$$

or $$\frac{n}{n'} = \frac{\sin\theta}{\sin\theta'} \tag{3.27}$$

Equation (3.27) represents Snell's law that related the refractive indices $(n \text{ and } n')$ of the two compound mediums with angles of the incidence (θ) and refraction (θ'), when the rays pass through the

interface of them. Mathematically $\sin\theta$ can be expressed by a Taylor's series

$$\sin\theta = \theta - \frac{\theta^3}{3!} + \frac{\theta^5}{5!} - \cdots \tag{3.28}$$

For small value of θ, only the first term is need to be used $(\sin\theta \approx \theta)$. This approach is called a paraxial approximation of ray tracing (first order optics) that lead to the paraxial form of Snell's law as follows

$$n\theta = n'\theta' \tag{3.29}$$

In first order optics, the merging wave from segment corresponding to these paraxial ray's is essentially spherical and will form a perfect image at point P as shown in figure 3.5. Therefore, the lens maker's formula can be driven using the optical path determination shown in figure 3.6 as follows [**Yoo 2005**]

$$\frac{nr(s_o + r)\sin\theta}{P_o} = \frac{n'r(s_i - r)\sin\theta}{P_i} \tag{3.30}$$

where P_o is the distance of incident rays between object and surface of lens, P_i is the distance of reflected rays between image and lens, s_o is the distance between object and surface of lens, s_i is the distance between image and surface of lens, r is the radius of curvature, n, n` are the refractive indices of air and medium respectively, and θ is the angle between incident rays and normal ray to the surface which pass through to the center of curvature. By using the paraxial approximation, one can find the lens maker's formula as follows

$$\frac{n}{s_o} + \frac{n'}{s_i} = \frac{n'-n}{r} \tag{3.31}$$

While, in the third order optics, the paraxial approximation is somewhat unsatisfactory if rays from marginal rim of a lens are considered.

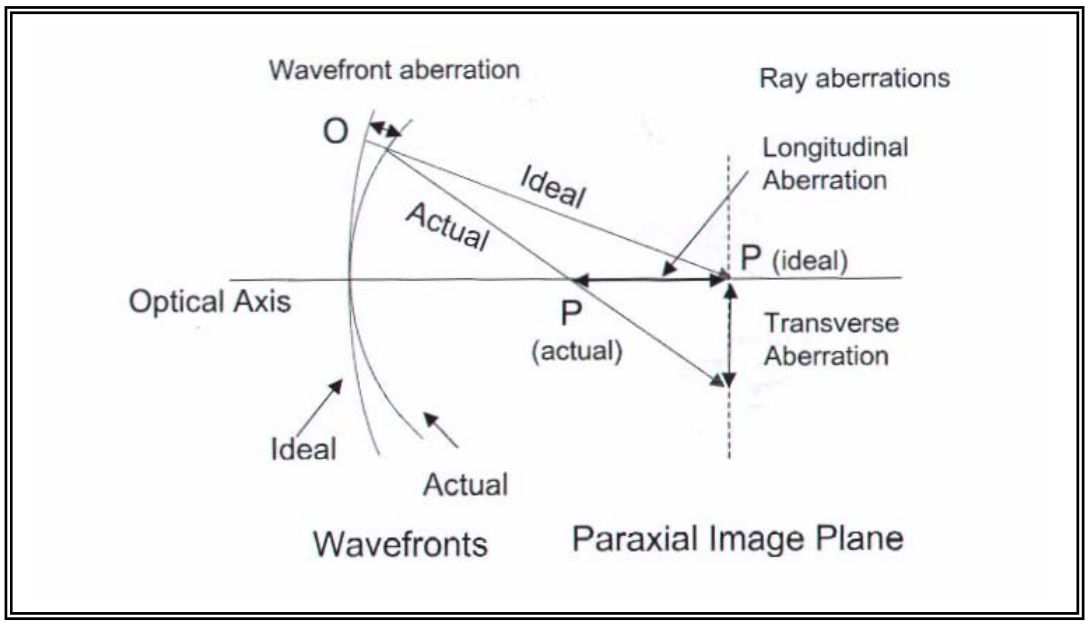

Figure 3.5: Ideal and actual wavefronts.

3.5 Optical System Aberrations

In this case the maker's lens formula will contains another term related by the aberration due to including the marginal rays beside the paraxial ray. If considering two wavefront leaving an optical system as shown in figure 3.6 as in the following:

$$n.\overline{SO} + n'.\overline{OP} = n.s_o + n'.s_i \tag{3.32}$$

If one define the aberration for a certain point on the lens as

$$\Delta W = n.\overline{SO} + n'.\overline{OP} - (ns_o + n's_i) \tag{3.33}$$

from the figure 3.6 and by using the law of cosine

so
$$\overline{SO}^{\,2} = (s_o + r)^2 + r^2 - 2(s_o + r)r\cos\theta \tag{3.34}$$

$$\overline{OP}^{\,2} = (s_i - r)^2 + r^2 - 2(s_i - r)r\cos(\pi - \theta) \tag{3.35}$$

substituting equations (3.34) and (3.35) into equation (3.24), then the OPL can be determined:

$$\begin{aligned} OPL = {} & n[(s_o + r)^2 + r^2 - 2(s_o + r)r\cos\theta]^{1/2} \\ & + n'[(s_i - r)^2 + r^2 - 2(s_i - r)r\cos(\pi - \theta)]^{1/2} \end{aligned} \tag{3.36}$$

Beyond the paraxial approximation, keeping terms to fourth order in θ

$$\sin\theta \approx \theta - \frac{\theta^3}{3!} \text{ and } \cos\theta \approx 1 - \frac{\theta^2}{2!} + \frac{\theta^4}{4!} \tag{3.37}$$

Recognizing that $\theta = \frac{h}{r}$, where *h* is the height above the optical axis then

$$\begin{aligned} \overline{SO}^{\,2} &= (s_o + r)^2 + r^2 - 2(s_o + r)r[1 - \frac{h^2}{2r^2} + \frac{h^4}{24r^4}] \\ &= s_o^2 + \frac{h^2(r + s_o)}{r} - \frac{h^4(r + s_o)}{12r^3} \end{aligned} \tag{3.38}$$

$$\begin{aligned} \overline{OP}^{\,2} &= (s_i - r)^2 + r^2 - 2(s_i - r)r[1 - \frac{h^2}{2r^2} + \frac{h^4}{24r^4}] \\ &= s_i^2 + \frac{h^2(r - s_i)}{r} - \frac{h^4(r - s_i)}{12r^3} \end{aligned} \tag{3.39}$$

$$\overline{SO} = s_o\left[1 + \frac{h^2(r + s_o)}{s_o^2 r} - \frac{h^4(r + s_o)}{12s_o^2 r^3}\right]^{1/2} \tag{3.40}$$

$$\overline{OP} = s_i\left[1 + \frac{h^2(r - s_i)}{s_i^2 r} - \frac{h^4(r - s_i)}{12s_i^2 r^3}\right]^{1/2} \tag{3.41}$$

if h^2=0 then a paraxial approximation is occur, for h^2<<1 the term in parentheses is small and can be substituted using Binomial expansion as follows

$$[1 + x]^{1/2} \approx 1 + \frac{x}{2} - \frac{x^2}{8} + \cdots \tag{3.42}$$

keeping terms h^4 only

$$\overline{SO} = s_o\left[1 + \frac{h^2(r + s_o)}{2s_o^2 r} - \frac{h^4(r + s_o)}{24s_o^2 r^3} - \frac{h^4(r + s_o)^2}{8s_o^4 r^2}\right]^{1/2} \tag{3.43}$$

$$\overline{OP} = s_i\left[1 + \frac{h^2(r - s_i)}{2s_i^2 r} - \frac{h^4(r - s_i)}{24s_i^2 r^3} - \frac{h^4(r - s_i)^2}{8s_i^4 r^2}\right]^{1/2} \tag{3.44}$$

substitute $\overline{SO}$ and $\overline{OP}$ in equation (3.32) obtained

$$\begin{aligned} \Delta W = {} & \frac{h^2}{2}\left[\frac{n}{2s_o}\left(\frac{1}{s_o} + \frac{1}{r}\right)^2 + \frac{n'}{2s_i}\left(\frac{1}{r} - \frac{1}{s_i}\right)^2\right] \\ & - \frac{h^4}{8}\left[\frac{n}{s_o}\left(\frac{1}{s_o} + \frac{1}{r}\right)^2 + \frac{n'}{s_i}\left(\frac{1}{r} - \frac{1}{s_i}\right)^2\right] \end{aligned} \tag{3.45}$$

$$\Delta W = \frac{h^2}{4}\left[\frac{n}{s_o}\left(\frac{1}{s_o}+\frac{1}{r}\right)^2 + \frac{n'}{s_i}\left(\frac{1}{r}-\frac{1}{s_i}\right)^2\right] - \frac{h^4}{8}\left[\frac{n}{s_o}\left(\frac{1}{s_o}+\frac{1}{r}\right)^2 + \frac{n'}{s_i}\left(\frac{1}{r}-\frac{1}{s_i}\right)^2\right] \quad (3.46)$$

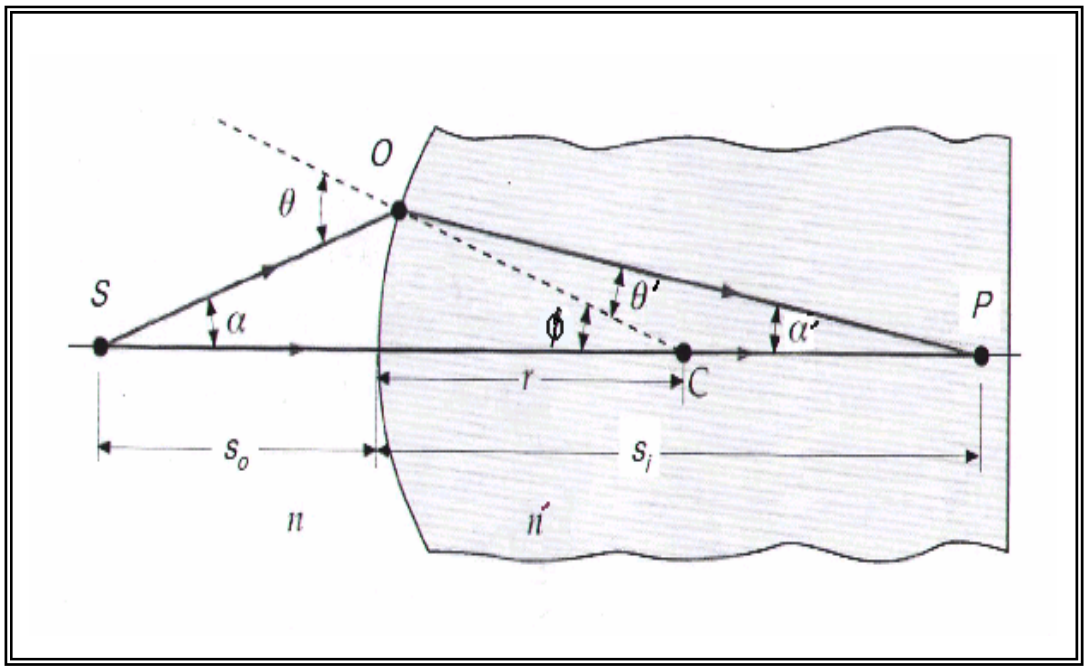

Figure 3.6: Optical system of two wavefronts.

Aberration like coma, astigmatism, and field curvature are called field aberration or ***off-axis*** because they vary with field of angle, and vary according to some power of the angle of the incident ray with respect to the optical axis. For a particular optical system, their magnitude depends on the optical design. While the spherical and distortion aberrations have a magnitude is constant over the field, so they called ***on-axis***. These aberrations have the same form as off-axis except that they do not depend on the field angle. The aberrations are measured in the transfer pupil. If the wavefront were unaberrated, one would obtain a perfect image of spot. In the presence of aberrations, individual spot are deviated. By fitting a mathematical function to these deviations (in the terms of the

Zernike polynomials), the coefficients of the aberrations are obtained **[Spot Optics 2006]**.

A particular image point is specified by giving the paraxial image coordinates (x_o,y_o) as shown in figure 3.7. The wavefront can be expanded as a power series in the four variables (x,y) (the exit pupil coordinates) and (x_o,y_o) (the coordinates of the image point).

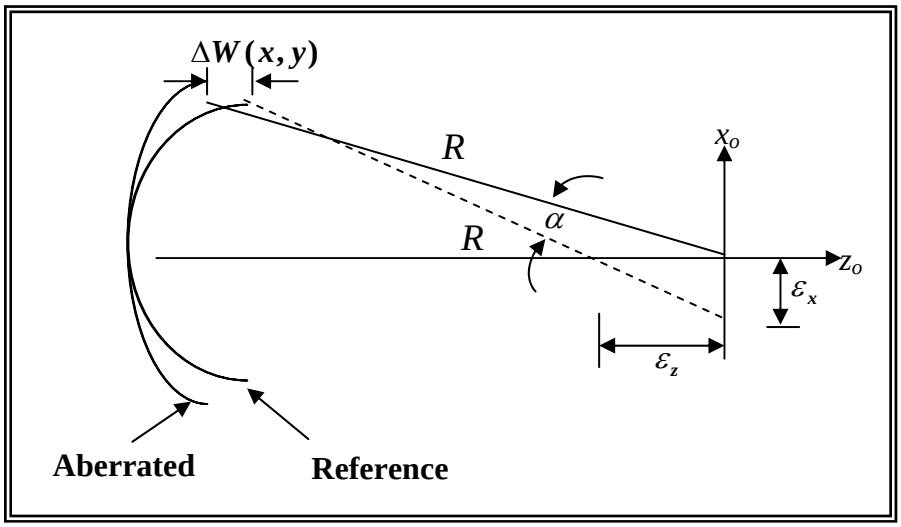

Figure 3.7: Transverse (ε_x) and longitudinal (ε_z) aberrations.

Due to the rotational symmetry, the wavefront distribution W must not change if there is a rigid rotation of the x_o,y_o and x,y axes about the z axis. It is possible to select the coordinates system such that the image point lies in the plane containing the x and z axes , is identically equal to zero. Hence, W can be expanded as

$$\begin{aligned} W(x,y,x_o) &\equiv W(x^2+y^2, xx_0, x_o^2) \\ &= a_1(x^2+y^2) + a_2 x x_o + a_3 x_o^2 \\ &+ b_1(x^2+y^2)^2 + b_2 x x_o(x^2+y^2) + b_3 x_o^2 x^2 + b_4 x_o^2(x^2+y^2) \\ &+ b_5 x x_o^3 + b_6 x_o^4 + \ldots + \textit{fifth and hight order terms.} \end{aligned} \tag{3.47}$$

The first term of equation (3.47) represents what is commonly called defocus, which is a longitudinal shift of the center of the reference

sphere, while the second term is the transverse shift of the center of the reference sphere, which called tilt. The third term gives rise to a phase shift that is constant across the exit pupil. When considering monochromatic light, these three terms normally have coefficients equal to zero. The six terms coefficients b_1 to b_6 are of third degree aberrations. The five first third-order are often called Seidel aberration **[Wyant and Creath 1992].** The exit pupil coordinates can be expressed in polar coordinates, as

$$x = h\cos\beta \tag{3.48}$$

and,

$$y = h\sin\beta \tag{3.49}$$

the radial coordinate ρ is usually normalized so that it is equal to 1 at the edge of the exit pupil (note that the height h of every point in the marginal plane is equal to the distance toward the optical axis ρ) . Using polar coordinates, the wavefront expansion of equation (3.47) can be written in terms of wavefront aberration coefficients C_{imn} as follows;

$$\begin{aligned} W(x_o,\rho,\beta) &= \sum_{j,m,n} C_{klm} x_o^k l\cos^m\beta \qquad \text{with } k = 2j+m, l = 2n+m \\ &= C_{200}x_o^2 + C_{111}x_o\rho\cos\beta + C_{020}\rho^2 \\ &+ C_{040}\rho^4 + C_{131}x_o\rho^3\cos\beta + C_{222}x_o^2\rho^2\cos^2\beta \\ &+ C_{220}x_o^2\rho^2 + C_{311}x_o^3\cos\beta. \end{aligned} \tag{3.50}$$

Or Siedel aberration coefficients S

$$\begin{aligned} W(x_o,\rho,\beta) &= \frac{1}{8}S_I\rho^4 + \frac{1}{2}S_{II}x_o\rho^3\cos\beta + \frac{1}{2}S_{III}x_o^2\rho^2\cos^2\beta \\ &+ \frac{1}{4}(S_{III}+S_{IV})x_o^2\rho^2 + \frac{1}{2}S_V x_o^3\cos\beta. \end{aligned} \tag{3.51}$$

The names of the wavefront aberration coefficients and their names are given in table 3.1, while figure 3.8 shows the departure of the wavefront ΔW due to the five Seidel aberrations from an ideal spherical wavefront form [**Wyant and Creath 1992**].

Table 3.1 Wavefront and Siedel aberration coefficients.

Wavefront aberration coefficient	**Name**	**Siedel aberration coefficients**	**Function of**
C_{200}	Piston		
C_{111}	Tilt		
C_{020}	Defocus		
C_{040}	Spherical	$\frac{1}{8}S_I$	ρ^4
C_{131}	Coma	$\frac{1}{2}S_{II}$	$x_o\rho^3\cos\beta$
C_{222}	Astigmatism	$\frac{1}{2}S_{III}$	$x_o^2\rho^2\cos^2\beta$
C_{220}	Field curvature	$\frac{1}{4}(S_{III}+S_{IV})$	$x_o^2\rho^2$
C_{311}	Distortion	$\frac{1}{2}S_V$	$x_o^3\rho\cos\beta$

From the binomial expansion, the wavefront contains a spherical aberration and an associated defocusing is given as;

$$\Delta W = C_{020}\rho^2 + C_{040}\rho^4 \tag{3.52}$$

Compare equation (3.49) with (3.50), the coefficients of defocusing and spherical aberration will be given as;

$$C_{020} = \frac{1}{4}\left[\frac{n}{s_o}\left(\frac{1}{s_o}+\frac{1}{r}\right)^2 + \frac{n'}{s_i}\left(\frac{1}{r}-\frac{1}{s_i}\right)^2\right] \tag{3.53}$$

$$C_{040} = \frac{1}{8}\left[\frac{n}{s_o}\left(\frac{1}{s_o}+\frac{1}{r}\right)^2 + \frac{n'}{s_i}\left(\frac{1}{r}-\frac{1}{s_i}\right)^2\right]$$

The ray from an axial point that makes an appreciable angle with the axis will intersect the axis in front or behind the Gaussian focus. The point at which the rays from the region near the center of the aperture

(paraxial rays) intersect the axis is called the paraxial or Gaussian focus. The point at which the rays from the edge of the aperture (marginal rays) intersect the axis is called the marginal focus as shown in figure 3.7.The normalized coordinate components of the spherical aberration are

$$\varepsilon_x = -\frac{4RC_{040}}{d_o} x(x^2 + y^2) \tag{3.54}$$

and $$\varepsilon_y = -\frac{4RC_{040}}{d_o} y(x^2 + y^2) \tag{3.55}$$

where d_o is again the geometrical pupil radius. Since the aberration is symmetrical about the principal ray, the transverse aberration due to third-order spherical aberration can be written as

$$\varepsilon_x = \varepsilon_y = -\frac{4RC_{040}}{d_o} \rho^3 \tag{3.56}$$

The wavefront aberration with respect to the new reference sphere is

$$\Delta W = C_{040}\rho^4 + \frac{\varepsilon_z d_o^2}{2R^2}\rho^2 \tag{3.57}$$

then $$\varepsilon_x = \varepsilon_y = -\frac{4RC_{040}\rho^3}{d_o} - \frac{\varepsilon_z d_o \rho}{R} \tag{3.58}$$

As the image plane is shifted, there is a position for which the circular image is a minimum; this minimal image is called the circle of least confusion. As shown in figure 3.9, this image position corresponds to the position where the ray from the rim of the pupil (marginal ray) meets the caustic. It can be shown that the image position for the circle of least confusion occurs three-quarters of the way from the paraxial focus to the marginal focus, and hence its radius, RC_{040}/d_o, one-quarter the radius of the image at the paraxial focuses. Therefore, the resulting wavefront aberration is [**Wyant and Creath 1992**]

$$\Delta W = C_{040}(\rho^4 - 1.5\rho^2) \tag{3.59}$$

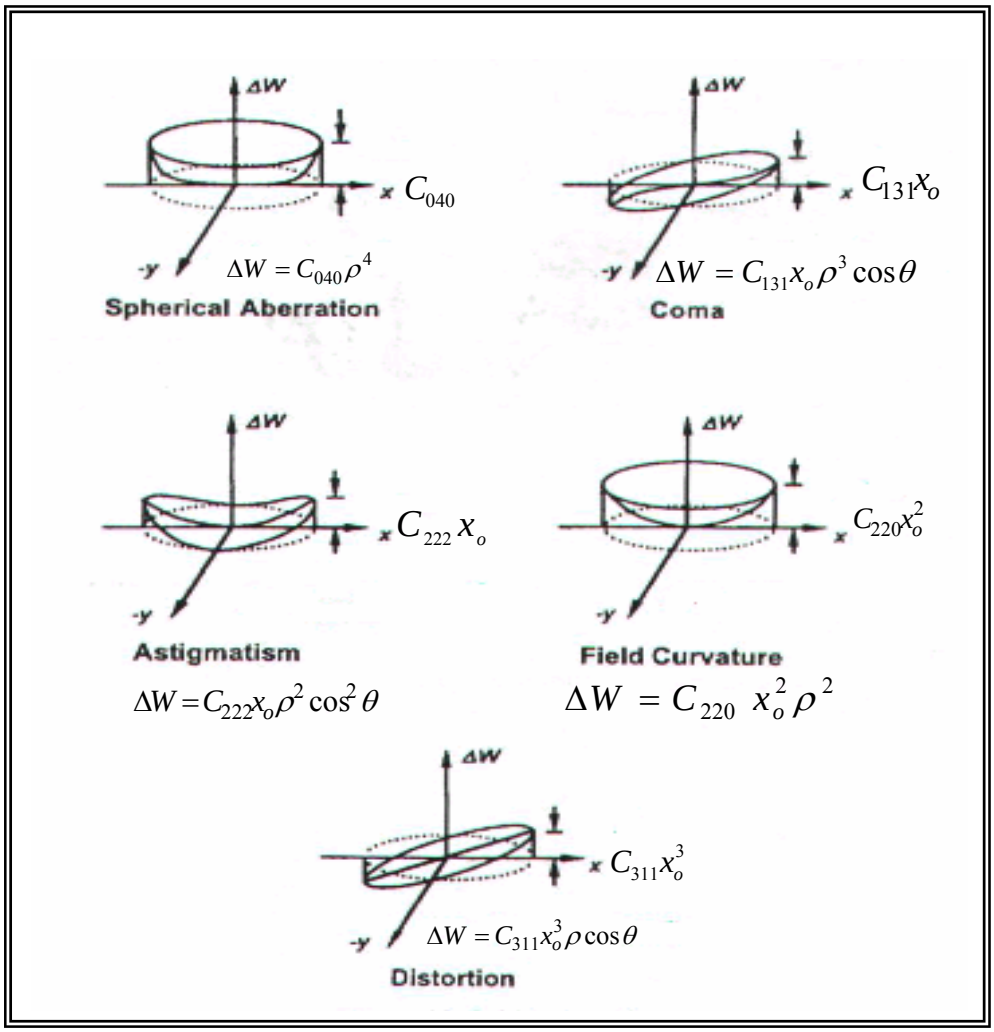

Figure 3.8:Wavefront aberrations **[Wyant and Creath 1992]**.

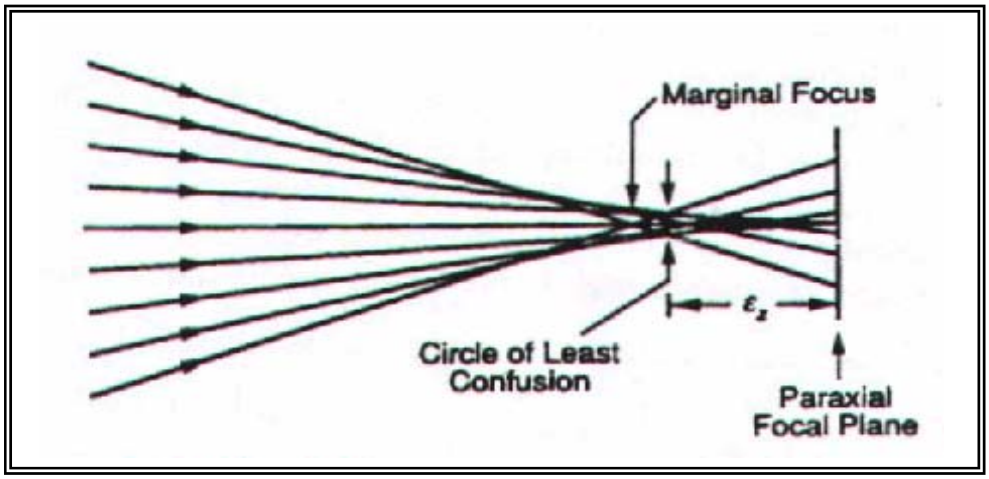

Figure 3.9: The circle of least confusion **[Wyant and Creath 1992]**.

3.6 Image Formation Model

Optical systems produce two effects on an image: projection and degradation due to the effects of diffraction and lens aberrations. Image formation model provide the tool that by which can improve image quality by correction the aberration. Physical optics describe the image degradation due to **(1)** the wave nature of light **(2)** the aberration of imperfectly designed and manufactured optical systems [**Weisstein 1999**].

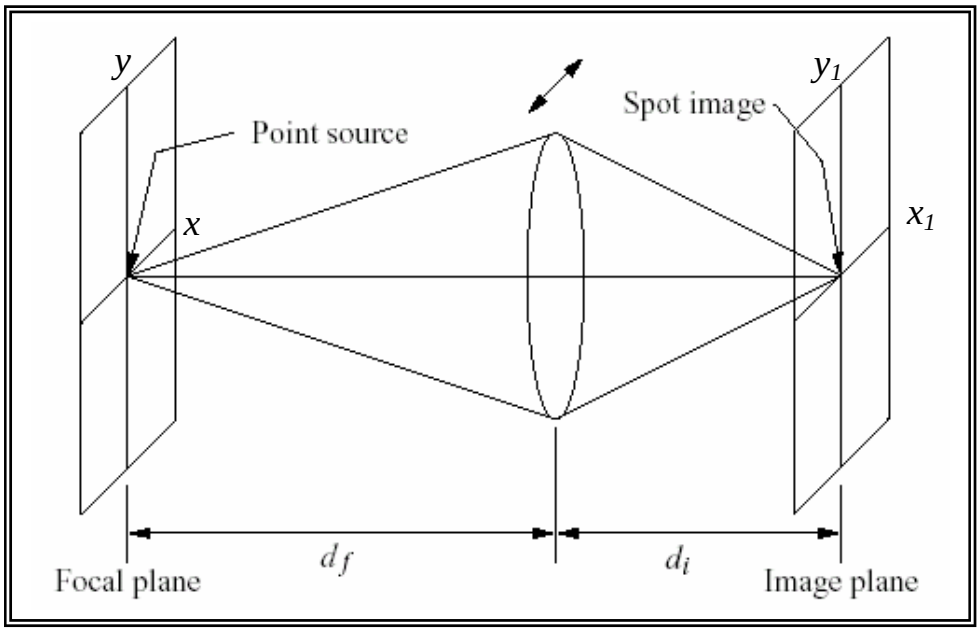

Figure 3.10: Simple optical system.

When an optical system produces an image using perfectly incoherent light, then the function that describes the intensity in the image plane produced by a point in the object plane is called ***point speared function*** (PSF). This function usually is written ***h(x,y;x1,y1)***. The input (object intensity pattern) and output (image intensity pattern) are shown in figure 3.10, they related by the simple convolution equation:

$$g(x,y) = f(x_1,y_1) \otimes h(x,y;x_1,y_1) \qquad (3.60)$$

this is more formally written as

$$g(x,y) = \iint f(x_1, y_1) h(x - x_1, y - y_1)\, dx_1\, dy_1 \qquad (3.61)$$

However, convolutions can be very computationally intensive. Fourier transform is used for solving this equation. A Fourier transforms converts information in the space domain into frequency domain, where it can be described as a linear combination of appropriately weighted sine and cosine. Convolution in the space domain with multiplications in the frequency domain as follows

$$G(u,v) = F(u,v) \cdot H(u,v) \qquad (3.62)$$

where u and v are frequency coordinates, $G(u,v)$, $F(u,v)$, and $H(u,v)$ are Fourier transforms of $g(x,y)$, $f(x_1,y_1)$, and $h(x,y;x_1,y_1)$ respectively. The function $H(u,v)$ is called the transfer function, and in the case of the optical systems, it is the optical transfer function or OTF. The OTF is a complex function, composed of real and imaginary parts:

$$OTF(u,v) = \left|H(u,v)\right| e^{i\Phi(u,v)} \qquad (3.63)$$

The real portion, or $\left|H(u,v)\right|$ is called the ***modulation transfer function*** (MTF), which is normalized to unity at zero spatial frequency, and the function $\Phi(u,v)$ is termed the ***phase transfer function*** (PTF). The PSF describes the image quality. These two functions are related by the ***pupil function*** (P) [**Optikos 1999**].

3.7 Pupil Function

The mathematical expression that describes an actual wavefront as it passes through the exit pupil is called a pupil function. When this function is expressed in normalized coordinates of a usual optical system

(both diffraction and aberration are exist), it is understood to have zero value outside the unit- radius circle.

$$\begin{aligned} &P(x,y) = P_o(x,y)e^{-iknW(x,y)} && when\,(x^2+y^2) \le 1 \\ &P(x,y) = 0 && otherwise \end{aligned} \qquad (3.64)$$

where *k* is the wave number, *n* is the refractive index, and *W(x,y)* is the wavefront aberration. For spherical aberration the rotationally symmetric pupil function is

$$P(x,y) = P_0 e^{-inkC_{040}\rho^4} \qquad (3.65)$$

If defocusing is included, then **[Wyant and Greath 1992**]

$$P(x,y) = P_0 e^{-ink(C_{040}\rho^4 + C_{020}\rho^2)} \qquad (3.66)$$

The perfect optical system (diffraction limited; no aberration) indicates that in such a system an incident diverging spherical wavefront of uniform amplitude is transformed into a converging spherical wavefront of uniform amplitude. When the system is a diffraction-limited system, the complex amplitude $P(x,y)$ is a real constant and the wave aberration function $W(x,y)$ is equal to zero [**Goodman 1996**].

$$\begin{aligned} &P(x,y) = P_o && when\,(x^2+y^2) \le 1 \\ &P(x,y) = 0 && otherwise \end{aligned} \qquad (3.67)$$

Analytically, one can conclude that the ideal optical system, the pupil function is real and represented by delta function distribution where the image of a point source is a point as shown in figure 3.7.

$$\begin{aligned} &P(x,y) = P_o && at\ the\ center \\ &P(x,y) = 0 && otherwise \end{aligned} \qquad (3.68)$$

The amplitude function $P_o(x,y)$ of the pupil function is extremely difficult to measure. The typical variations in the amplitude have far less

effect on the image than the typical variations in phase, which is contained in the wave aberration function $W(x,y)$. The phase characteristics can quit conveniently be measured interferometrically. So, the amplitude of the pupil function is assumed constant, and all aberration effects can be attributed to the wave aberration function [**Williams and Becklund 1989**].

3.8 Point Spread Function

Geometrical optics in the paraxial approximation predicts that the image of a point produced by an image forming optical system is a point, such system is ideal and the point separation represented by delta function as shown in figure 3.11-a. Thus, PSF for a normalized illumination given as follows

$$\begin{aligned} PSF &= 1 \qquad \textit{at the center} \\ PSF &= 0 \qquad \textit{otherwise} \end{aligned} \tag{3.69}$$

Actually, the image of a point produced by a real optical system is not a point but a small, blurred spot. This is due to diffraction and various forms of aberrations. The blurred spot image of a single point is called the point spread function PSF of the optical system [**Davidson 2006**]. For a lens with a circular aperture of diameter D_o, the PSF at usual case is the zero–order Bessel function (J_o)

$$PSF = \frac{p\pi}{\lambda^2 (f/no)^2} \left| \int_0^1 P(x,y)\, J_o\left[\left(\frac{\pi r}{\lambda (f/no)}\right).\rho \right] \rho \, d\rho \right|^2 \tag{3.70}$$

where

$$J_o(x) = \sum_{m=0}^{\infty} \frac{(-1)^m (x/2)^{2m}}{(m!)^2} \tag{3.71}$$

PSF of the diffraction pattern of a circular aperture having a rotationally symmetric pupil function $P(x,y)$ in the presence of aberration,

which is illuminated with uniform beam of total power *p* contained within the circular aperture.

In the perfect optical system, the PSF is the ***Airy disc***, which is the Fraunhofer diffraction pattern for a circular pupil (i.e. there are diffraction rings centered at the image plane) as shown in figure 3.11-b. The paragon of PSF ***(Airy pattern)***, which produced by a perfect optical system having a perfectly circular aperture stop is shown in figure 3.12 [**Williams and Becklund 1989**].

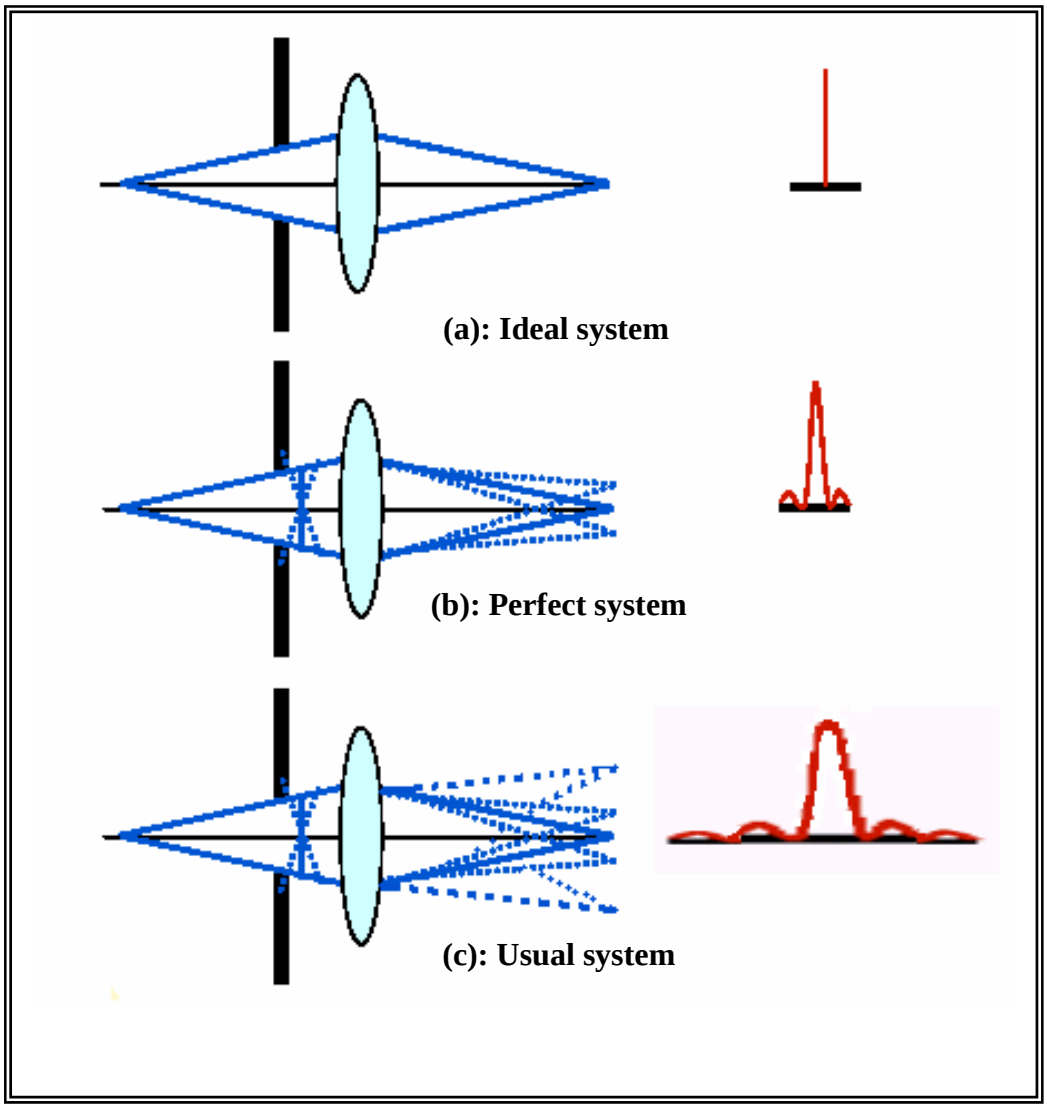

Figure 3.11: PSF of ideal, perfect, and usual systems.

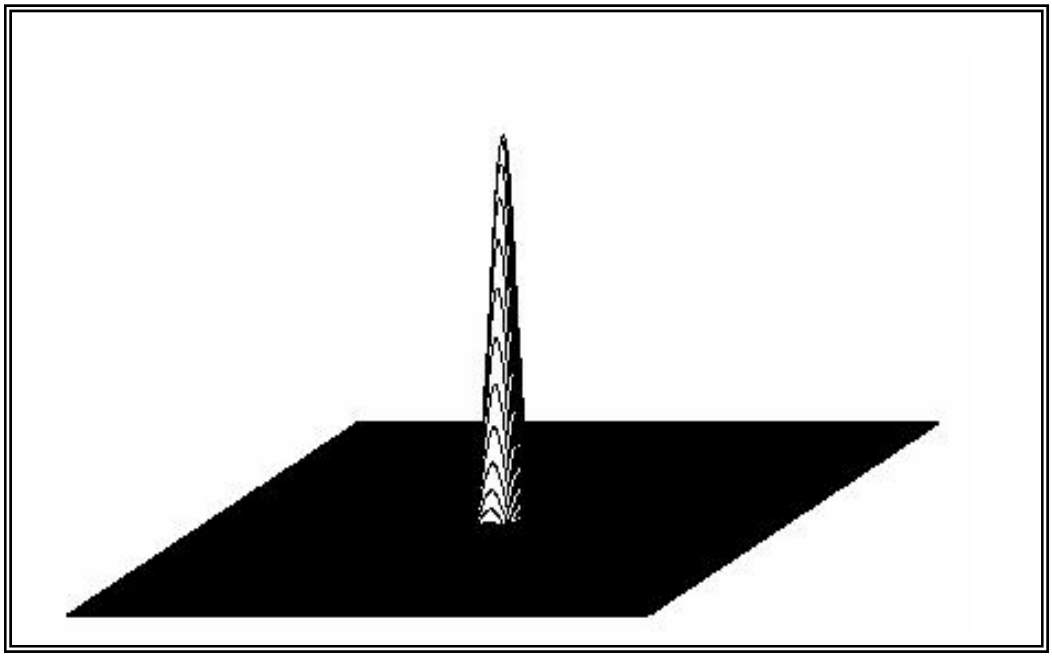

Figure 3.12: Paragon of a perfect PSF.

Using the Huygen's principle we can derive the PSF of an optical system. The pupil function takes a value of one inside the aperture and zero outside. If the illumination is incoherent and varies randomly from one point to another, then the system is linear in intensity and the PSF is the square modulus of $h(x,y)$. Thus the incoherent PSF is the power spectrum of the pupil function.

$$PSF = \left|h(x,y)\right|^2$$
$$PSF = \left|FT\{P(x,y,x_1,y_1)\}\right|^2 \qquad (3.72)$$

For a lens with a circular aperture in a narrow band incoherent light, the PSF is given by:

$$PSF = \frac{p\pi}{\lambda^2\left(f/no\right)^2}\left|\int_0^1 J_o\left[\left(\frac{\pi r}{\lambda(f/no)}\right).\rho\right]\rho\, d\rho\right|^2 \qquad (3.73)$$

where $r = \sqrt{x_1^2 + y_1^2}$ which is the radial distance measured from the optical axis in the image plane [**Weisstein 1999**].

In the usual optical system, both aberration and diffraction exist. Thus, due to the coalition effect of the diffraction and aberration, the separation of any point seems to be larger than that of a perfect, and the central spot will be surrounded by a plenty of a brighter rings as shown in figure 3.13-c.

Since an optical system can be completely described by either the PSF or the transfer function. A point source in the focal plane will produce an expanding spherical wave, part of which enters the lens. The refractive action of the lens slows and delays axial rays more near the center of the lens than the edge, converting the expanding spherical wave into another spherical wave converging toward the image point [**Weisstein 1999**]**.**

3.9 Spot Diagram

When a system of rays originally at a single object point is constructed, so that the rays are uniformly distributed over the entrance pupil, the plot of their consequent intersections with the image plane is called a ***spot diagram***. The size of spot diagram shows to extent of the energy distribution and the shape is due to the type of aberration. When the spot diagram has been reduced to a size comparable to that of the central fringes in a diffraction pattern, ray theory causes to be as useful as wave theory [**Williams and Becklund 1989**].

In the ideal optical system case where there are no diffraction and aberration, the image of the object is focused in one point, as shown in figure 3.13-a. This is an ideal case, which does not exist since it assumes that the optical system has no diffraction and aberration. Perfect optical system is practically diffraction limited when aberration does not exist.

In all cases of ideal, perfect and usual, the accumulation of the rays at the image plane follow ***Gaussian distribution*** taking into account the image point shift due to the diffraction and aberration. Thus, the image spot consists of rings surrounded the bright central spot as shown in figure 3.13-b and 3.13-c. The size of the spot depends on the amount of the aberration exists in the optical system.

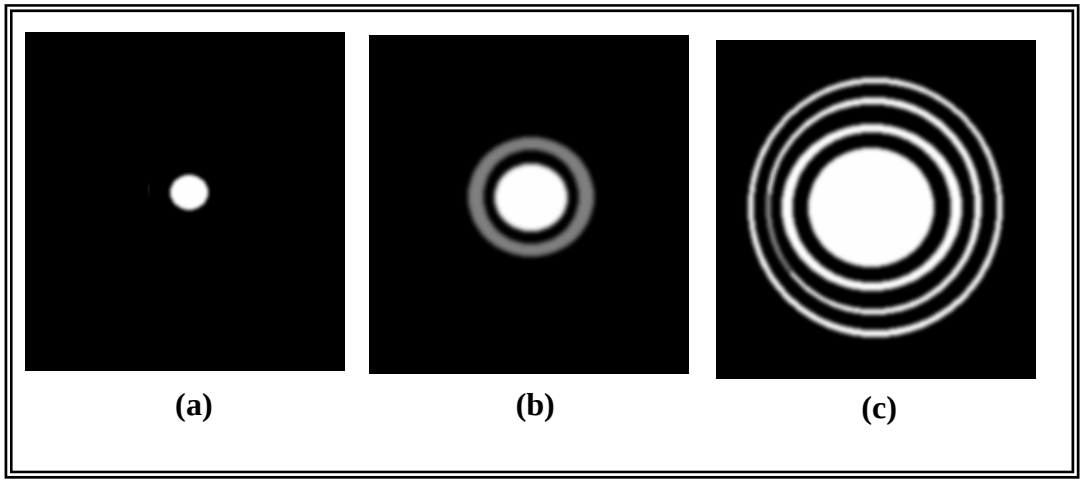

Figure 3.13: Spot distribution of ideal, perfect, and usual optical systems.

In general, the performance of a lens or lens system in a specific circumstance should be determined by the ray trace. The effect on the spot size caused by spherical aberration is strongly depending on *f*/no. The spot size caused by diffraction increases linearly with *f*/no, thus for some lens types, spot size at first decreases and then increases with *f*/no, meaning that there is some optimum performance point where both aberration and diffraction combine to form a minimum [**Fundamental Optics 2004**].

The spot size (Z) is an important parameter since it determines the optical system efficiency. Theoretically the following relationship gives the size of the spot formed by a single lens under diffraction limited

condition. The diameter of the first dark ring of the Airy rings is given by:

$$Z = 2.44\lambda(f / no) \tag{3.74}$$

$$f / no = \frac{f}{D_O} \tag{3.75}$$

where f is the effective focal length, and D_o is the diameter of the aperture. The effective diameter of the blur is one half of the above equation (3.74) in (μm).

If one deals with a usual optical system, some modifications should be imposed on equation (3.74) to correct the computed spot size formed by the optical system. The modification includes the addition of an spherical aberration term. Hence, the size of the spot formed by an optical system can be calculated from the following equation [**Scott 1959**].

$$Z_T = 2.44\lambda(f / no) + \frac{Af}{(f / no)^3} \tag{3.76}$$

where *A* is a constant given by the following expression [**Scott 1959**]

$$A = \frac{n+2}{n(n-1)^2} R^2 - \frac{4(n+1)}{n(n-1)} R + \frac{3n+2}{n} + \frac{n^2}{(n-1)^2} \tag{3.77}$$

and

$$R = \frac{r_2 + r_1}{r_2 - r_1} \tag{3.78}$$

where r_1, r_2 are the radii of the lens, and n being the refractive index of the last lens in the optical system. Figure 3.9 shows that the ray paths near the image plane of a system afflicted with third-order spherical aberration. It is apparent that the minimum diameter blur spot for this system occur at a point between the marginal focus and paraxial focus. This point three quarters of the way from the paraxial focus to the marginal focus and the diameter of spot can be determine geometrical due to spherical aberration by

$$Z = \frac{1}{2} \Delta W \tan\theta \tag{3.79}$$

ΔW can be given in equation (3.79), θ is the angle of the final slop of the marginal ray through the system [**Smith 1966**].

3.10 Depth of Focus

The concept of depth of focus rests on the assumption that for a given optical system, there exists a blur (due to defocusing) of small enough size such that it will not adversely affect the performance of the system. The depth of focus is the amount by which the image may be shifted longitudinally with respect to the some reference plane and introduced no more than the acceptable blur. The depth of field is the amount of which the object may be shifted before the acceptable blur is produced. The size of the acceptable blur may be specified as the linear diameter of the blur spot or as an angular blur, the angular subtense of the blur spot from the lens. Thus, the linear and angular blurs (Z and β) respectively and the distance *D* are related by

$$\beta = \frac{Z_T}{D} \tag{3.80}$$

For a system in air, where a primed symbol refer to the image size quantities. From the figure 3.14 it can be seen that the depth of field δ for a system with clear aperture *A* can be obtained from the relationship

$$\frac{\delta}{\beta(D \pm \delta)} = \frac{D}{A} \tag{3.81}$$

This expression can be solved for the depth of field, giving

$$\delta = \frac{D^2 \beta}{(A \pm D\beta)} \tag{3.82}$$

Note that the depth of field toward the optical system is smaller than that way from the system. When δ is small with respect to the distance *D*, this reduced to

$$\delta = \frac{D^2 \beta}{A} \tag{3.83}$$

For the image size, the relationship is

$$\delta' = \frac{D'^2 \beta}{A} = \frac{f^2 \beta}{A} = f\beta(f/no) \tag{3.84}$$

The depth of focus in term of linear blur spot size *B* can be obtained by substituting equation (3.83) into equation (3.84). Also, noted that the depth of field δ and depth of focus δ' are related by the longitudinal magnification of the system as follows [**Smith 1966**]

$$\delta' = m^2 \delta \tag{3.85}$$

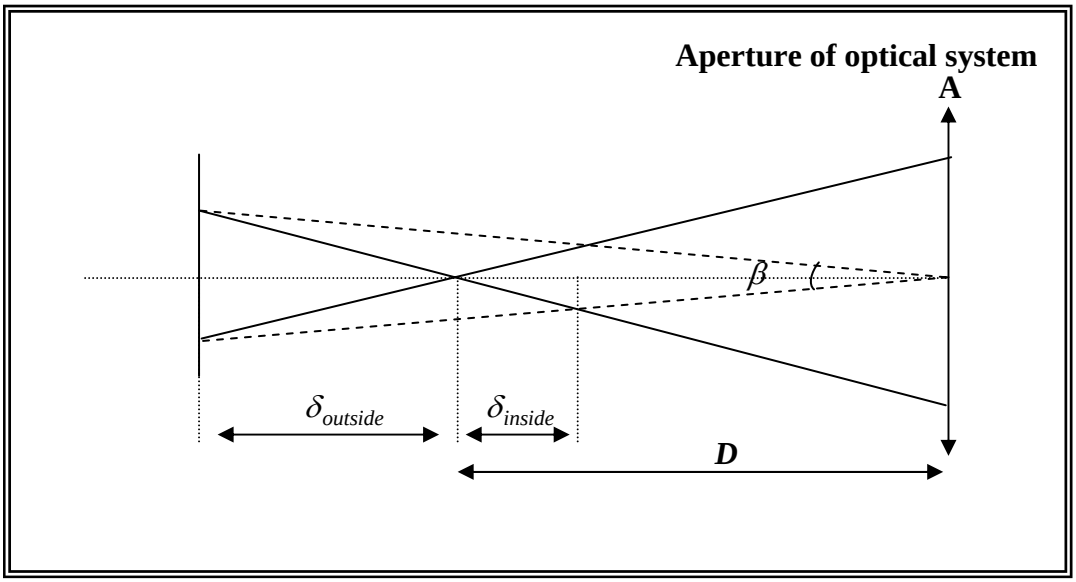

Figure 3.14: Depth of focus.

3.11 Optical Transfer Function (OTF)

OTF can be derived from the point spread function, which has been described as the image of an axial point object formed by diffraction limited system. When the pupil is circular, the calculation of OTF is not straightforward. The OTF will clearly be circularly symmetric, it suffices to calculate OTF along the positive f_x axis. As illustrated in figure 3.15, the area of the circular sector A+B [**Goodman 1996**].

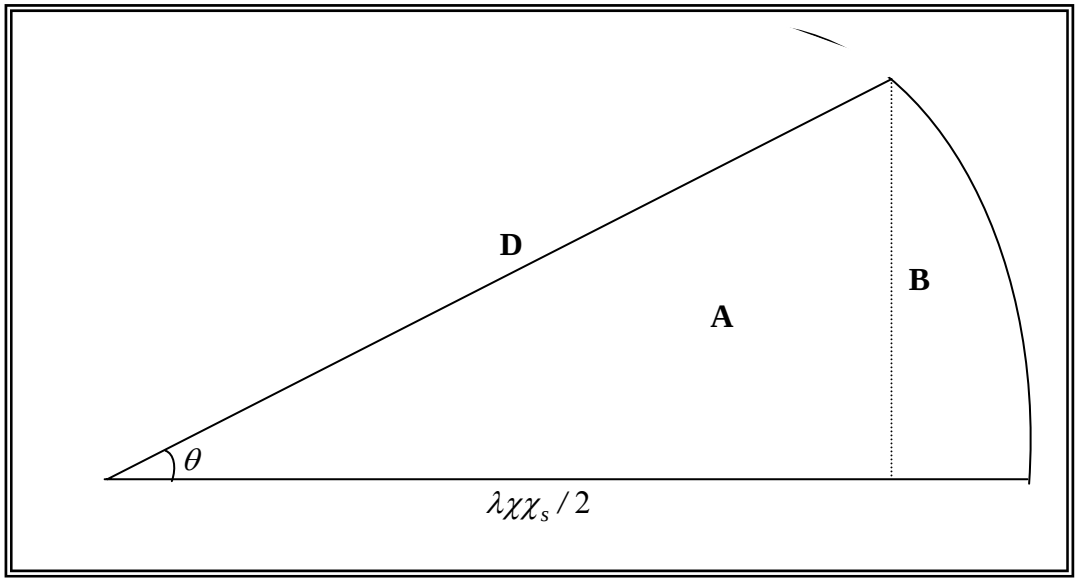

Figure 3.15: overlapped area of two MTF curves.

$$Area(A+B)=\left[\frac{\theta}{2\pi}\right]\pi D^2 \qquad (3.86)$$

$$Area(A+B)=\left[\frac{\arccos(\lambda\chi\chi_s/2D)}{2\pi}\right](\pi D^2) \qquad (3.87)$$

While the area of the triangle $A+B$ is

$$Area(A+B)=\frac{1}{2}(\frac{\lambda\chi\chi_s}{2})\sqrt{(D)^2-(\frac{\lambda\chi\chi_s}{2})^2} \qquad (3.88)$$

Finally, we have

$$OTF(\chi_s,0)=\frac{4[area(A+B)-area(A)]}{\pi D^2} \qquad (3.89)$$

or, for general radial distance f_s in the frequency plane, The relation by which, one can determine the perfect OTF is given as;

$$OTF(f_s)=\left[\frac{2}{\pi}\left(arccos\left(\frac{f_s}{f_c}\right)-\frac{f_s}{f_c}\right)\sqrt{1-\left(\frac{f_s}{f_c}\right)}\right] \qquad (3.90)$$

where f_s is the spatial frequency and $f_c=1/\lambda(f/no)$ which is the value of the cutoff frequency. Figure 3.16 shows the perfect OTF is a real function (phase=0) for a normalized spatial frequency range of $0\le f_s/f_c\le 1$ mm^{-1}. The OTF plot shows that every optical system

operates as a low-pass filter with a specific cutoff frequency**.** Therefore, any quantity directly derived from the nonzero frequency range has significance for a more general OTF than the value of the perfect OTF

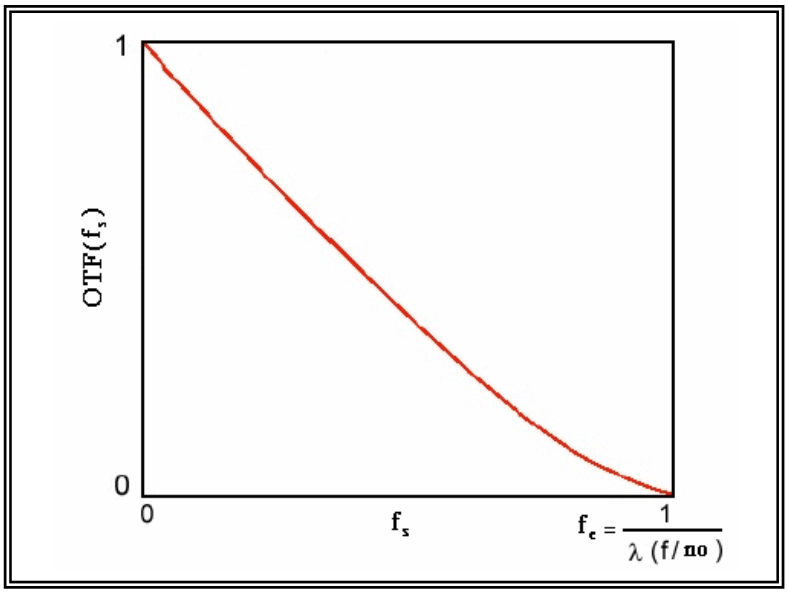

Figure 3.16: Perfect OTF.

In the usual optical system, the aberration described as a distortion in the wave emerging from the exit pupil. Therefore, the optical transfer function is given as [**Goodman 1996**];

$$OTF(f_s) = \iint_a \exp\left\{-ink\left[W(x+\frac{f_s}{2}, y) - W(x-\frac{f_s}{2}, y)\right]\right\} \text{dxdy} \qquad (3.91)$$

Simplification in the integrand can be achieved by defining an ***aberration difference function*** as follows:

$$\Delta W(x, y, f_s) = \frac{1}{f_s}\left[W(x+\frac{f_s}{2}, y) - W(x-\frac{f_s}{2}, y)\right] \qquad (3.92)$$

The wave aberration is a function of the coordinates x and y where the ray passes through the pupil sphere and the distance of object point. The defocusing and spherical aberration appears on the wavefront as a distortion affecting OTF by the wavefront function of equation (3.91).

Therefore, by substituting equation (3.92) into equation (3.91), the OTF relationship becomes;

$$OTF(f_s) = \iint_a \exp[-ink f_s \Delta W(x, y, f_s)]\,dxdy \qquad (3.93)$$

Equation (3.93) represents the OTF, which may leads to a spatial frequency dependent complex variable whose modulus is the MTF and whose phase describes the PTF. Thus the incoherent OTF is the power spectrum of the PSF.

$$OTF = \left|FT\{PSF\}\right|^2 \qquad (3.94)$$

3.12 Modulation Transfer Functions (MTF)

The resolution and performance of an optical system design can be characterized by MTF, which is a measurement of the system design ability to transfer contrast from the spatial domain into the frequency domain at a specific resolution. Computation of MTF is a mechanism that is often utilized by optical manufactures to incorporate resolution and contrast data into a single specification [**Davidson 2006**].

A type of target commonly used to test the performance of an optical system consist of a series of alternating light and dark bars of equal width, as indicate in figure 3.17-a. Several sets of patterns of different spacing are usually imaged by the system under test and finest set which the line structure can be discerned is considered to be limit of resolution of the system, when a pattern of this sort is imaged by an optical system, each geometric line (i.e. of infinitesimal width) in the object is imaged as a blurred line, whose cross section is the line spread function. Figure 3.17-b indicates a cross section of the brightness of the bar object. Figure 3.17-d show the effect of the image blurs on

progressively finer patterns. It is apparent that when the illumination contrast in the image is less than the smallest amount that the system can detect, the pattern can no larger be "resolved"[**Smith 1966**]. The amount of detail in an image is given by a resolution of the optical system, and is customarily specified in line pairs per millimeter. A line pair is one cycle of a light bar and dark bar of equal width and has a contrast of unity. Contrast is defined as

$$Contrast = \frac{I_{\max} - I_{\min}}{I_{\max} + I_{\min}} \tag{3.95}$$

where I_{max} is the maximum intensity produced by an image (white bar) and I_{min} is the minimum intensity (black bar). MTF is a plot of contrast, measured in percent, against spatial frequency measure in one pairs per millimeters. This graph is customarily normalized to a value of 1 at zero spatial frequency as shown in figure 3.17 [**Davidson 2006**].

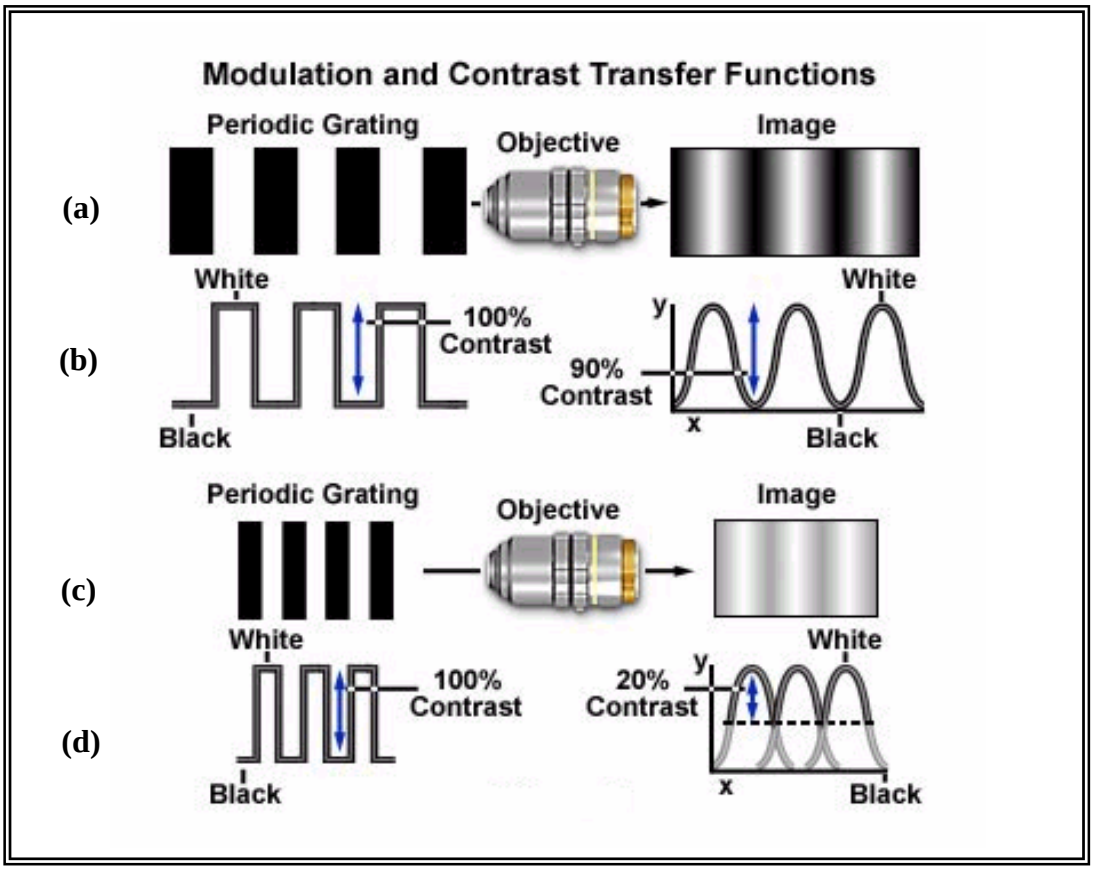

Figure 3.17: Modulation and Contrast transfer function [**Davidson 2006**]

A plot of MTF against frequency f_s as shown in figure 3.18 is thus almost universally applicable measure of the performance of an image forming system, and can be applied not only to lenses but film, image tube, and even complete system such as camera carrying aircraft.

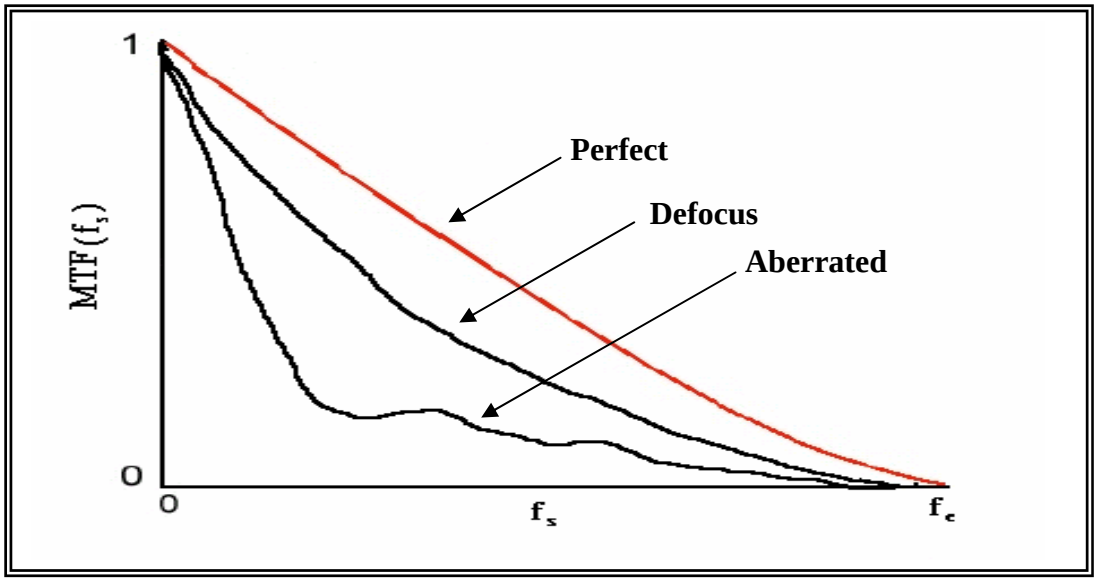

Figure 3.18: MTFs of perfect, defocus, and aberrated systems.

Chapter two

IR Homing Head

Chapter Contents

2. IR H0MING HEAD

2.1 Introduction

All the electromagnetic radiations transport energy. Infrared (***IR***) radiation covers that portion of the electromagnetic spectrum that lies between visible light and microwave where certain phenomena are associated with this relatively narrow slice of the electromagnetic spectrum. Optics is often defined as being concerned with radiation visible to the human eye; however, in view of the expansion of optical application in the regions of the spectrum on either side of the visible region, it seems not only prudent but necessary to include certain aspects of the infrared and ultraviolet region in many discussions [**Smith 1966**]. However, it should be mentioned that the IR window considered in the present research lies in the region 3-5 μm where the transmission of IR radiation is about 0.9 [**Hudson 1969**], which is the maximum transmission in the IR region of the spectrum.

The principal differences between the optics of infrared systems and visual optical systems result from the image size requirements in the two portions of the spectrum. In the visible and near infrared, semiconductor detectors, photographic plates, and the eye are capable of resolutions in the tens of micrometers and smaller range of dimension. In the deep infrared, beyond two micrometers wavelength, the current state of the art yields detectors with effective resolution areas from the order of millimeters down to one hundred micrometers in size. Thus, the optics required for the latter regions need not produce the high resolution common in visual optics. Great advantage of this fact is taken to make the IR optics simpler.

No matter how perfect in design or construction, any optical system is limited in its resolution by diffraction. The effect of this limitation depends on the size of the optical system and the wavelength of the radiation forming the image. In geometrical optics a point object produces a point image. In fact an image of a point source produced by an ideal optical system has a central maximum of intensity surrounded by diffraction rings **[Scott 1959].**

The application of IR techniques has been known since the beginning of the twentieth century. As early as 1910, many workers were intrigued by the possibility of heat seekers and were proposing a wide variety of IR search devices. In the 1920's the availability of the thallous sulfide detector encouraged a new generation of workers to reinvent IR search devices. When the lead sulfide photon detectors were developed at the end of 1940's which is sensitive in the 1 to 3 μm window, German applications of the IR missile guidance appeared [**Vnderhill 1947**] Further developments were introduced in the early 1960's when small and reliable cooling devices became available up to yet.

2.2 Components of IR Homing Head

Along their sequence from the target until the image, the components of IR homing head are discussed in the following sections in details.

2.2.1 Infrared Target

The term "target" refers collectively to those objects that IR systems are designed to detect. Although specific details on the military application

of IR technique and the radiating characteristics of some targets are classified by the military, reasonably accurate estimates can often be made by applying the radiation laws and certain other information readily available in the open literature **[Hudson 1969].**

Calculation of the IR radiation emitting from the hot target (for example; aircraft jet) can be carried out by using Planck's radiation law for the detector operating in the IR region of interest (3-5) μm. The most sensitive detector operating in this region is the indium antimonide and the lead selenide.

The parameters going from the target to the IR homing head are described and the calculations of the parameters of interest are given. The spectral distribution of radiance exitance of blackbody at temperature T_{BB} (K) is given by [**Hudson 1969**].

$$w_\lambda(\lambda, T_{BB}) = c_1 \lambda^{-5} [e^{\frac{c_2}{\lambda T_{BB}}} - 1]^{-1} \qquad (2.1)$$

In units of $Wcm^{-2}\mu m^{-1}$, where

$$c_1 = 2\pi hc^2 = 3.741832 \times 10^{-12} Wcm^2 \qquad (2.2)$$

$$c_2 = \frac{hc}{k} = 1.438786\, mK \qquad (2.3)$$

where c_1 and c_2 being the radiation constants, h is Planck's constant, k is Boltzmann's constant, and c is speed of light.

The spectral emittance of the blackbody in the spectral region between wavelength λ_a and λ_b can be obtained by integration of the Planck's law in this interval of spectrum.

$$w_{\lambda_a}^{\lambda_b} = \int_{\lambda_a=3}^{\lambda_b=5} w_\lambda(\lambda, T_{BB})\, d\lambda \tag{2.4}$$

Evaluation of emittance (exitance) of a blackbody can be done by the method of reduced coordinates [**Gaussorgues 1984**].

Define $$X = \frac{\lambda}{\lambda_{\max}} \tag{2.5}$$

and $$Y = \frac{w_\lambda(\lambda, T_{BB})}{w_\lambda(\lambda_{\max}, T_{BB})} \tag{2.6}$$

using this assumption, Planck's equation can be written as

$$Y.w_\lambda(\lambda_{\max}, T_{BB}) = w_\lambda(\lambda, T_{BB}) \tag{2.7}$$

so, equation (2.4) can be written in the form

$$\int_{\lambda_a=3}^{\lambda_b=5} w_\lambda(\lambda, T_{BB})\, d\lambda = w_\lambda(\lambda_{\max}, T_{BB})\lambda_{\max} \int_{X_1}^{X_2} Y\, dX \tag{2.8}$$

similarly

$$\int_0^\infty w_\lambda(\lambda, T_{BB})\, d\lambda = \sigma T_{BB}^4 = w_\lambda(\lambda_{\max}, T_{BB})\lambda_{\max} \int_0^\infty Y\, dX \tag{2.9}$$

where $\sigma = 5.67 \times 10^{-12}\ \mathrm{Wcm^{-2}K^{-4}}$ which is Stefan's constant, equations (2.8) and (2.9) can be reduced to the following equation

$$w_{\lambda_a}^{\lambda_b} = \int_{\lambda_a=3}^{\lambda_b=5} w(\lambda, T)\, d\lambda = \sigma T^4 \frac{\int_{X_1}^{X_2} Y\, dX}{\int_0^\infty Y\, dX} \tag{2.10}$$

$$w = \sigma T^4 [Z(X_2) - Z(X_1)] \tag{2.11}$$

where $Z(X)$ is assumed to be

$$Z(X) = \frac{\int_{X1}^{X2} \mathrm{Y}\, dX}{\int_0^\infty \mathrm{Y}\, dX} \tag{2.12}$$

$$\lambda_{max}(\mu m) = \frac{P_n}{T(K)} \tag{2.13}$$

where $P_n = 2898$, $T(K)$ is the jet nozzle temperature which is equal to 850K, and

$$X_1 = \frac{\lambda_1}{\lambda_{\max}} \tag{2.14}$$

$$X_2 = \frac{\lambda_2}{\lambda_{\max}} \tag{2.15}$$

The spectral radiant intensity is related by the area of the jet nozzle (A) and spectral radiant emittance (w) as follow

$$I = \frac{wA}{\pi} \qquad (W/Sr) \tag{2.16}$$

the standard value of A is 3660 cm^2 [**Hudson 1969**], therefore the spectral radiant intensity of interest is

$$I = \frac{w_3^5 \times 3660}{\pi} \quad (W/Sr)$$

2.2.2 Atmosphere Transmission (τ_a)

The thermal radiation transmits through the atmosphere until it is reaching to the optical part of the homing head. Then, it transmits the optical elements to produce an IR image for the target on the detector. The mathematical description of the two transmissions is giving as follows

It is unfortunate that most IR systems must view their targets through the Earth's atmosphere. Before it reaches the IR sensor the radiant flux from the target is ***(a)*** selectively absorbed by several of the atmospheric gases**,*****(b)*** scattered away from the line of sight by small particles**,** and ***(c)*** suspended in the atmosphere. In the IR portion of the spectrum the absorption process

possesses a far more serious problem than does the scattering process. The molecule responsible for each absorption band is either water vapor/carbon dioxide, or ozone. Fog and clouds strongly scatter and are, in effect, opaque to IR radiation. As a consequence, IR systems cannot be considered to have a true all weather capability. On the other hand, transmission through rain is good.

Atmosphere transmission τ_a can be approximated with analytical function easy to use in computation.

$$\tau_a = e^{-\beta_{ato} R} \qquad (2.17)$$

where *R* is the range between the target and the homing head, which can be expressed by path length and β_{atm} is the attenuation factor of the atmosphere.

The attenuation factor of the atmosphere is depending of several elements which are present in the atmosphere [**Hudson 1969**].

$$\beta_{atm} = \beta_{aerosl} + \beta_{water} + \beta_{moleculer} \qquad (2.18)$$

β_{aerosl} for the particles in suspension in the air, it can be expressed as a function of the horizontal visibility. The following values are commonly used in the bandwidth $(3-5)\mu m$. Visibility (R_v) in kilometers is the only input value needed to determine β_{aerosl} by using the equations given in table 2.1.

β_{water} is a function of the quantity of water in the atmosphere, i.e humidity. The $\beta_{moleculer}$ is a function of the gas molecules composing the atmosphere. $(\beta_{water} + \beta_{moleculer})$ is a mean value along the considered range which is dependant mainly of:

1-The range itself.

2- The humidity, i.e dew point temperature.

The values of $(\beta_{water} + \beta_{moleculer})$has been computed by means of *LOWTRAN* code and given in table 2.2. The β_{atm} may be determined by using the appropriate value obtained from tables (2.1 and 2.2).

Table 2.1: Equations to approximate β_{aerosl} [**Fisher 1966**].

Aerosal Model	$(3-5)\mu m$
Maritime	2.24/ R_v
Rural	0.42/ R_v
Urban	0.60/ R_v
Dry	1.76/ R_v

Table 2.2: $(\beta_{water} + \beta_{moleculer})$as a function of range (path length) and dew point T_{dp} temperature [**Fisher 1966**].

Range (km)	**$T_{dp}(^oC)$**												
	-20	-15	-10	-5	0	5	10	15	20	25	30	35	40
0.5	.602	.643	.691	.745	.810	.880	.956	1.03	1.12	1.22	1.33	1.43	1.55
1.0	.381	.411	.446	.486	.529	.576	.629	.685	.747	.810	.875	.947	1.02
2.0	.246	.268	.292	.318	.349	.381	.415	.452	.490	.532	.576	.622	.672
4.0	.161	.176	.192	.211	.231	.252	.275	.299	.325	.351	.379	.410	.443
8.0	.107	.117	.129	.141	.154	.168	.183	.199	.215	.233	.252	.275	.300
16.0	.072	.079	.087	.095	.104	.113	.123	.133	.145	.158	.173	.190	.210

The important parameter is visibility. According to the U.S Weather Bureau, visibility refers to the maximum distance at which objects such as mountains, buildings, or towns can be seen and identified with the unaided eye **[Hudson 1969].** For any given pulse input to the search set detector the visibility factor is a function of the detector/ noise filter combination **[Genoud 1959].** On a clear day, when the visibility factor is greater than 15km from a heavy overcast cloud layer with a base just below 700*m* the linear depolarization (or degree of coherence) value increases gradually with a penetration depth into the cloud starting at values very close to zero at the base of the cloud, reaching a value of 0.17 at an altitude of 780*m* **[Houston and Carswal 1978]** The attenuation coefficient as a function of the meteorological visibility range R_v at various weather conditions is shown in figure 2.1. The values of R_v in table 2.3 at various weather conditions have been used in a computer program for determining the range.

Table 2.3: Meteorological visibility range at various weather conditions.

R_v (km)	Weather Condition
0.01-0.5	**Very Bad** (dense fog, very dense snow, dense snow).
0.5-2	**Bad** (moderate snow, haze “moderate snow”, very dense rain)
2-10	**Medium** (dense rain, moderate rain)
10-20	**Good** (without precipitation “light rain”)
20-50	**Very Good** (clear atmosphere without precipitation)
50-150	**Excellent** (very clear atmosphere)

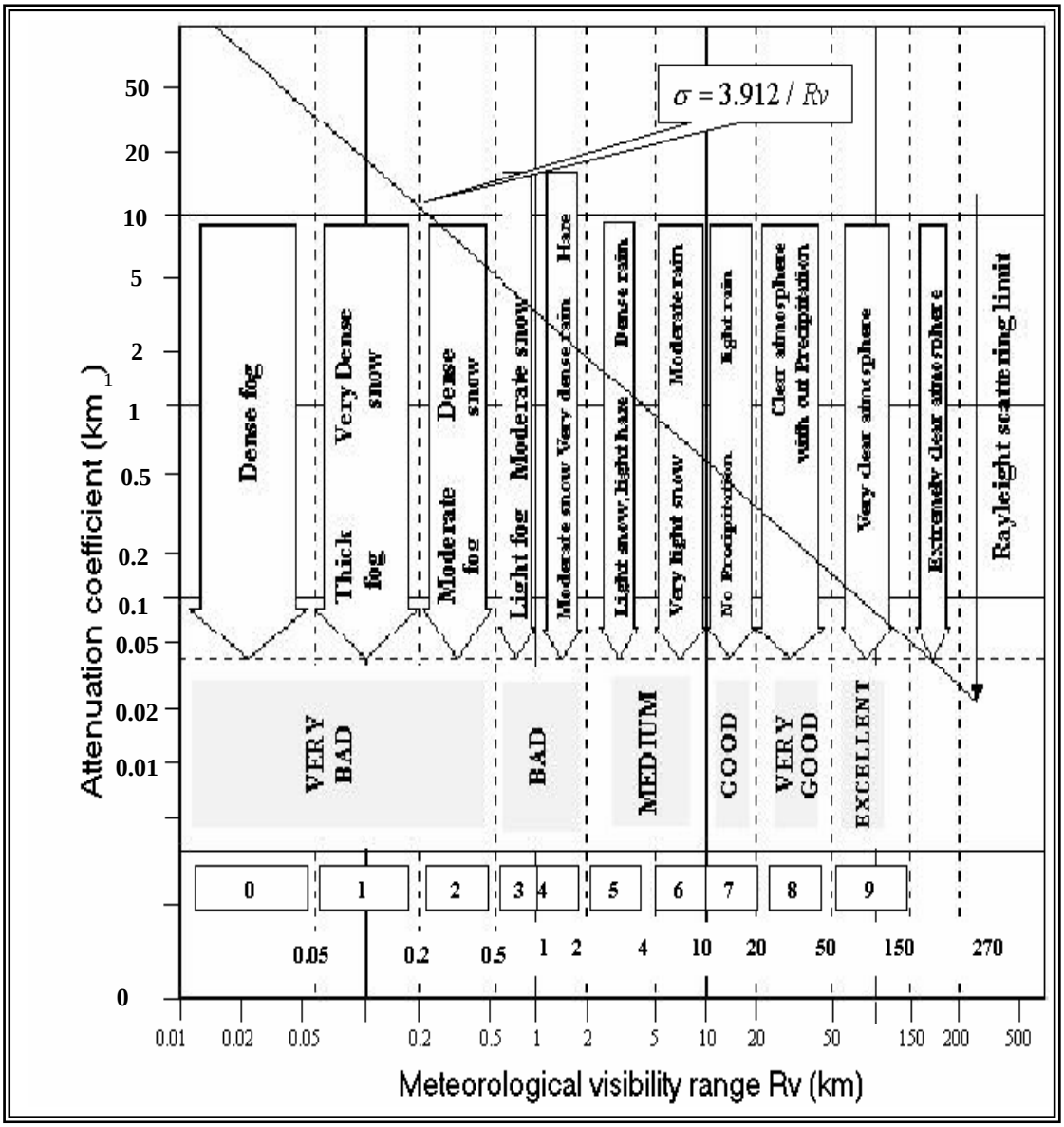

Figure 2.1: Meteorological visibility range at various weather conditions **[Houston and Carswal 1978]**.

2.3 Optoelectronics Components of IR Homing Head

The optoelectronic components of an IR homing head are shown in figure 2.2. The general description of the optical components needs to be described in this section, leaving the theoretical description to the next

chapter which is dedicated to the optical consideration of the homing head. The following elements are described:

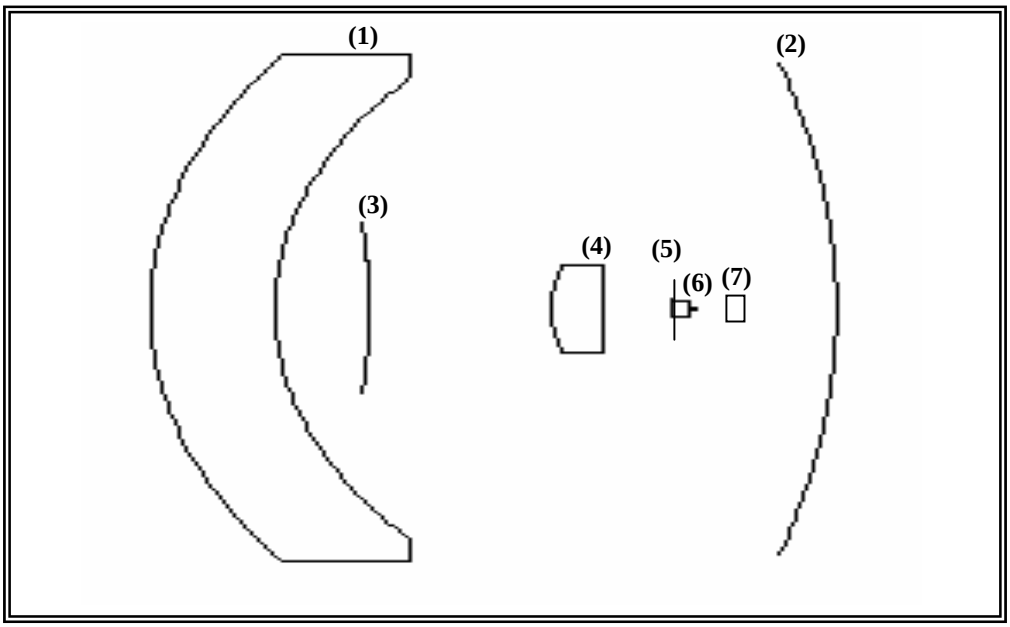

Figure 2.2: Optical system design for IR homing head. (1 is a dome, 2 and 3 are mirrors, 4 is a correcting lens, 5 is reticle, 6 is collecting lenses, 7 is detector.)

1. Dome

Figure 2.2 shows a dome, a primary mirror, and a secondary mirror which is located between the spherical mirror and the dome. The dome introduces spherical aberration opposite to that of the primary mirror. It also produces significant amounts of higher-order on-axis aberrations. It is interesting to note that although the paraxial power of the dome is equal and opposite to that of the primary mirror, this means the dome is a highly non-linear element with aberration. Since the dome center is near the center of the aperture, the dome affects the off-axis rays almost identically as the on-axis rays. In optical terms, the principal ray of the system is perpendicular to the dome surface so that almost no off-axis aberrations are generated by the

dome. In conventional systems the dome material is usually MgF_2, which is usually a single crystal possesses high optical transmittance as shown in figure 2.3. The growth of such crystal is obtainable by either conventional methods or hot pressing technique of the MgF_2 powder. Both methods require advanced technology and high cost. In the present work, this material has been replaced by calcium aluminate glass ($CaAl_2O_3$) due to its desirable specifications particularly its high optical transmittance and simple manufactors as shown in figure 2.4. This means that the reflectance is very low. The suggested calcium aluminate glass does not need advanced technical requirements for its preparation. For 3-5 μm wavelength band, the choices of window material usually include calcium aluminate glass, sapphire, magnesium fluoride, silicon, and possibly zinc sulphide. The hardest material being sapphire is considered environmentally as the best choice for air to air missiles, but cost can prevent it use as shown in figure 2.5 **[Baker 1983]**. The stop image that subtends the smallest angle at the center of window since it determines the field of view, if the aperture stop is small **[Longhurst 1967]**.

The window used either flat plate or dome, must withstand the flight profile stated for its application. The mechanical properties should be strong enough to prevent castographic failure. The likely cause of this would be cracking and fracturing due to the thermal and stress loads imposed on the window during the first five second of flight. This is the critical time of buildup of stress and external temperature. A high temperature differential between external and internal surfaces may be inducing thermal stress leading to cracking. This will not be so great a problem if the material has a

high thermal conductivity [**Baker 1983**]. Sapphire is the superior window material in many ways. Because of its extreme surface hardness, it exhibits high internal transmittance all the way from vacuum UV to middle IR. The external transmittance of sapphire window can safely be made much thinner than the windows of other materials. Its properties are shown in table 2.4.

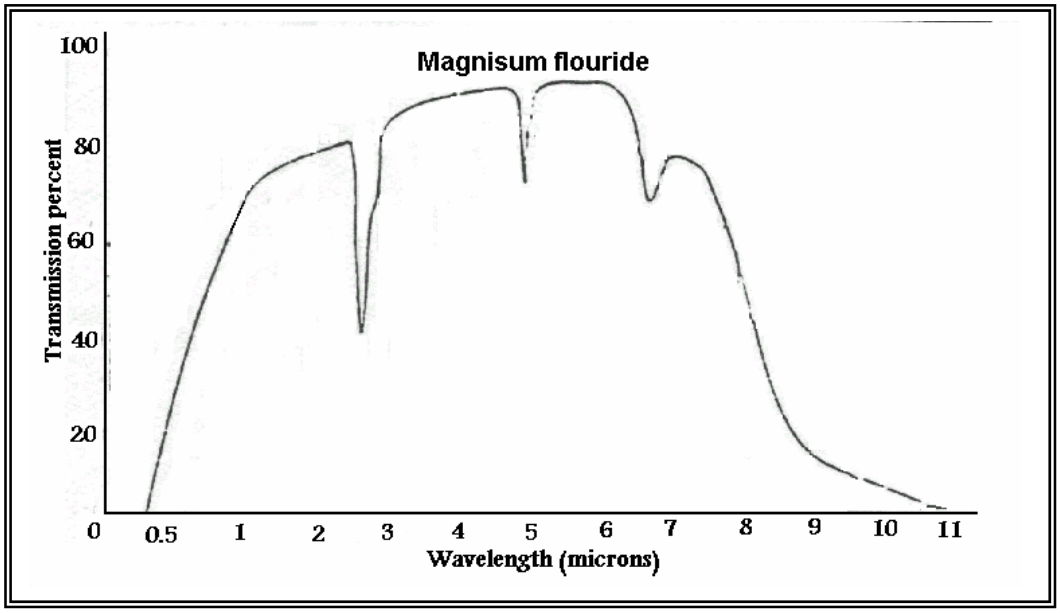

Figure 2.3: Optical transmission of MgF_2 [**Fundamental optics 2004**].

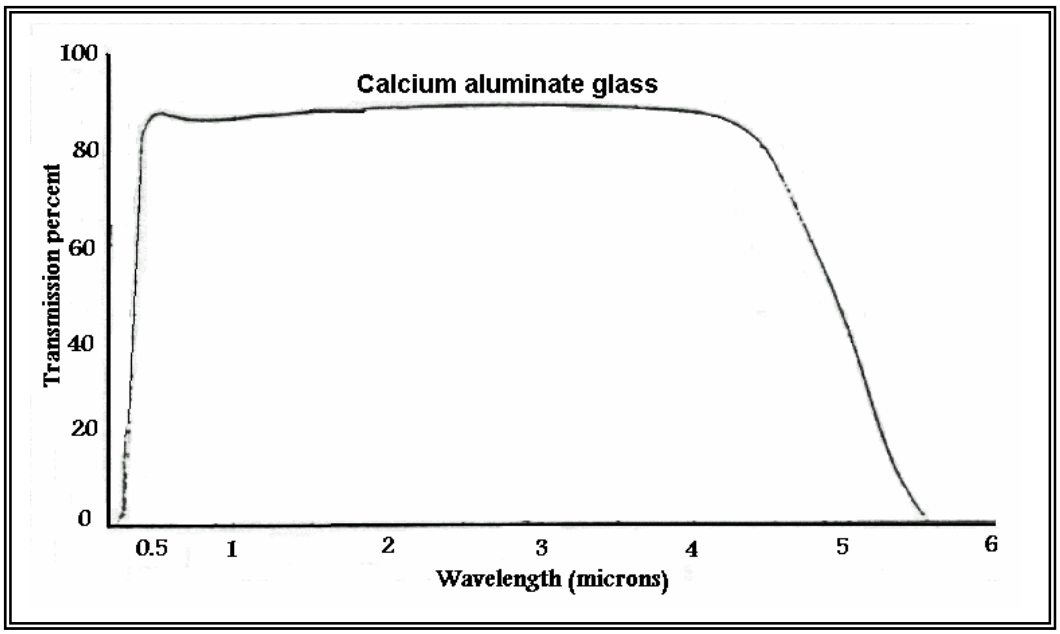

Figure 2.4: Optical transmission of $CaAl_2O_3$ [**Chung 1997**].

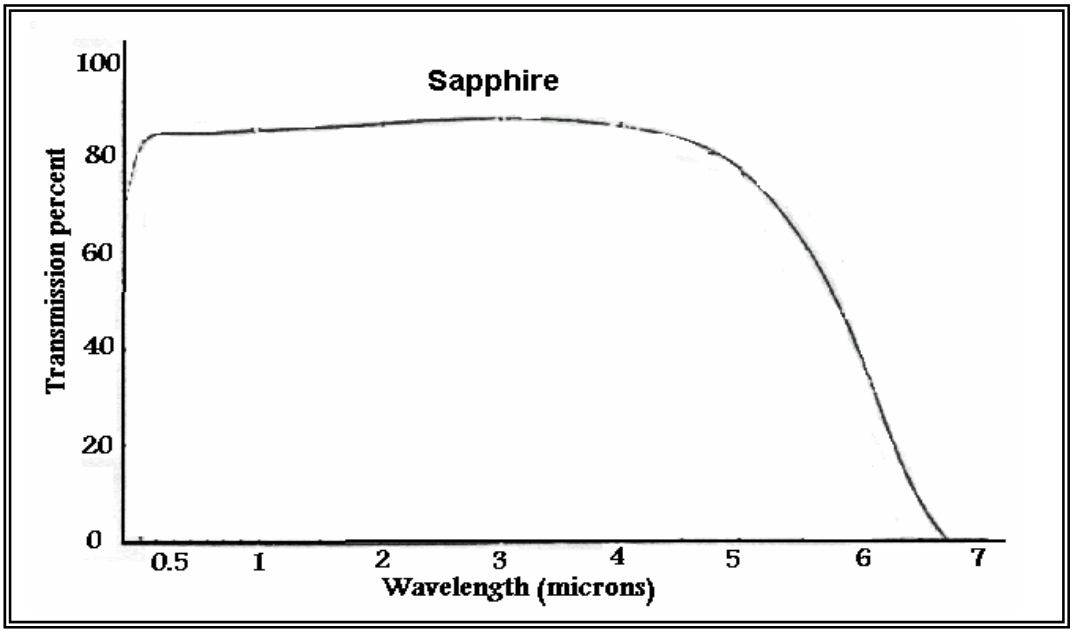

Figure 2.5: Optical transmission of sapphire (Al_2O_3)
[**Fundamental optics 2004**].

2. Primary mirror

The primary mirror introduces spherical aberration and since this element is used as the aperture stop, coma and astigmatism are also introduced. In attempting to improve the resolution, the first logical step was to investigate the use of a more complicated primary mirror. This was done by using thin-lenses. The study of a mangin (back surface) mirror showed that by keeping the power of the lens constant and just bending the lens, the astigmatism remains constant, coma decreases, and the spherical aberration decreases through zero and then increases negatively. If this mirror were used to correct coma, the spherical aberration would have a reversed sign, and the dome would no longer be able to correct the residual spherical aberration. Therefore, a correcting lens is required to cancel the remaining spherical aberration [**Dubner 1959**].

3. Secondary mirror

Using thin lens formulas, an investigation has been made on a mangin secondary mirror. The system is composed of the primary mirror and mangin secondary mirror. The optical aberration varies rapidly as a function of lens bending. At the point where spherical aberration is near zero, the mangin secondary mirror behaves in much the same manner as the dome, that is, for large changes in spherical aberration there is little change in either coma or astigmatism. Thus, a dome can now be chosen independent of the spherical aberration required; the mangin mirror can supply the residual spherical aberration.

4. Correcting lens

Since both the mangin primary and the mangin secondary mirrors required a correcting lens in front of the focal plane, a thorough analysis was made of a system consisting of a glass dome, a primary mirror, a plane secondary mirror, and a lens. The first objective was to find a configuration, which would yield zero coma. It was found that for any particular lens power, the lens could be bent so that there would be no coma. For zero coma, astigmatism and spherical aberration were functions of lens power **[Dubner 1959].**

5. Reticle

The reticle is a selective modulator that is most efficient against point source targets. For the highest modulation efficiency, the opening in the reticle should match the size of the target image. In practical designs, they may be up to three times as large as the size of the image [**Hudson 1969**].

Typical reticles have extremely fine patterns and require great care in their manufacture. Figure 2.6 shows the geometry of the reticle pattern which is used in the optical system for IR homing head. The encoding method used in this reticle type is the frequency modulation (FM). The first problem in the design of an IR homing head is to code the position of the target signal $\Delta f \neq 0$ in the field of view, in such a way that the homing head will know which direction to move in order to bring the target to the center of the field $\Delta f = 0$. Infrared homing head system usually generate their tracking information by a scanning process that produce relative motion between an optical formed image of the target and a reticle located in the image plane [**Fisher 1966**].

The most common ways in which the chopping reticle may be used are a nutating system and a rotating system [**Nichols 1959**]. In nutating system, the optical axis of the homing is rotated at an angle to the axis of the reticle. This causes the image to move about on the reticle in a circular fashion; and, if there is a target in the field of view, it will be modulated by the reticle pattern as its image moves about. In a rotating system, the optical axis of the homing head and the axis of the reticle are common, but the reticle rotates in the image plane. In this case, the rotating pattern in the image plane will modulate the target image to give the error signal.

In the present design, the nutating system is considered. The loop of nutation is concentric with the reticle center when the target is on the axis; it is eccentric when the target is off the axis.

The light then travels through the reticle, becoming frequency-modulated and falls onto the detector. The output signal *u* of the detector, being the voltage proportional to the light intensity, is also frequency-modulated and it sent to a discriminator which electronically demodulate the signal to yield a final output signal v, which, being the voltage proportional to the instantaneous frequency of *u*, is used to control the orientation of the tracking system to perform the aiming function.

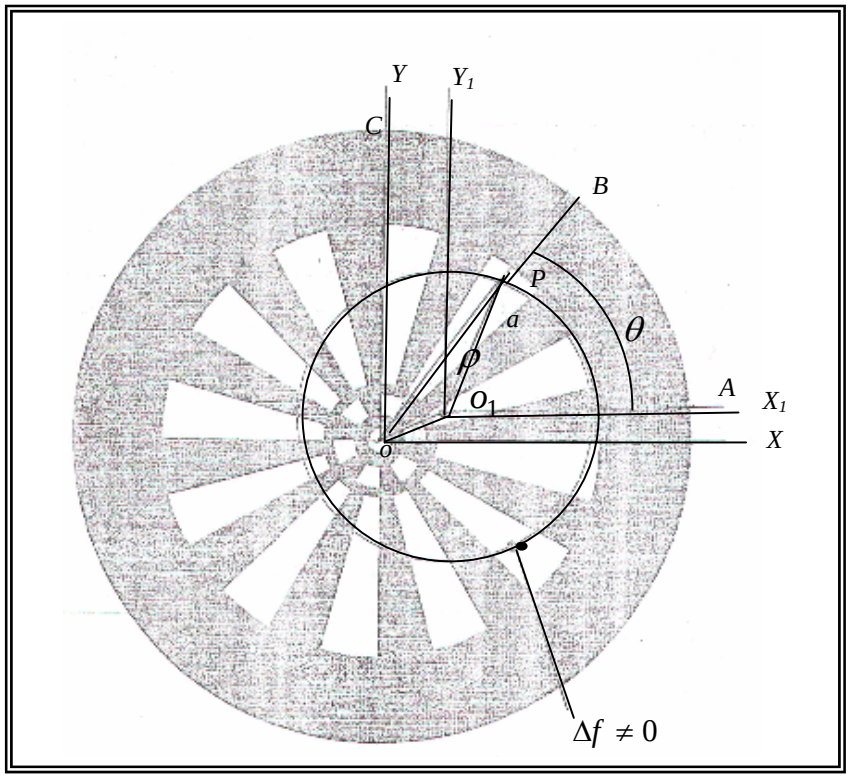

Figure 2.6:The FM reticle used in the homing head system.

There are three important parameters to be considered in the signal processing of the electronic circuits in a FM system:

i. Center frequency.

ii. Frequency bandwidth.

iii. Degree of contrast.

All three can be understood through the analysis of the behavior of the image spot nutating in the reticle plane. We use here the analytically point model developed by Chao and Chu [**Chao and Chu 1988**] to establish the analytical results for individual parameters.

The point model considers the image spot in an ideal point as shown in figure 2.6. The image point *P* nutate with a constant angular velocity Ω along a circular loop of radius *a* around the center O_1, which in general does not coincide with the reticle center *O*. The reticle comprises $2m$ (*m* is the a positive integer) equally spaced spokes of alternating transmittance 0 (opaque) and 1 (transparent). In the system OXY, the polar coordinates of O_1 and *P* are (r_1, θ_1) and (ρ, θ), respectively.

The detector output voltage is proportional to the target intensity behind the reticle, which is

$$u(t) = \int_{-\infty}^{\infty}\int_{-\infty}^{\infty} r(\vec{x},t)P(\vec{x},t)d^2\vec{x} \qquad (2.19)$$

where $r(\vec{x},t)$ is the intensity transmittance function of the reticle, and $P(\vec{x},t)$ is the intensity distribution function of the image. The function *P* can be written as

$$P(\vec{x},t) = \delta[X - X'(t)]\delta[Y - Y'(t)] \qquad (2.20)$$

where $X'(t)$ and $Y'(t)$ are the instantaneous positional coordinate of the image point. For the function $r(\vec{x},t)$ notice that the reticle is stationary so $r(\vec{x},t) = r(\vec{x})$. From the figure 2.6.

$$\frac{\theta}{2\pi} = \frac{b}{2m} \qquad (2.21)$$

where *b* stands for a non integer parameter that takes different values in different spokes. For example, in the spokes OAB, *b* takes the values $0 \prec b \prec 1$. Thus we have

$$r(\vec{x}) = STP[\sin(m\theta)] \tag{2.22}$$

where $$STP(\omega) = \begin{cases} 1 & \omega \geq 0 \\ 0 & \omega < 0 \end{cases} \tag{2.23}$$

equation (2.19) can be then written as

$$u(t) = \int_{-\infty}^{+\infty}\int_{-\infty}^{+\infty} STP[\sin(m\theta)]\delta(X - X')\delta(Y - Y')dXdY \tag{2.24}$$

$$= STP[\sin(m\theta)]$$
$$= STP[\sin(argument)]$$

According to the definition of FM demodulation, the signal ν is:

$$\nu(t) = \frac{d}{dt}(argument) = m\frac{d\theta}{dt} \tag{2.25}$$

a method of differentiation with respect to θ can be done by replacing the differentiation with respect to *t* in equation (2.25) by the differentiation with respect to *s*, the arc length. Transforming the coordinates $O_1X_1Y_1$ to system OXY and transform the function $\nu(t)$ to $\nu(\theta)$, where θ is proportional to *t*, one can obtain

$$\nu(\theta) = m\Omega - m\Omega\frac{r_1}{a}\cos(\theta - \theta_1) \tag{2.26}$$

because θ is a function of *t*, the equation is of the form

$$\nu(t) = \nu_o - f(t) \tag{2.27}$$

where $\nu_o = m\Omega$ and $f(t) = m\Omega\frac{r_1}{a}\cos(\theta - \theta_1)$ (2.28)

Comparison of this expression with the definition for instantaneous frequency of an FM signal. i.e. $\omega = \omega_o + f(t)$, reveals that ν behaves like demodulated FM signal.

Central Frequency

If the target is tracked correctly, that is, when the target is on the axis, there should be no lateral deviation, i.e, r_1 =0. Then from equation (2.28), we see that

$$\nu = \nu_0 = m\Omega = constant \qquad (2.29)$$

This implies that the tracking system should work in the sense that ν approaches a constant. The constant value $m\Omega$ is the center frequancy.

Frequency bandwidth

Referring to equation (2.29) a type relation of ν verses θ is shown in figure 2.7.

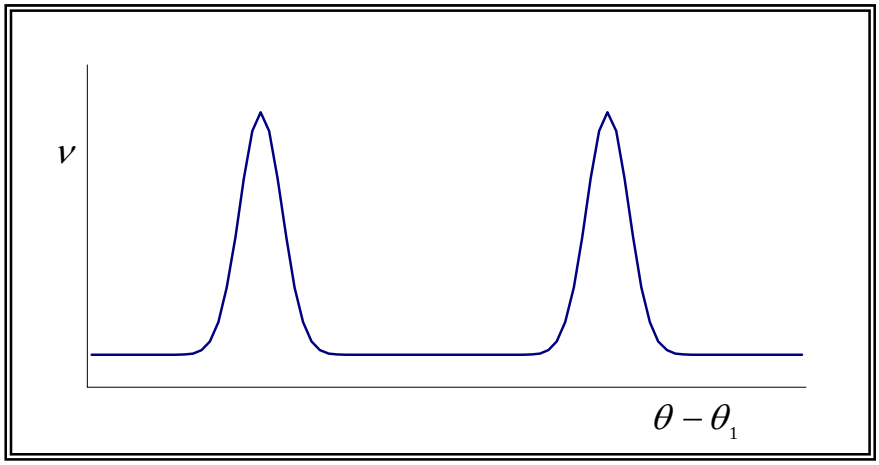

Figure 2.7: Signal output after demodulation

It should be remarked that there are ν_{max} and ν_{min} on the curve. The difference between them is the frequency bandwidth at $\theta - \theta_1 = \pi$

$$\nu_{\max} = m\Omega(1 + \frac{r_1}{a}) \tag{2.30}$$

and at $\theta - \theta_1 = 0$

therefore $$\nu_{\min} = m\Omega(1 - \frac{r_1}{a}) \tag{2.31}$$

thus the frequency bandwidth is:

$$\Delta\nu = \nu_{\max} - \nu_{\min} = 2m\Omega\frac{r_1}{a} \tag{2.32}$$

therefore one can understand the behavior of ν anywhere on the reticle, e.g. $\nu_{\max}$ and $\nu_{\min}$ simply through geometrical interpretation. This would be a useful theoretical support to simplify the design process of the infrared homing head.

Degree of contrast

The degree of contrast is defined as

$$G = \frac{\nu_{\max} - \nu_{\min}}{\nu_{\max} + \nu_{\min}} \tag{2.33}$$

the low value of *G* is undesired, therefore, the designs of the reticle should arrange the reticle spokes so as to obtain the best value of *G*. The value of *G* is always be obtained with the range $0 \le G \le 1$. *G*=1 implies a pure FM signal; *G*=0 implies no FM signal.

Calculation of the modulation parameters mentioned in this paragraph is carried out using the measure data **[Mohammed and Mustafa 2001]**. The required data for the calculation are the numbers of spokes pair pertaining to the homing head reticle, namely, 2m=12 or m=6, the angular frequency measure of the homing head gyroscope using the test band apparatus is 100 *Hz*, also the measure dimensional parameters of the reticle which where

found to be $r_1 = 2\mu m$ and $a = 4\mu m$. Using the measured data given above, the following important parameters for the digital signal processing for the homing head are calculated as follows:

$$\upsilon_o = 2m\Omega$$
$$= 12 \times 100 = 1200\ Hz$$

This value represents the FM signal without modulation (the case of $\Delta f = 0$). This value leads to calculate the modulation time of one spoke of the reticle $\tau_1 = 1/\upsilon_o$ =0.833 *ms*, while the period of the gyroscope $\tau_2 = 1/100 = 10\ ms$. Furthermore, υ_{max}, υ_{min}, $\Delta\upsilon$ can be calculated using the relations (2.30), (3.31), and (2.32).

$$\upsilon_{max} = 12 \times 100\left(1 + \frac{2}{4}\right) = 1800\ \ Hz$$

$$\upsilon_{min} = 12 \times 100\left(1 - \frac{2}{4}\right) = 600\ \ Hz$$

and $\Delta\upsilon = \upsilon_{max} - \upsilon_{min} = 1800 - 600 = 1200\ \ Hz$

Also the contrast $G = \dfrac{\upsilon_{max} - \upsilon_{min}}{\upsilon_{max} + \upsilon_{max}} = \dfrac{600}{2400} = 0.25$

The calculated results were in good agreement with the results obtained from the homing head test bench given in reference Mohammed and Mustafa. These parameters are of great importance for the design of the homing head digital signal processor mentioned in figure 1.1.

6. collecting lenses

Which is used to collect the radiation and form an image by the focusing process. The main purpose of the collection part is to focus the radiation on the optical axis to produce a spot image on the detector's active

area. For good focusing, a Germanium lenses are used after the reticle to collect income rays.

The reason of using the Germanium is because it is characterized by higher refractive index then the other optical elements, in addition to higher transmission at region of interest ($3-5\ \mu m$) as shown in figure 2.8.

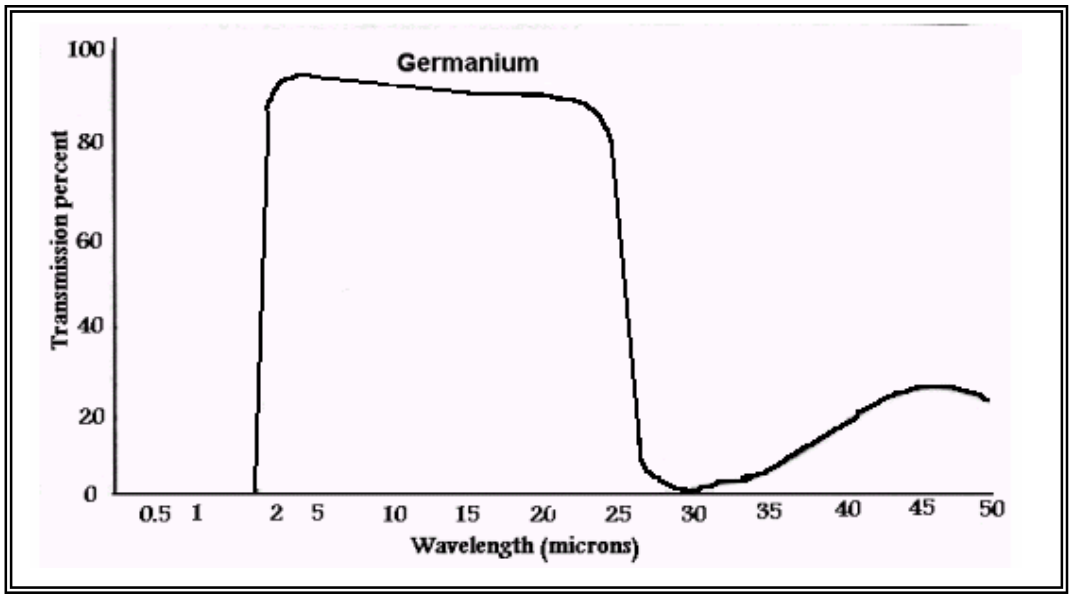

Figure 2.8: Optical transmission of AR coated Ge
[**Fundamental optics 2004**].

7. Detectors

During the war world II lead sulphide Gudden, Kasper, Kutzcher and others, manufactured photoconductive cells in Germany but the methods of production have not been published. In 1944 methods of manufacturing of PbS and PbSe cells were developed at the Admiralty Research Laboratory in Britain and by American workers, from 1945 onwards [**Wilman 1948**]. Both vacuum sublimation and chemical deposition for forming suitable films of PbS were exploited. Peak sensitivity in PbS cells occurs at about 2.7 μm at

room temperature, while a spectral response curve for a PbSe extends to $3.5\,\mu m$ at low temperature. The detectivity was about $10^8\,cmHz^{1/2}W^{-1}$, and the response time of the prepared cells were of the orders of 10^{-5} seconds [**Starkiewics 1948**].

The InSb cooled p-n junction detector was prepared using sliced single crystal of InSb. The detector characterization was measured with the slice mounted in a demountable metal Dewar system for cooling the detector at $90K$ [**Avery 1957**]. A spectral response between $(3-5.6)\mu m$ was observed, and response time of $2\times10^{-7}\,s$ obtained. Because of the best sensitivity of this detector in the IR region $(3-5)\mu m$, this detector is widely used in thermal imaging and in IR homing for missile guidance. Consider a simple p-n homojunction photovoltaic detector, electron-hole pairs generated within a diffusion length of the junction diffuse to the depletion region and accelerated in opposite directions. In this way, minority carriers become majority carriers on the other side of the junction which shifts the current- voltage curve down as shown in figure 2.9. The magnitude of the photocurrent is given by [**Michel and Razeghi 1998**].

$$I_{ph} = \eta q A_j \phi \qquad (2.34)$$

where η is the quantum efficiency, q is the electronic charge, A_j is the junction area, and ϕ is the incident flux. Photodiode can operate at any point on the current- voltage characteristics, but reverse bias is generally used for high frequency applications to reduce the RC time constant of the device.

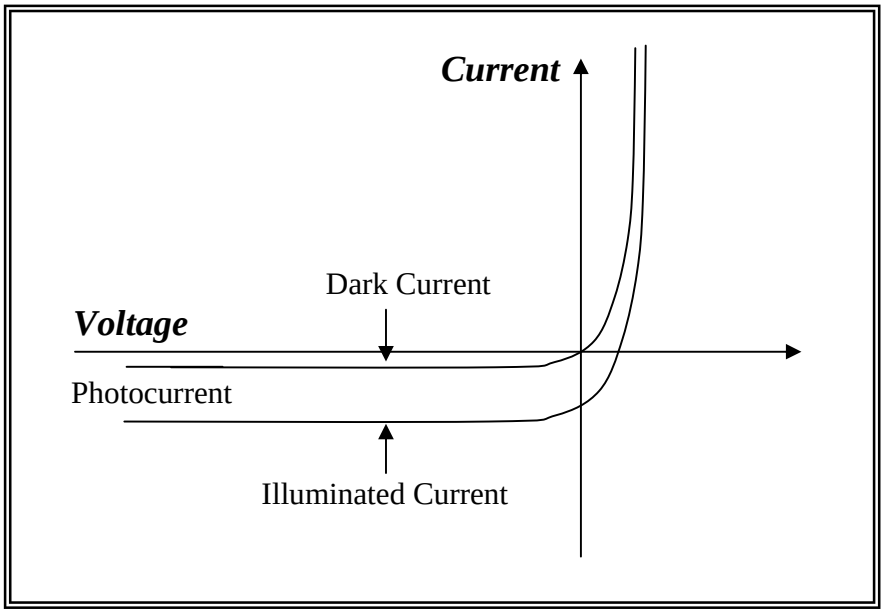

Figure 2.9: Photodiode current-voltage curve.

The most important figure of merit for this photodiode, which takes the major importance in search or tracking range evaluation is the detectivity *D**.The detectivity of a thermal noise limited photodetector is given by [**Michel and Razeghi 1998**]:

$$D^* = \frac{\lambda \eta q}{hc} \frac{\left(R_o A_j\right)^{1/2}}{\left(4kT\right)^{1/2}} \qquad (2.35)$$

where λ is the wavelength, *h* is the Planck's constant, *c* is the velocity of light, $R_o A_j (\Omega.cm^2)$ is the zero- bias resistance area product, *k* is Boltzmann's constant, and *T* is the temperature. For the best performance under given operating conditions (wavelength and temperature), the value of $\eta \left(R_o A_j\right)^{1/2}$ should be maximized.

Detectivity is an important parameter that influences the range of the IR homing head system. A good detector has high detectivity. The detectivity is a function of the following factors:

i. Wavelength of the incident radiation,

ii. Temperature of the detector, and

iii. Area of the detector.

It is not easy to achieve a theoretical relationship between the detectivity and temperature of the detector. This is why the detector temperature is always given with any measurements of the detectivity. For instance, the InSb detector is usually used at $77K$ ($D^* = 9 \times 10^{10}\ cmHz^{1/2}W^{-1}$). Figure 2.10 shows the variation of the detectivity with the absolute temperature for different materials of the detector. It is seen that there is always a temperature at which the detectivity of the detector is at its maximum value.

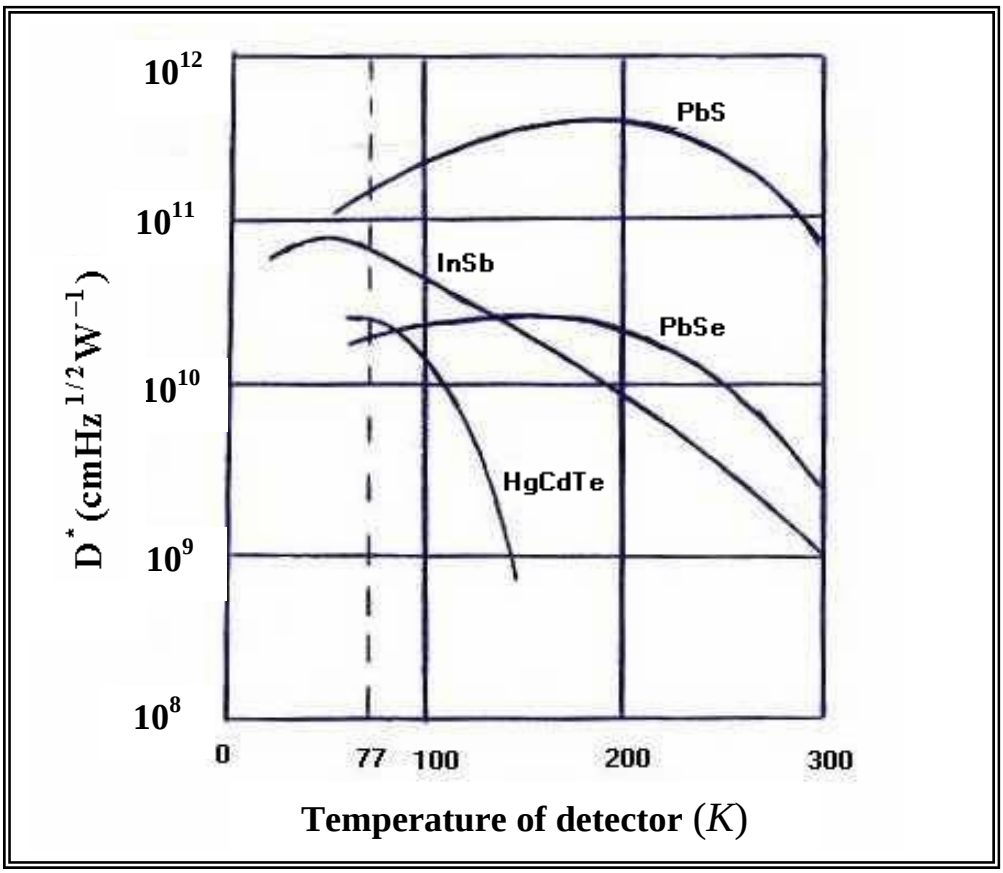

Figure 2.10: Detectivity versus temperature [**Michel and Razeghi 1998**].

2.4 Optical properties of IR materials

The optical properties such as transmittance, reflectance, refractive index, optical homogeneity, and wavelength variation of these properties are themselves significant. For these properties the major importance in search and tracking range evaluation is the optical transmittance (τ_o). Within the optical elements, some of the radiation may be absorbed by the material. If T is the transmission of a unit thickness of material, the transmission through a thickness of i unit will be given by [**Smith 1966**].

$$\tau_o = T^i \tag{2.36}$$

This relation is often state in the following form

$$\tau_o = e^{-ai} \tag{2.37}$$

where a is called the absorption coefficient and equal to $-\log_e T$, for light normally incident on the boundary, the reflection is given by

$$R = \frac{(n'-n)^2}{(n'+n)^2} \tag{2.38}$$

where n' and n are the indices of two media. Thus, it can be seen that transmission through an optical elements a sort of product of its surface transmission and its internal transmission. So the transmission of the surface

$$R + \tau_o = 1 \tag{2.39}$$

or, $$\tau_o = 1 - R$$

$$\tau_o = 1 - \frac{(n'-n)^2}{(n'+n)^2} \tag{2.40}$$

then, $$\tau_o = \frac{4n}{(n+1)^2} \tag{2.41}$$

For Germanium for example (n = 4)

$$\tau_o = \frac{4 \times 4}{25} = \frac{16}{25} = 0.6$$

The optical properties of some IR materials used in this work can be shown in table 2.4.

Table 2.4 Optical material features [**Weast, Astle, and Bayer 1984-1985**].

Material	**Name**	**Ref. Index**	**Crystallo-Graphy**	**Density (g/cm^3)**	**Transmittance at $(3-5)\mu m$**
$CaAl_2O_3$	Calcium Aluminate Glass	1.643	Crystalline (Cubic)	2.981	0.94
Ge	Germanium (coated)	4.025	Crystalline (Cubic)	5.33	0.97
Al_2O_3	Sapphire	1.675	Crystalline (Tetragon)	3.98	0.93
MgF_2	Magnisum Fluoride	1.34	Crystalline	3.18	0.97

2.5 The Range

The solution to the problem of determining the maximum range by using the design parameters mentioned in (chapter one) at which an IR device can detect a target requires the following details: **(a)** the analysis of the spectral radiant properties of the target, **(b)** the absorption in the intervening space, **(c)** the characteristics of the radiation-gathering system, and **(d)** the response of the passive-range equation. The parameters affecting

the range are, for example, target emission characteristics, atmospheric attenuation, detector parameters, radiation collection system, and background characteristics [**Larmore 1959**].

In many applications of interest, the maximum range in which an IR system can detect or track the target is required. A generalized range equation is therefore necessary to show the design tradeoffs available to the system engineer. The only prior assumption is that the limiting source of system noise is that from the detector. If this condition is not met because of poor design or improper installation procedure, the detection range will be less than that predicted by the generalized equation [**Hudson 1969**].

The range calculations have some of complexity and difficultly because of the many parameters shared within. These parameters derived from the basic concepts of emitting, transporting, and transmitting the infrared radiation through different mediums. The spectral irradiance from an unresolved target is

$$H_\lambda = \frac{I_\lambda \tau_a(\lambda)}{R^2} \tag{2.42}$$

where τ_a is the spectral atmosphere transmittance of the path between sensor and the target, R is the range distance to the target, and I is the spectral radiant intensity of the target *(W/Sr).* A spectral radiant power incident on the detector is

$$P_\lambda = H_\lambda A_o \tau_o(\lambda) \tag{2.43}$$

where A_o is the area of the entrance aperture of the optics (cm^2) and $\tau_o(\lambda)$ is the optical transmittance. The signal voltage from the detector is

$$S = P_\lambda \Re(\lambda) \tag{2.44}$$

where $\Re(\lambda)$ is the spectral responsively of the detector (*V/W*). For real spectral interval, the signal voltage can be found by integrating over the interval

$$S = \frac{A_o}{R^2} \int_{\lambda_1}^{\lambda_2} I_\lambda \tau_a(\lambda) \tau_o(\lambda) \Re(\lambda)\, d\lambda \qquad (2.45)$$

The signal-to-noise ratio is found by introducing the RMS value of the noise from the detector [**Larmore 1959**]

$$S/N = \frac{A_o}{NR^2} \int_{\lambda_1}^{\lambda_2} I_\lambda \tau_a(\lambda) \tau_o(\lambda) \Re(\lambda)\, d\lambda \qquad (2.46)$$

Unfortunately this equation cannot be solved implicitly since the atmospheric transmission term is a function of λ and *R*. The other wavelength dependent terms complicate the evaluation of the expression because the integration involves. So, the term $I_\lambda\, d\lambda$ is replaced by *I*, the radiant intensity between λ_1 and λ_2. The term $\tau_a(\lambda)$ is replaced by τ_a which is the average value of the atmospheric transmission between λ_1 and λ_2. Similarly, $\Re(\lambda)$ is replaced by $\Re$ which is the average value of the responsibility between λ_1 and λ_2. Adopting these changes, the solution of equation (2.46) be

$$R = \left[\frac{A_o I \tau_a \tau_o \Re}{N(S/N)} \right]^{1/2} \qquad (2.47)$$

the performance of the detector is more appropriately described by detectivity (D^*) than its responsively

$$\Re = \frac{S}{HA_d} \qquad (2.48)$$

where A_d is the area of the detector, and D^* is the detectivity given as

$$D^* = \frac{S(A_d B)^{1/2}}{NHA_d} \tag{2.49}$$

where B is the equivalent noise bandwidth (Hz).

then $$\Re = \frac{ND^*}{(A_d B)^{1/2}} \tag{2.50}$$

if the instantaneous field of view of the sensor is *IFOV* (Sr), the area of the detector is found it in equation (1.2).

where f is the equivalent focal length of the optics, which given as follows [**Boutry 1961**]

$$\left.\begin{aligned} f_{lens} &= \frac{-r_1 r_2}{(n-1)[r_1 - r_2 - \frac{(n-1)}{n}t]} \\ f_{mirror} &= \frac{r}{2} \end{aligned}\right\} \tag{2.51}$$

where r_1 and r_2 are the radii of the curvature, n is the refractive index, and t is the thickness of the lens, while r is the radius of curvature of the mirror. So the effective focal length (f) of the system consist of lenses and mirrors given by

$$\frac{1}{f} = \frac{1}{f_1} + \frac{1}{f_2} - \frac{t}{f_1 f_2} \tag{2.52}$$

It is convenient to characterize the optics by their numerical aperture *NA*

$$NA = \frac{D_o}{2f} \tag{2.53}$$

where D_o is the diameter of the entrance aperture of the optics. By substituting these values and replacing A_o by $\pi D_o^2 / 4$, the range equation becomes

$$R = \left[\frac{\pi D_o (NA) D^* I \tau_a \tau_o}{2(IFOV \times B)^{1/2}(S/N)}\right]^{1/2} \tag{2.54}$$

In order to see more clearly how the various factors affect the maximum detection range, it is convenient to regroup the terms as follows [**Hudson 1969**]:

$$R_{\max} = [I\tau_a]^{1/2}[\frac{\pi}{2}D_o(NA)\tau_o]^{1/2}[D^*]^{1/2}\left[\frac{1}{(IFOV \times B)^{1/2}(S/N)}\right]^{1/2} \qquad (2.55)$$

The first term $[I\tau_a]$ is related to the weather conditions. The second term $[(\pi/2)D_o(NA)\tau_o]$ depends on D_o and NA of the optical system design of the homing head. The third term represents the detectivity D^*. The fourth term $[1/((IFOV \times B)^{1/2}(S/N))]$ includes the optical system characteristics according to the signal processing principles. In order to use the equation (2.55) for the homing head system analysis, the radiant intensity of the target as a function of the angles should be taken into consideration.

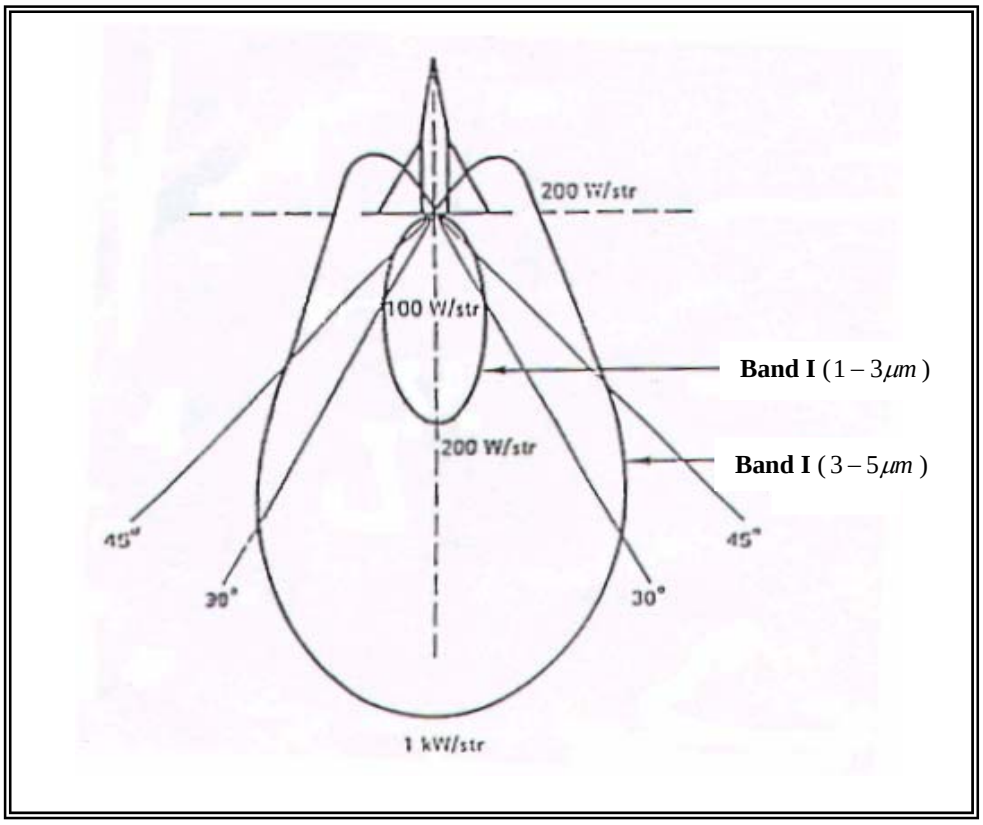

Figure 2.11: Radiant intensity versus angles [**private communication**].

Lambert's cosine law states that the radiant intensity is proportional to the cosine of the angle measured from the normal to the surface of the source. Therefore, the cosine distribution can be used to describe the angular distribution of radiant intensity through a view angle from a radiating source by the following form [**Nussbaun 1998**]

$$I = I_o \cos\theta \tag{2.56}$$

where, I is the distributed intensity, I_o is the maximum intensity, and θ is the view angle of the homing head with respect to the normal of the source surface [**Hudson 1969**] as shown in figure 2.11. Thus, the final range equation should be angle dependent and can be written as:

$$R_{\max} = [I_o \cos\theta\, \tau_a]^{1/2}[\frac{\pi}{2} D_o(NA)\tau_o]^{1/2}[D^*]^{1/2}\left[\frac{1}{(IFOV \times B)^{1/2}(S/N)}\right]^{1/2} \tag{2.57}$$

The detail analysis of this range equation is given in chapter four.

Chapter Four

COMPUTATIONAL RESULTS AND DISCUSSION

Chapter Contents

4. COMPUTATIONAL RESULTS AND DISCUSSION

4.1 Introduction

The optics part of the IR homing head is the field of interest since the current main goal is to design an optical system for IR homing head and analyze all the effective parameters of the suggested system. Knowledge in this field has been kept confidential and publications have been classified. Therefore, any investigation in this field requires a good knowledge of the physical principles related to the design and detection processes in addition to high level programming.

The present computational work passes through four stages. The first stage is improving the optical system design (OSD). The improvement is carried out by changing the material of the dome with a newly used material has an additional characteristics related by its plentifulness and industrialization technique. The features of the adopted optical system are fitted to make its performance is better. This stage regarded as a production of new generation with same characteristics and less cost.

The second stage is descriptive investigation utilize to choose the optical parameters that describe the performance of the suggested OSD. The chosen effective parameters are used to determine the efficiency of the suggested OSD. The third stage is the calculations stage, which includes the effective parameters determination in addition to maximum range evaluation. The fourth stage includes a quantitative and qualitative analysis on the results of both the effective parameters, which indicates how the suggested system is capable to perform good imaging, and the range results at different expected situations which is a function of how

the suggested OSD can be safely applied practically. The following block diagram in figure 4.1 shows the main sequence of operations of the computational work.

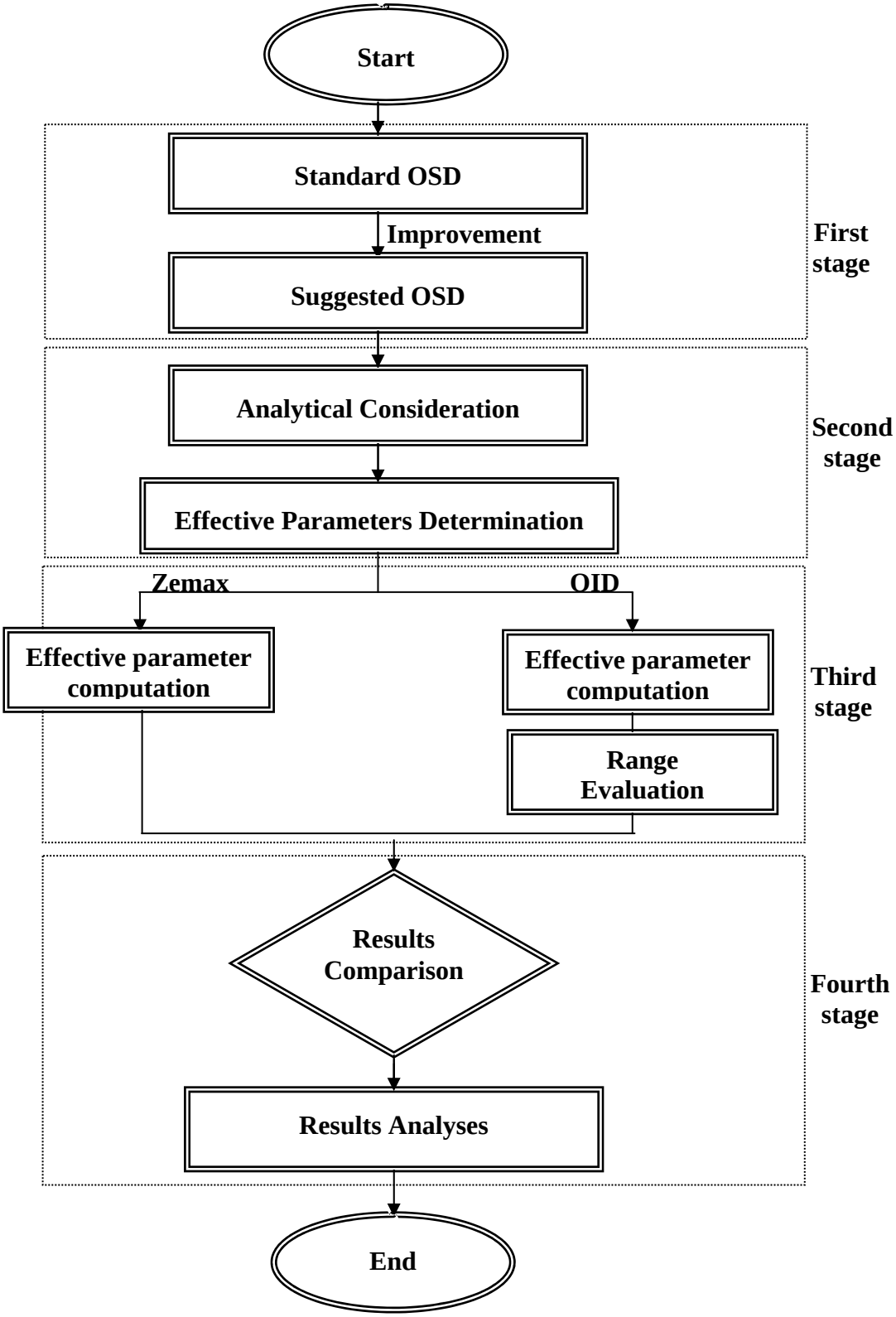

Figure 4.1 Block diagram of the sequential operations of the present computations work

4.2 OSD Improvement

The improvement process covers two topics, the ***optical materials improvement*** and the ***optical elements improvement***. The optical materials improvement includes changing the optical materials of the dome which greatly affect the performance of the OSD. The optical elements improvement includes fitting the optical features of the elements in the system in order to focus the rays that defocus due to change of dome material. The improvement is done by means of Zemax software. This software can model, analyze, and assist in the design of optical systems. It allows very rapid interactive design. Selecting options from either dialog boxes or pull-down menu provide accesses to most Zemax features. Figure 4.2 shows a standard OSD used normally in homing heads, while table 4.1 presents the optical features of each element share in this design of interest

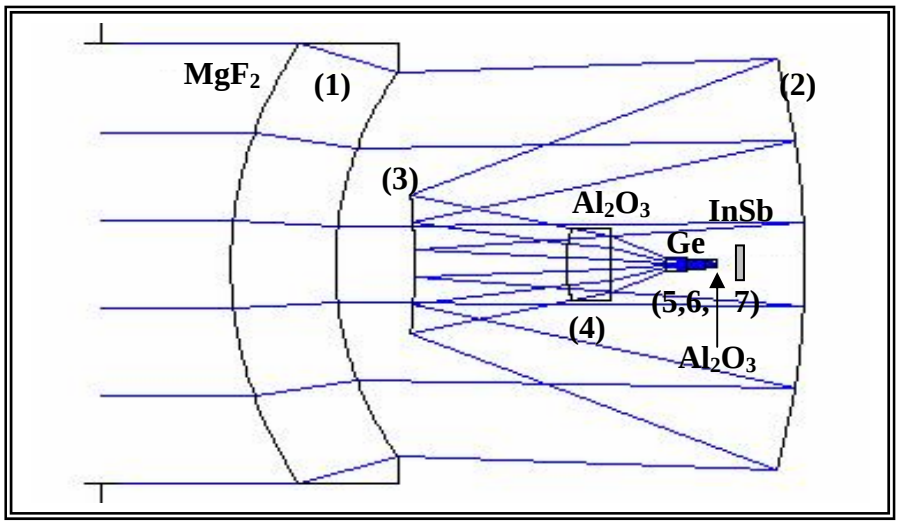

Figure 4.2 Standard OSD of a homing head
[**Mohammed and Mustafa 2000**].

The improvement has been carried out on this standard design to achieve an improved one. The following brief account describes how the improvement process has been performed on each element in the system

Table 4.1: Optical data of the standard design.

S. no.	R_1(mm)	R_2(mm)	Thic(mm)	Dist (mm)	Element type	Material
1	36.73	33.5	3.23	10	Lens	MgF_2
2	-82	-82	0	34	Mirror	
3	-141.25	-141.25	0	-29	Mirror	
4	46.88	-115.8	1.80	10.56	Lens	Sapphire
5	Infinity	4.70	3.20	3.66	Lens	Germanium
6	-2.66	Infinity	2.80	0	Lens	Germanium
7	-2.89	1.25	1.25	0	Lens	Sapphire

4.2.1 Optical Material Improvement

In the current suggested optical system design, the conventional dome material MgF_2 single crystal of refractive index 1.34 has been replaced by newly chosen material $CaAl_2O_3$ (calcium aluminized glass) of refractive index 1.643. The replacement make the refraction of income rays is greater. In order to fit the suggested design and make the focusing is possible, the radius and thickness of the dome have both been changed.

4.2.2 Optical Element Improvement

This improvement takes into consideration some important parameters such as the relatively large diameter of the aperture and the proper size optical system. The improvement process implemented on each optical element was performed by the following manner.

(a) dome diameter (aperture)

The diameter of the dome has a considerable effect on the system operation. The diameter of about 7 cm will receive more radiations and this requires a large diameter and higher curvature for the primary mirror in order to be able to collect all the rays incident on the face of the secondary mirror. From the present investigation, it has been found that the large diameter of the dome causes distortion to the spot, which becomes far from being perfect. The spot in this case is characterized by a series of bright rings around the center as shown in figure 4.3-a.

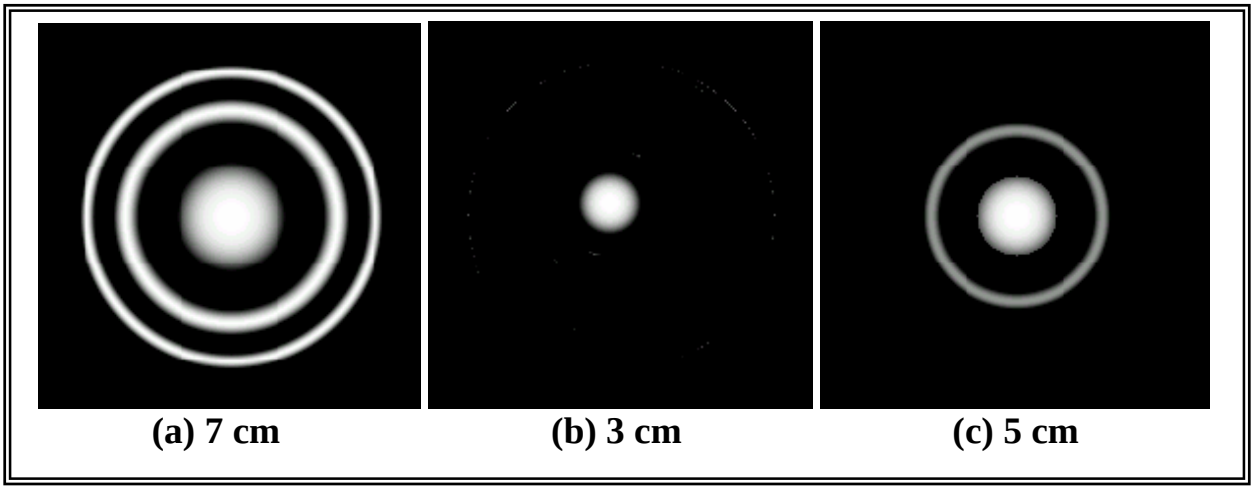

(a) 7 cm **(b) 3 cm** **(c) 5 cm**

Figure 4.3 Diagram of spots for different aperture diameters.

A 3 *cm* diameter of the dome allows fewer rays to be received which are close to the optical axis. These rays produce a clear spot with small size and the bright rings disappear because of the reduction in aberration. This case however cannot describe the spot image well since the spot size is very small because of the few IR radiations received. The spot of very small size shown in figure 4.3-b is not useful for the purpose of tracking.

Depending on the above analysis, one can conclude that a dome of about 5 *cm* in diameter is very proper to describe the spot image since the spot will be clear and the amount of diffraction is very small. Therefore,

this value of the dome diameter is adopted in the suggested OSD in order to produce the intended spot as that shown in figure 4.3-c.

(b) dome distance

The optical system size means the size of the constituent optical elements and their distance of separation, in addition to their diameter, curvature, and thickness. The size of the adopted optical system is represented by the dome aperture and the distance between the dome and the primary mirror that has been fixed at 3.6 cm.

(c) primary mirror

The function of the primary mirror is highly affected by its distance from the dome. The computations have shown that increasing the dome-primary mirror distance will give rise to closer angles of reflection for the off-axis and paraxial rays; thus better focusing will be achieved. Therefore, one can say that a high quality spot depends, among other parameters, on the distance between the dome and the primary mirror. However, there is a limitation to this distance. A short distance requires a high radius of curvature for the primary mirror to enable the rays to be collected on the surface of the secondary mirror. In this case it has been noticed that the off-axis and the paraxial rays will be reflected towards the secondary mirror at angles where the difference between them is high. This situation will lead to poor focusing. The above discussion shows that the distance between the dome and the primary mirror in the suggested optical system design will limit the curvature of the primary mirror.

(d) secondary mirror

The radius of curvature of the secondary mirror is related to the distance separating it from the primary mirror. A small radius of curvature of the secondary mirror will increase the reflection angles of the

rays which are collected in the vicinity of the secondary mirror that makes focusing on the detector rather difficult. However, a secondary mirror of large radius of curvature will make the rays to be collimated on the optical axis far from the mirror due to angles of reflection. This case would require that the secondary mirror should be followed by a correction lens of the double convex type with large radii of curvature. Therefore, it is important that the curvature of the secondary mirror need to be at a value which makes the reflected rays very close to the convex lens and hence the correction lens will need small curvature for better focusing.

(e) correction lens

The double convex correction lens is the fourth element in the optical system. It has an important role in the focusing process. Its position from the secondary mirror is at a distance less than its focal length which has the advantage of keeping the image erect up to the detector's position. In addition, the value of its radius of curvature should be such that the emerging rays are collimated very close to the optical axis.

(f) collection lens

The collection lens is the last optical element that will be included in the improvement process. It is used for focusing the rays on the detector. It is possible to use a combination of lenses for better performance. There are two important parameters in the improvement for this lens (or lenses) namely, the radius of curvature of both surfaces of the lens and its thickness. These two parameters may be employed to achieve the intended focusing in order to collect the radiation to form a desirable spot.

4.3 The Suggested OSD

The processing of aberration is a very important task in the optical system design, because of its high effect on the image quality. The long range optical system design consists of two optical parts. The first is the ***correction part*** whose function is to reduce the optical aberrations, and the second is the ***collection part*** which is used to collect the radiation and form an image by the focusing process. In the present work only the spherical aberration and defocusing have been taken into account whereas other aberrations have been neglected due to they were processed well, which make their effect is little on the image quality. Moreover, the spherical aberration and defocusing are reduced by changing the features of some optical elements in the correction part, in order to bring them to the lowest possible value.

The suggested optical system design consists of the two above mentioned parts. The correction and collection parts consist of four and three optical elements respectively. The following is a brief description of the optical elements of these two parts (see figure 4.4).

(a) dome

The dome is a meniscus lens used to separate the received radiation on the face of the second element (primary mirror, **b**). The material of the dome is $Ca.Al_2O_3$, which has desirable optical properties.

(b) primary mirror

The primary mirror is a concave one used for receiving the radiation traversing the dome and deliver them to the surface of the third element which is the secondary mirror, **c**. It may also be used to reduce the spherical aberration.

(c) secondary mirror

The secondary mirror is a convex one where the radiation coming from the concave mirror are reflected to be collimated by the fourth element, **d**. The function of this mirror is to bring back the radiation towards their original direction at a higher density and close to the optical axis**.**

(d) correction lens

It is a plano-convex lens used to correct spherical aberration. It also converges the radiation towards the collection part. Figure 4.4 shows the correction part of the optical system design where the radiation passes through the dome and then converges by other elements, while table 4.2 lists the optical features of each element in its structure.

(e) collection lenses

They have the most effect on the focusing and the change of their characteristics will make the rays to be more dispersed. Thus, their material remains germanium, while their optical features are varying according to the need of focusing. The detector represents the last surface in the optical system. The main purpose of the collection part is to collect and focus the radiation on the optical axis to produce a spot image on the detector's active area. The spot size must have a small value (about 50% of the detector's diameter or that of the reticle spoke or less). The smallest size of the spot requires the solution of the following two important problems in order to achieve high resolution:

(i) Reducing spherical aberration to the lowest possible value, which is the task of the correction part.

(ii) Good focusing by the system elements which is the task of the collection part.

Actually, the second problem cannot be avoided unless the first is solved, i.e. the defocusing is always associated with the aberration. In the suggested design, fitting the radius of curvature, thickness, and distance between the optical elements solve both problems.

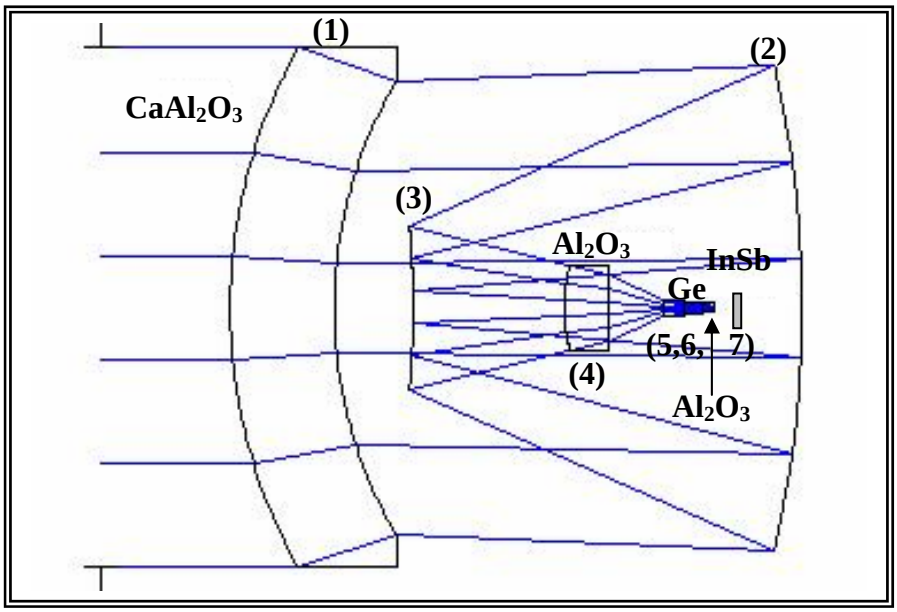

Figure 4.4: Complete suggested OSD.

Table 4.2: Optical data of the suggested OSD.

S. no	R_1(mm)	R_2(mm)	Thic(mm)	Dist (mm)	Element type	Material
1	40.81	34.31	8.00	10	Lens	$CaAl_2O_3$
2	-82.16	-82.16	0	36	Mirror	
3	-73.11	-73.11	0	-29.93	Mirror	
4	12.70	Infinity	3.40	11.65	Lens	Sapphire
5	Infinity	20.00	1.23	4.25	Lens	Germanium
6	-1.60	Infinity	0.30	0	Lens	Germanium
7	-1.00	Infinity	0.11	0	Lens	Sapphire

4.4 Analytical Considerations

The analytical consideration aims to show what are the effective parameters that can provide complete indication about how efficient the suggested OSD. Since the function of the OSD of an IR homing head is to detect and track a distant object, the accuracy of the calculations is very important. In order to achieve high accuracy, an analytical study on how to determine the effective parameters of the optical system has been performed. The analysis includes a test for some of well–known optical functions at different amounts of aberration and defocusing, then studying their behavior and how they are affected.

Zemax software has been used to present the behavior of the effective parameters correspondent to different amounts of spherical aberration. These aberrations are created by change the radius of curvature of the primary mirror to be –81.96, -82.06, -82.16, -82.26, and –82.36 *mm*. The results showed different amount of spherical aberration coefficient C_{040} of about 3.69, 4.54, 6.14, 8.77, and 12.77 while associated the defocusing coefficient C_{020} was about 9.29, 9.27, 9.26, 9.21, and 9.12 respectively at the middle infrared region ($\lambda = 4\ \mu$m). The increasing the radius of curvature of the primary mirror causes to increase the spherical aberration that simultaneous to the decrease of defocusing. It is seen that the adopted value in the suggested design (i.e. –82.16 *mm*) is the best since both the aberration and defocusing are balancing at best situation as shown in figure (4.5). It is expected that the condition of all the optical function be worse by going far from this value, but the important is choosing the greater changed function to be considered to use as an effective parameter in the current research.

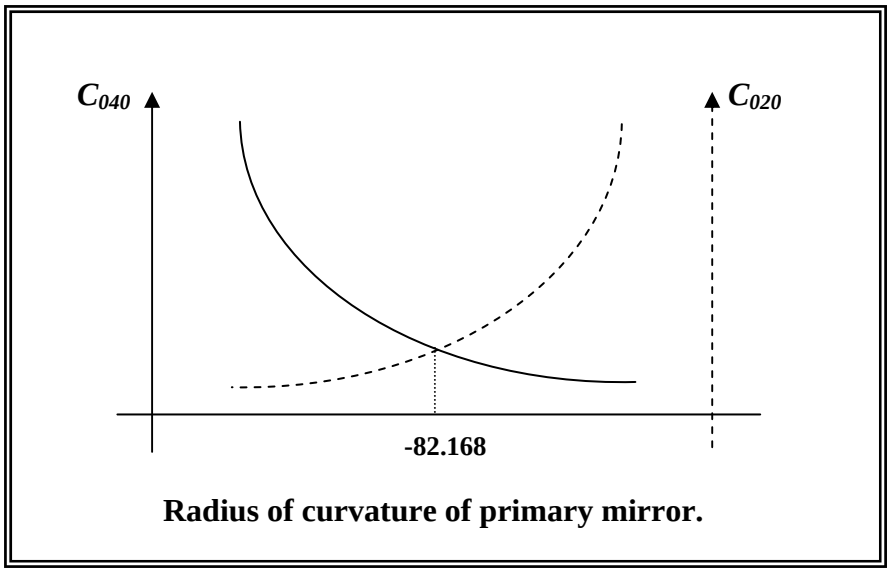

Figure 4.5: C_{040} and C_{020} behaviors.

The four cases of C_{040} and C_{020} are considered successively, the effect of the aberration and defocusing are noticed on the behavior of some utilized optical functions. According to the variation in the behavior of the optical function due to the aberration, the effective optical functions PSF,MTF, Spot diagram, and Spot size are chosen to be effective parameters for the suggested design. The following is a qualitative presentation on the behavior of the optical functions that found useful to specify the efficiency of the optical system, figures numbered (1), (2),… (5) belong to the five considered cases of aberration.

4.4.1 Point Spread Function

PSF determines the energy distribution in the image plane due to a point source located at the object plane, i.e. the paraxial image "point" at the image plane "speared" out. Therefore, PSF can be regarded as a measure for how efficient the optical system in spatial domain.

With no aberration the spread function is the Airy disc with rings centered at the point image plane. Since pupil function is real and

distributed according to the circle function, the PSF distributed according to the first order Bessel function documented by equation (3.71) which contains a central spot surrounded by diffraction rings.

In the current case of the suggested system, both diffraction and aberration exist. Thus, the pupil function is complex following equation (3.66). The complex pupil function make PSF distributed according to the zero order Bessel function. Because of existing the aberration term in the equation that describe the behavior of the PSF, the energy dispersed about the center of the image which may be leads to strengthen the brightness of the rings or increasing their number. Figure 4.6 shows the shapes of the PSF for the considered values of both C_{040} and C_{020}, which presents the behavior of the PSF for different amounts of aberration and defocusing.

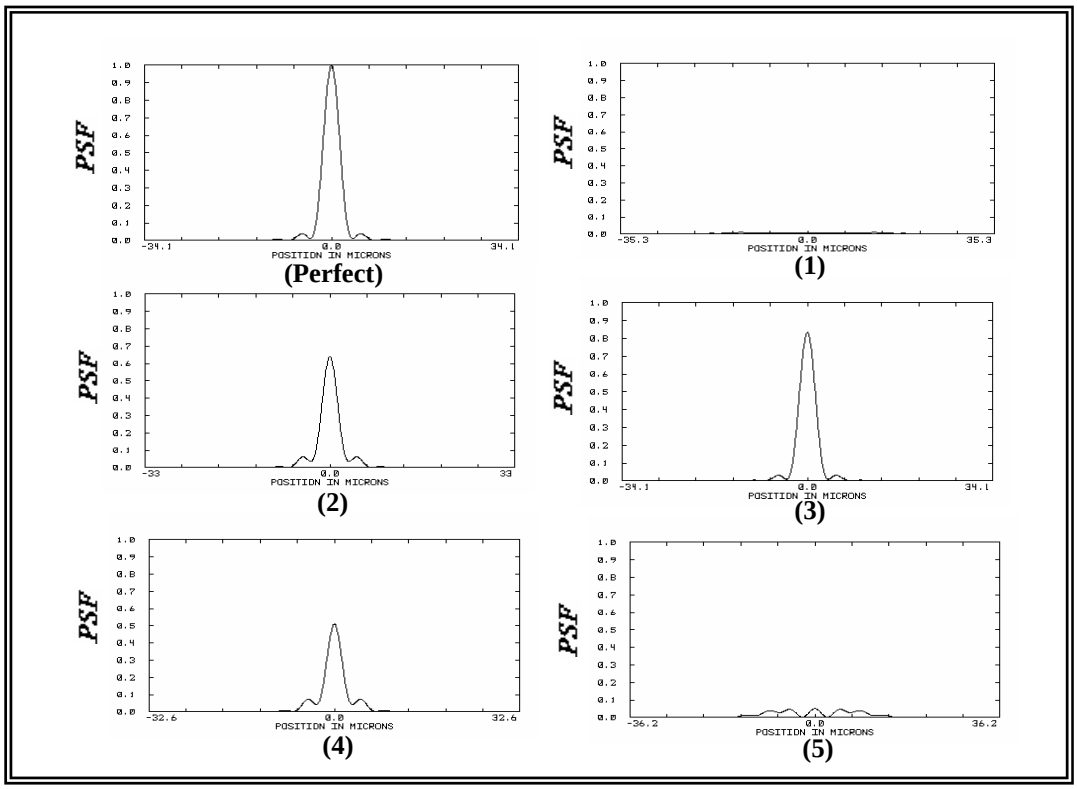

Figure 4.6: Different shapes of PSF versus aberration and defocusing.

It is seen that by increasing the aberration or defocusing, the amplitude of PSF is decreased and the surrounding ring is raised and their number may be increased, which ensure great sensitivity of PSF for the small changes of aberration.

4.4.2 Modulation Transfer Function

MTF is one of the most important parameters determines the efficiency of the optical system. MTF is very sensitive to many different types of aberrations. It may be described by a set of points as a function of frequency. A plot of this sort has a maximum value at zero frequency, which means that the OSD receives all the information of zero frequency. The relations refer that the maximum value of this curve is unity; therefore, it is a normalized curve. In other words, MTF values corresponding to a specific value of frequency in the MTF curve represents the percentage of the OSD to receive the information at that frequency. Therefore, the MTF value corresponding to a specific frequency indicates the amount of image contrast relative to the object contrast.

Analytically, MTF for an ideal image formed by an ideal OSD takes a value of unity at all frequencies, as shown in figure 4.7-a. It is seen that there is no cutoff frequency (i.e., all frequencies will pass through OSD) and the resolution of the images is identical to that of the object (i.e. the resolution percentage is 100%; natural). However, if the OSD is not good enough, where a dark image exists, the expected MTF will be as shown in figure 4.7-b; its values equal to zero for all frequencies (i.e. the resolution percentage is 0%), which implies that the cutoff frequency is equal to zero (i.e. no frequency will pass through OSD).

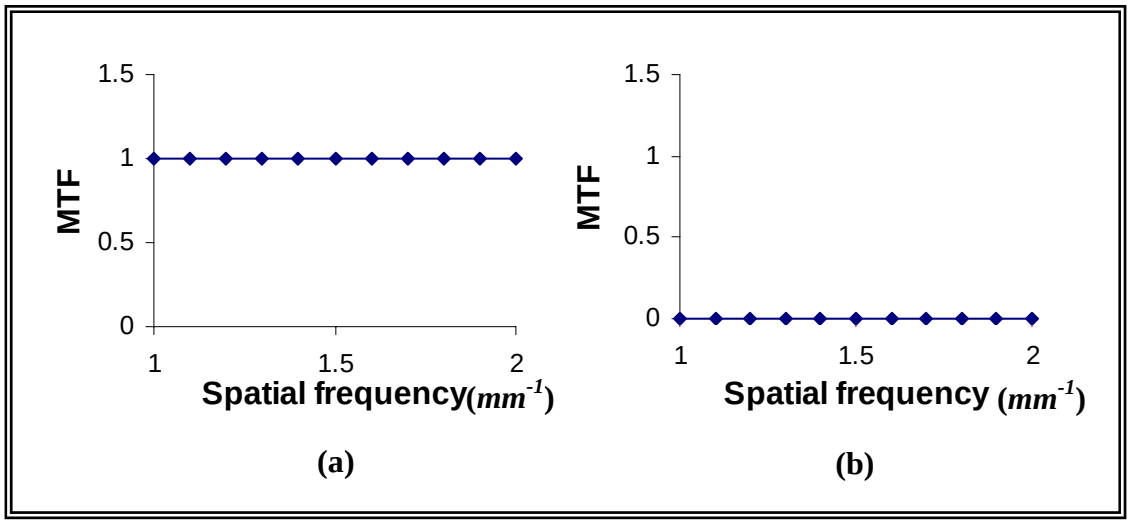

Figure 4.7: **(a)** Ideal MTF **(b)** Worse MTF.

If one deals with a perfect OSD, then the image will have a specific contrast and the behavior of MTF distribution depends on the frequency and its curve will decrease with increasing frequency until it reaches a zero value at the cutoff frequency. The computed MTF curve shown in figure 4.7-c is for a perfect optical system (i.e. there is no aberration).

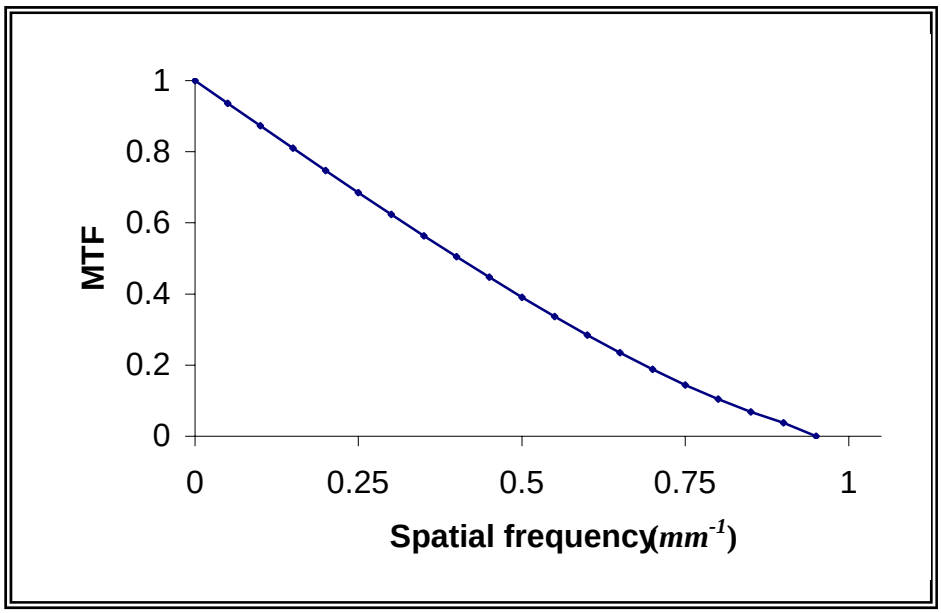

Figure 4.7: (**c**) Perfect MTF.

When an optical system has some aberrations its MTF curve will be different from that of the perfect one by its slope and behavior especially in the high frequency region, where the amount of the decay will increase and is proportional to the aberration. The signal in this region diffused with the background noise since both of them have same frequency, which interpret the oscillations occurred in the high frequency region.

In order to show the variation of MTF with the aberration, the amounts of aberration and defocusing agreed previously have been considered. Figure 4.8 shows the behavior of the MTF comparing with the perfect MTF for different amounts of aberration and defocusing, which prove the great sensitivity of the MTF curve to the aberration and defocusing. It is seen that the curve of the middle case is the best since it near to the perfect case. Also, the defocusing affect the decay of the MTF curve, while the aberration affects the smooth behavior of the MTF curve.

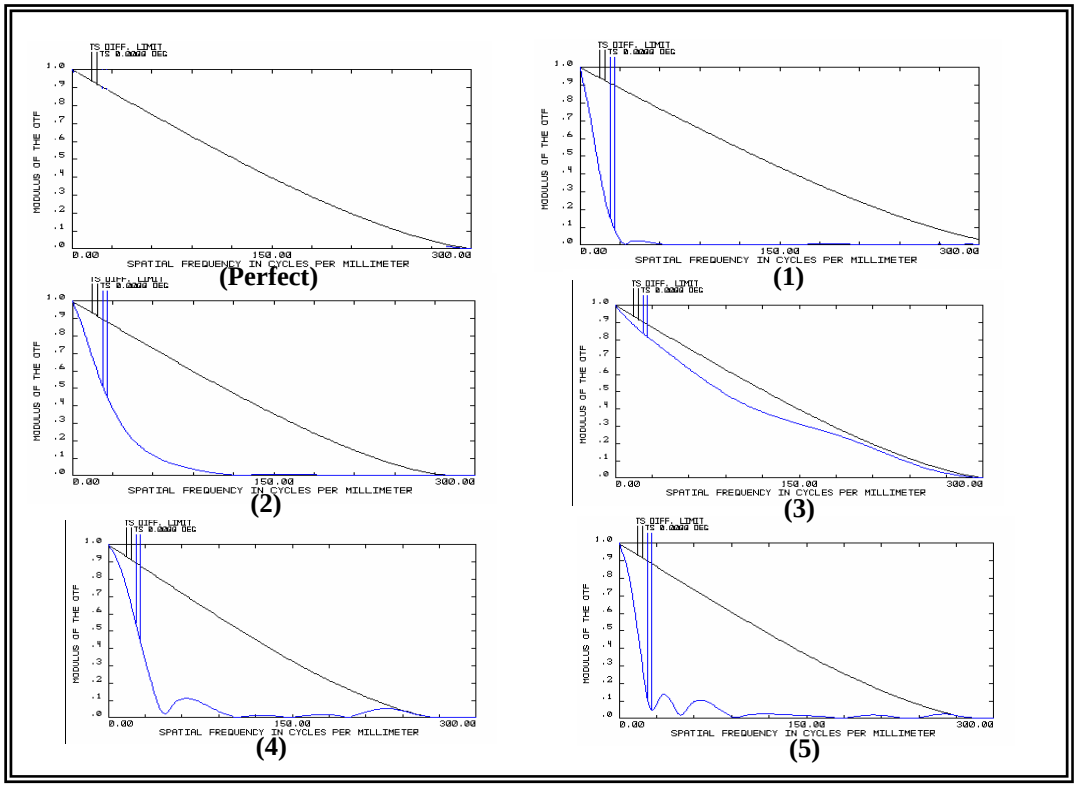

Figure 4.8: MTF curves for different amounts of aberration and defocusing.

4.4.3 Spot diagram

The resulting image achieved by any optical system is Gaussian distributed. The perfect system consist a perfect image diagram, which is a Gaussian illuminated with some of dim ring due to diffraction.

In the current case of suggested system, the image contains on a central bright spot of shape depending on the amount of aberration exist on the suggested optical system. Figure 4.9 shows the consideration of different amounts of aberration and defocusing. It seen that the aberration determines width of spot, number of surrounding rings, and their illumination, where the size of the central spot is appearing greater by increasing the amount of aberration or defocusing, also the number of the rings and their illumination are increased by increasing the amount of aberration or defocusing. Moreover, the aberration affects the number of rings around the central spot, while the defocusing affect the width of the central spot.

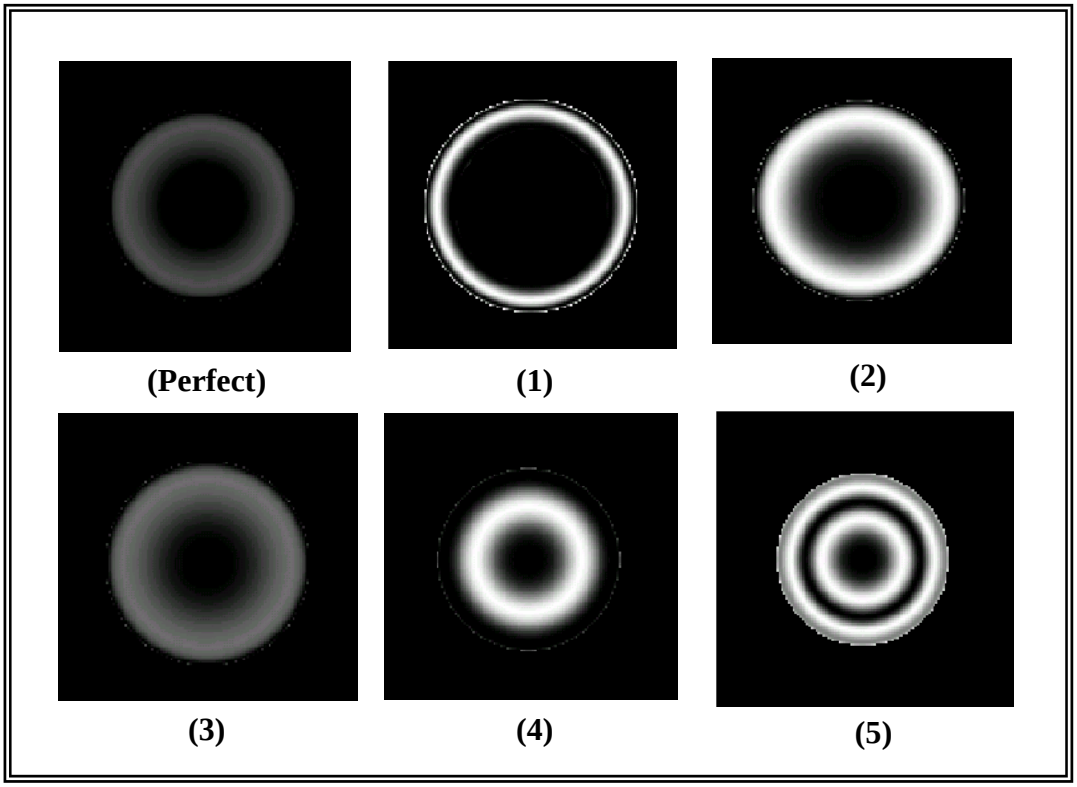

Figure 4.9: Spot diagram for the six values of C_{040} and C_{020}.

4.4.4 Spot Size

It is well-known the spot size is related by the depth of focus. In order to study the behavior of the spot size in the absence of aberration (with diffraction limit), equation (3.76) can be adopted. For the middle IR region at $\lambda = 4\mu m$, the *f/no* is the parameter affecting the spot size alone. In order to study the effect of *f/no* on the spot size, one can achieve different values for *f/no* by changing the curvature of the primary mirror in the suggested OSD. The different values of *f/no* are taken to be less than one, they give corresponding values for the spot size according to the linear relationship plotted in figure 4.10, which indicates that the slope of the linear relationship is equal to 2.44λ while the intercept is equal to zero.

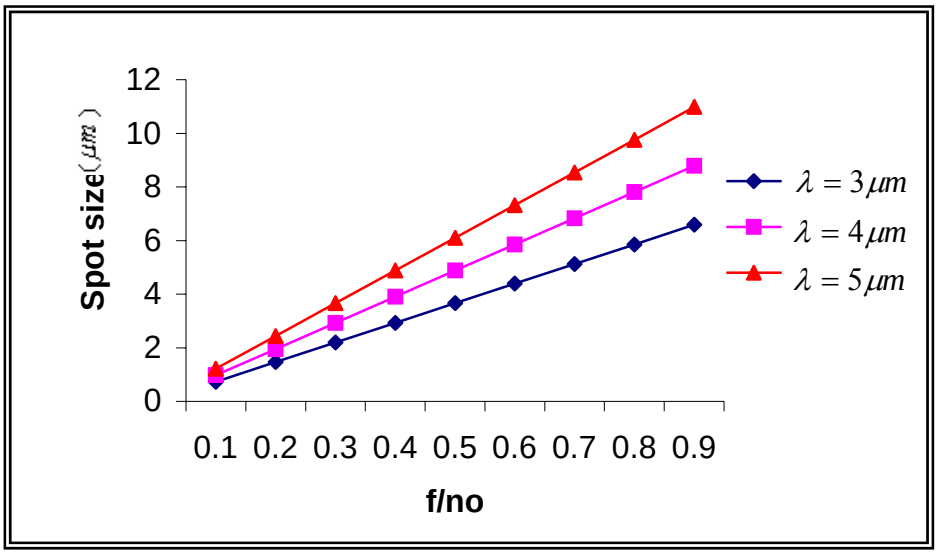

Figure 4.10: The spot size as a function of focal number (diffraction limited).

But when one deals with the aberration (without diffraction limit), then another relationship for the spot size depending on equation (3.74) can be employed where the spot size changes with *f/no* and λ as shown in figure 4.11. This figure pictures the reversion of the direct linear relation between the spot size and *f/no* into another is different. It is converted

into; (1) inversely relationship, and (2) exponential relationship. This conversion is due to the additional second term that has third power of *f/no* related by aberration. This term is dominant on the behavior of the spot size, while the divergence kept conserved with same differences in between, which interprets why the behaviors of total spot size for different wavelengths take larger values.

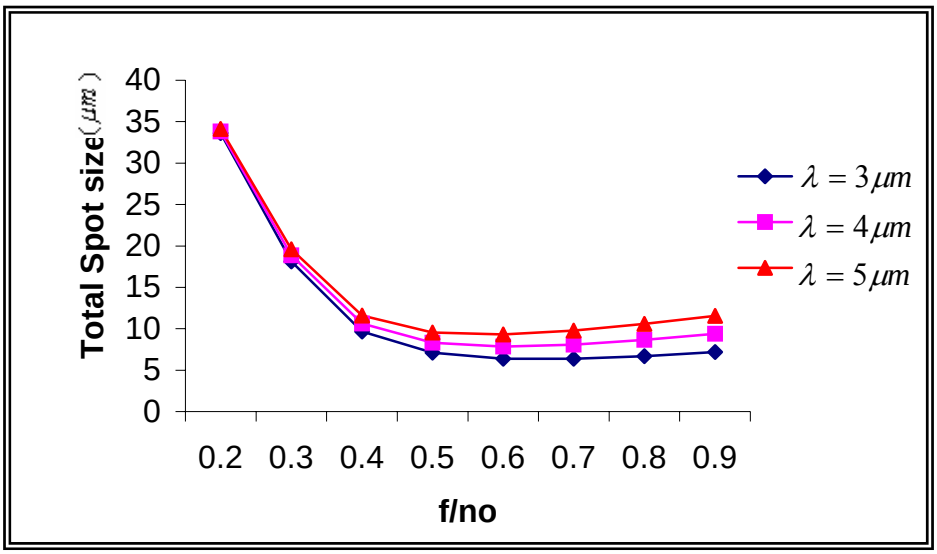

Figure 4.11: Total spot size as a function of focal number.

As a result, the lens produces a minimum spot size when the spot size due to aberration is smaller or equal to the diffraction limited spot size. Spot size due to diffraction increases linearly with *f/no*, whereas the total spot size decreases with *f/no* until a specific situation of minimum aberration at *f/no*=0.5 and then it increase slowly. This indicates that there is an optimum performance point where both aberration and diffraction limit combine to form a minimum spot size by the system. The effect on spot size by aberration is strongly dependent on *f/no* since the aberration term is inversely dependent on the cubic *f/no*. High power contains in equation (3.76) cause to make the total spot size decreases with increasing *f/no*, but it seems to be independent of λ between 3 and 5 μm at *f/no*<0.3 since the three behaviors are very close to each other.

In addition to the aberration, the spot size is mainly affected by defocusing. The effect of defocusing on the spot size is determined by the depth of focus. In order to describe how the defocusing affect the spot size in the suggested system, the depth of focus is computed by equation (3.84) for the considered focal numbers. Figure 4.12 shows the depth of focus as a function of *f/no*. It is noticeable that the decreasing of the spot size by increasing the *f/no* affects the direct relationship between the depth of focus and the *f/no*.

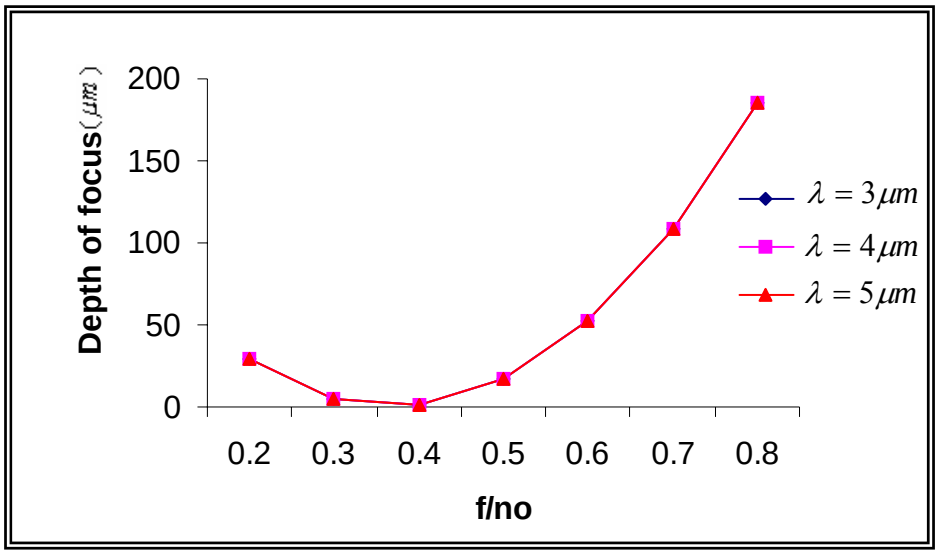

Figure 4.12: Depth of focus as a function of focal number.

The depth of focus (δ') contains minima corresponding to a focal number of 0.4, at *f/no* greater or less than that the δ' is increasing irrespectively. The increasing of δ' at small values of *f/no* is because of the opposite behavior of *Z* reduces the effect of the squared *f/no* in the relation of $\delta'(f/no)$, while increasing $\delta'(f/no)$ at large values of *f/no* is because little effect of spot size (*Z*) on the behavior of δ'. The variation of δ' due to defocusing measure the amount of shifting the image far away from the region of least confusion. The minimum δ' indicates minimum *Z* at least defocusing and indicates the image is taken at the region of least confusion. Also, it is shown that the increasing or

decreasing the *f/no* by same amount give different δ', this lead to conclude that the δ' is asymmetric around the least of confusion region. The irrespective increasing of δ' around the least confusion region is because of the least of confusion lie on 3/2 of the distance expanded from the paraxial focus into merdional focus.

It is should be mentioned that the *f/no* of the suggested system given by Zemax was 0.418, which refer to that the imaging was at the region of least confusion. This result ensures the optical feature improvement carried out previously and pointing to the safe use of equation (3.59) at the next computations.

4.5 Effective Parameters Computations

The proper choice for the effective parameters is the basis that the success of the design depends on, because of these parameters are candidate to describe the performance of the suggested system. The computations need to high level of programming, which prepare to design and implement specific software concern with the field of interest, this software is called ***OID***, which is an acronym for **O**ptical **I**nfrared **D**esign. It has been put forward in the Visual Basic programming language to show the different features of the optical system under consideration. Visual Basic language works through windows operating system, which easily displays the results graphically. By OID software, one can compute the effective parameters needed to describe the performance of any input optical system design; these parameters are ***PSF***, ***MTF***, ***spot diagram***, and ***spot size***.

It was capable to expand the software tasks to include multi-windows in the OID software, where for each interface there is a specific task. There is a specific window, used to input or change the optical features and another one used to display the ray tracing of the design under consideration as shown in figure 4.13 and 4.14.

In the following a detailed explanation about the computations of each effective parameter determined by OID. The result of the adopted parameters is comparing with the corresponding one that extracted by Zemax to ensure the correct path of computations, and then this result is compared with that of the perfect design to indicate how the adopted design is approaching to the perfect case.

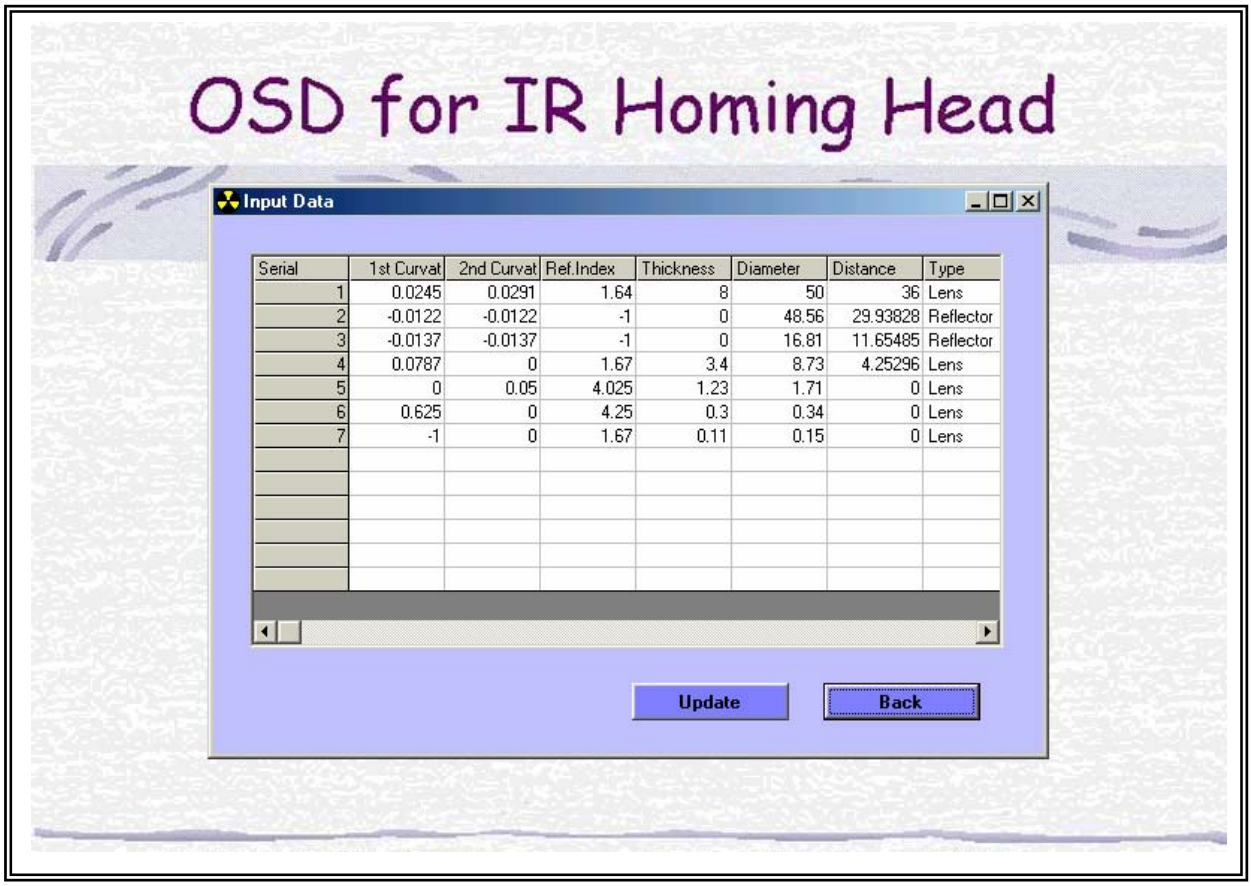

Serial	1st Curvat	2nd Curvat	Ref.Index	Thickness	Diameter	Distance	Type
1	0.0245	0.0291	1.64	8	50	36	Lens
2	-0.0122	-0.0122	-1	0	48.56	29.93828	Reflector
3	-0.0137	-0.0137	-1	0	16.81	11.65485	Reflector
4	0.0787	0	1.67	3.4	8.73	4.25296	Lens
5	0	0.05	4.025	1.23	1.71	0	Lens
6	0.625	0	4.25	0.3	0.34	0	Lens
7	-1	0	1.67	0.11	0.15	0	Lens

Figure 4.13: OID software input data window.

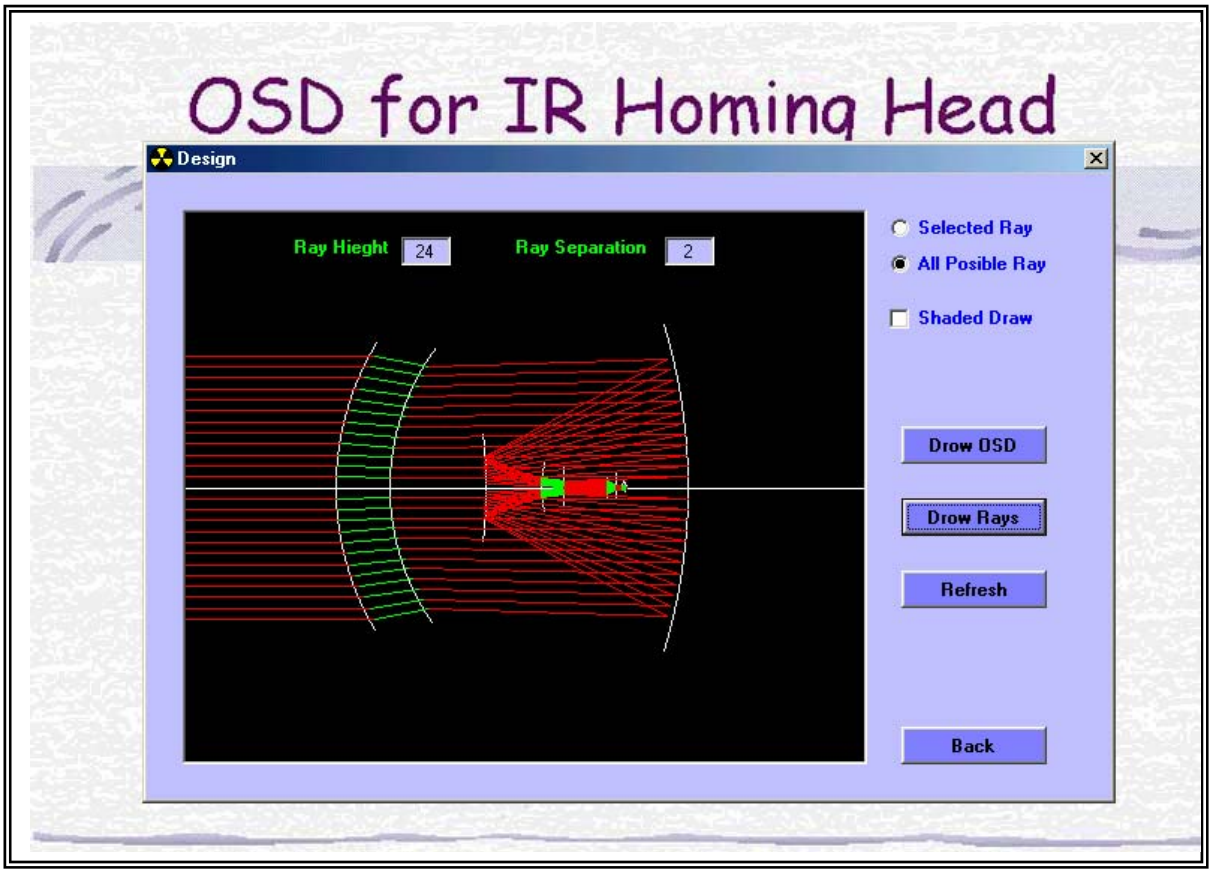

Figure 4.14: Ray tracing diagram by OID software.

4.5.1 PSF Computation

PSF is determined for both two cases of perfect and usual based on two adopted methods. Both of the two methods depend upon the pupil function during the calculations, the calculation of the pupil function is shown in flowchart present in figure 4.16 below.

The important parameter drive the behavior of the pupil function is the wave aberration function *W*. so, it interested to compute C_{040} first. C_{040} is computed depending on the data achieved by the ray tracing with regarding all the surfaces present in the suggested OSD according to the flowchart in figure 4.15. A detailed explanation about each method is presented in the following.

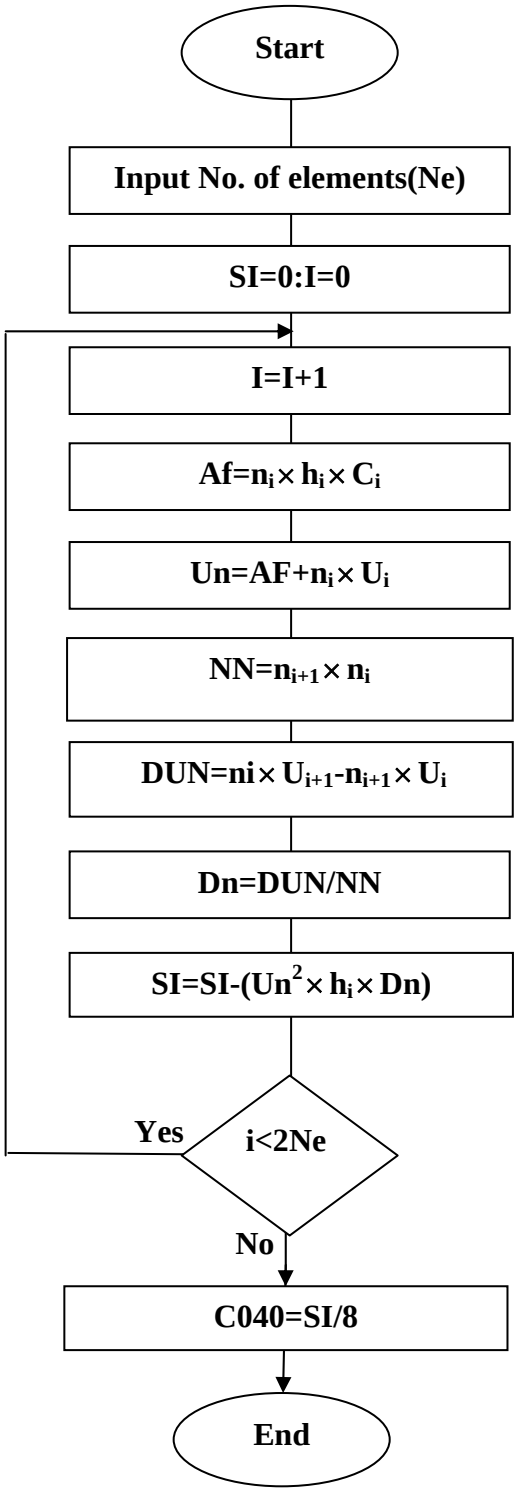

Figure 4.15: Flowchart of computing C_{040}.

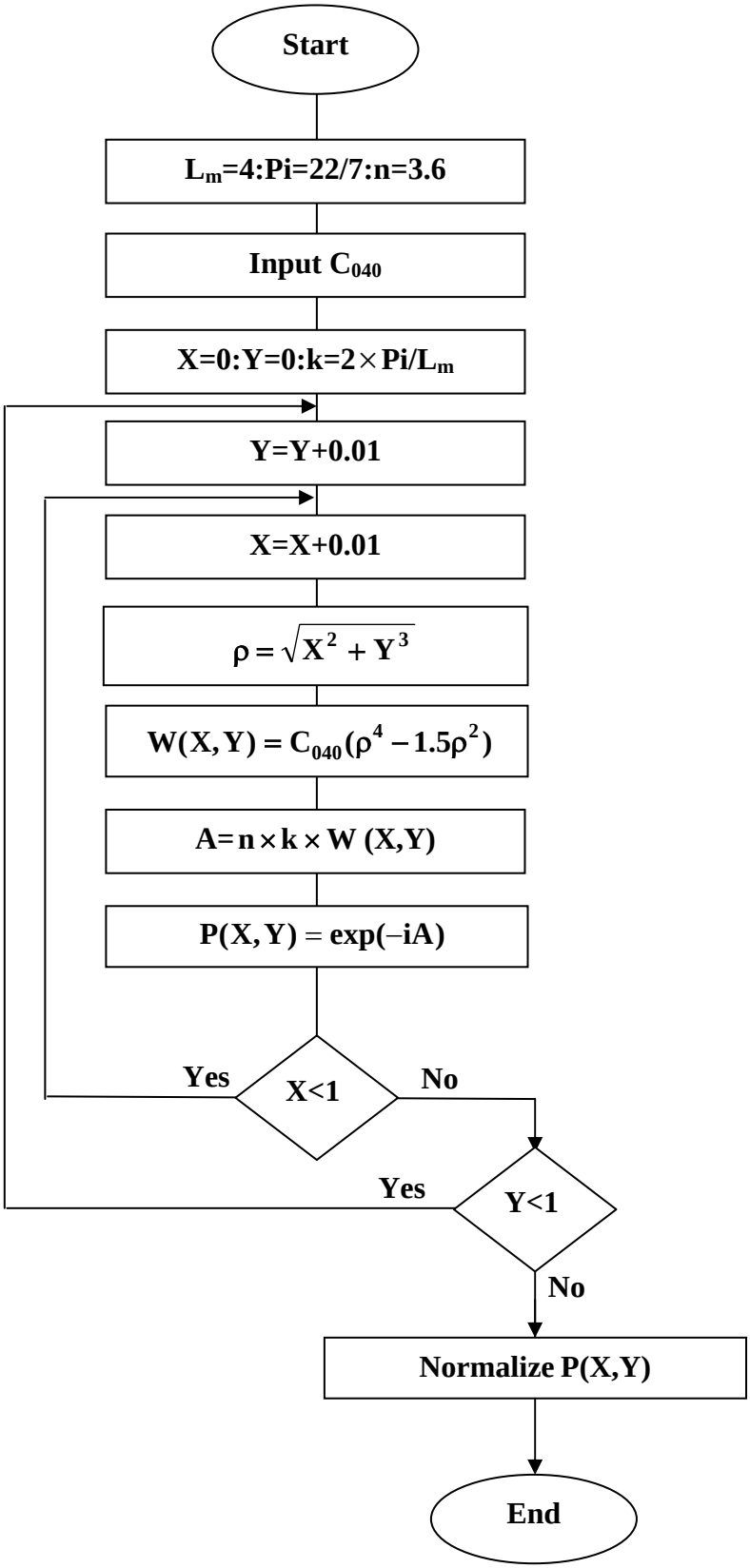

Figure 4.16: Flowchart of pupil function computation.

1. **Mathematical Method**

This method based on equations documented previously for both two cases of perfect and usual. Equation (3.73) is used to determine the shape of perfect PSF. The determination requires computing *f/no* by equation (3.75), which in turn need to find the effective focal length. The effective focal length is computed according to the following algorithm;

By assuming f_1 and f_2 are the focal lengths of the first two elements determined by equation (2.51), the effective focal length for the combination of current two elements in the suggested optical system calculated by using equation (2.52). Another time one can perform the same calculation to compute the new effective focal length for new combination with the next element by regarding the effective focal length is equal to f_1 and the focal length of the next element is equal to f_2. This is continuing until all lenses and mirrors in the suggested system are accounted. The expression for the combination focal length is the same whether the separation distance are large or small and whether f_1 and f_2 are positive or negative. Figure 4.17 present the flowchart of the effective focal length. The results of effective focal length can be shown in spot size results.

The following useful discrete formula of equation (3.73) can be used to determine the shape of the point spread function belong to a perfect optical system.

$$PSF(x,y) = \frac{p\pi}{\lambda^2 (f/no)^2} \left| \sum_{x=0}^{1} \sum_{y=0}^{1} J_o \left[\left(\frac{\pi\rho}{\lambda(f/no)} \right) \rho \right] \rho \right|^2$$

The image is divided into 100×100 points, thus both x and y needed to determine ρ are normalized and take multiples of 0.01 according to the position of the current point in the image.

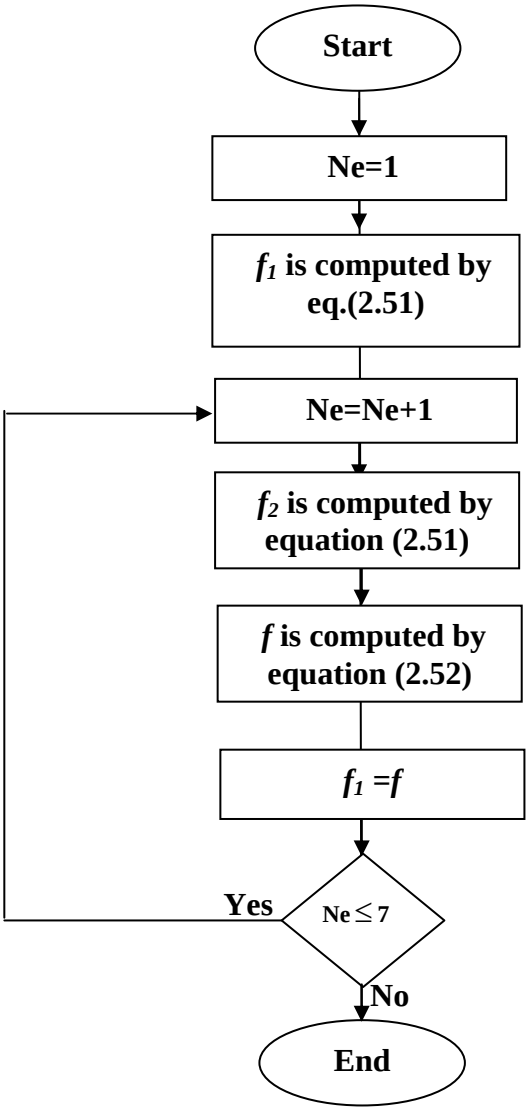

Figure 4.17: Flowchart for compute effective focal length

In the present case, the suggested optical system is usual and has some of aberration and defocusing. Thus, the following discrete formula of equation (3.70) is used to compute the usual PSF.

$$PSF(x,y) = \frac{p\pi}{\lambda^2 (f/no)^2} \left| \sum_{x=0}^{1} \sum_{y=0}^{1} P(x,y) J_o \left[\left(\frac{\pi\rho}{\lambda(f/no)} \right) \rho \right] \rho \right|^2$$

This equation contains an additional term within related by the aberration, which is the pupil function that given in equation (3.66). The flowchart present in figure 4.18 shows the procedure of computing the PSF for the perfect and suggested OSD.

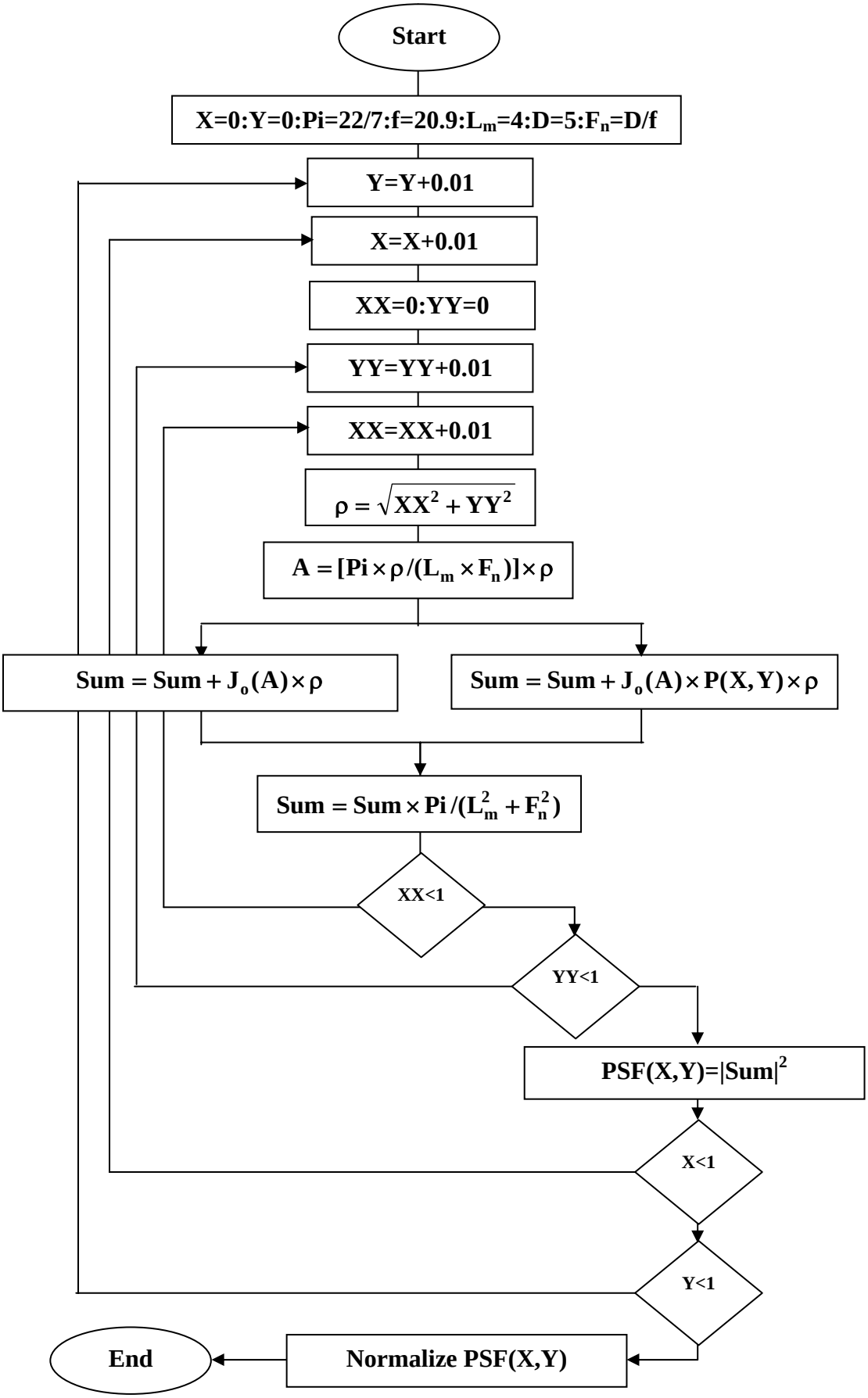

Figure 4.18: PSF flowchart of perfect and suggested OSD by mathematical method.

Figure 4.19-a shows the resulting PSF for the diffraction limited case, while the resulting PSF shown in figures 4.19-b, c, and d represent the averaging shape of PSF for the suggested OSD at wavelengths 3, 4, 5 μm one by once. Actually, PSF is two dimensional function, which is normally plotted as one dimension in purpose of seeing the amount of its speared. It should be mentioned that the computed effective focal length was about 19.6 *mm* by OID, while its correspondent value obtained by Zemax was about 20.09 *mm*. They are close each other.

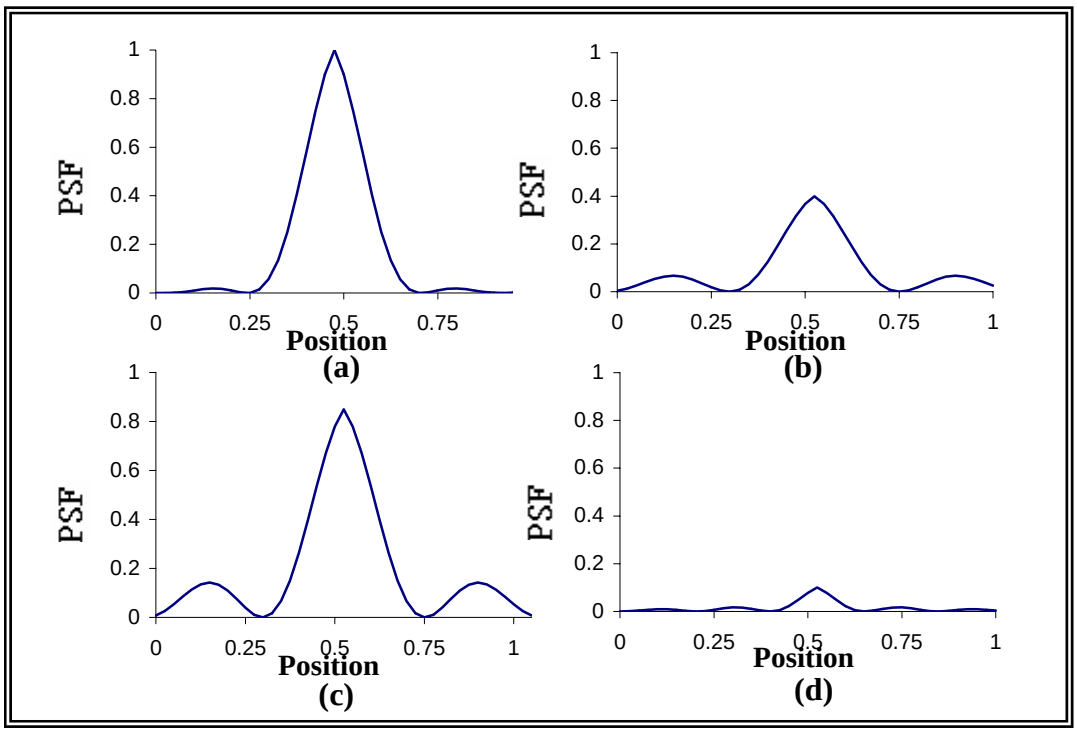

Figure 4.19: PSF shapes of the perfect and suggested design using the mathematical method by OID for the perfect and 3, 4, and 5 wavelengths.

2. **Fourier Transform Method**

This method is based on the theoretical basis which suggests that PSF is equivalent to the power spectrum of the pupil function. If the pupil function is perfect (i.e. perfect OSD) then PSF is computed using equation (3.72) is perfect too. When the aberration is taken in consideration (i.e. usual OSD) the PSF is computed by using equation (3.72) is usual and represents the average PSF of the suggested design. It

is shown that the PSF computation is just the transform of the pupil function, thus it represents the pupil function itself. The computation of the pupil function is detailed as follows.

In the case of perfect OSD; the pupil function is real and computed by equation (3.67). In the presence of aberration the pupil function is complex and represented by equation (3.66). For the suggested OSD, the parameter that dominant on the behavior of the pupil function is *W*. This parameter is computed previously in the first method. By assuming the illumination is normalized, the values of *P* will be in between 0 and 1. Where 0 is the black, 1 is the white, and the numbers in between them are the gray levels between the black and white. Figure 4.20 present the flowchart of computing the PSF for the perfect and suggested OSD. Figures 4.21 display the PSF of the perfect OSD and the correspondent PSF of the suggested OSD considered for the wavelengths of interest.

In overview, the PSF behavior contains on a central higher peak of width is greater than the width of that computed by the perfect OSD. It contains on sharper ring at wavelengths of 3 and 4 μm while there are two dim rings at 5 μm comparing with the perfect that contains on one dim ring. It thought that the sharper ring of the usual PSF is resulting due to existence of small amount of residual aberration in the suggested system. Therefore, it can be say that the suggested design transfer greater amount of energy carried in each ray come from the object plane into image plane.

It can be seen that the figures 4.21 and 4.19 have peaks are smaller than their correspondent of the perfect OSD shown in the same figures by very little percent of about 5% at $\lambda = 4\mu m$. This percent does not only

represent the dispersing of the energy during its traveling from the object plane into image plane due to diffraction, but there is an additional effect of aberration make the PSF curve appear more oblate.

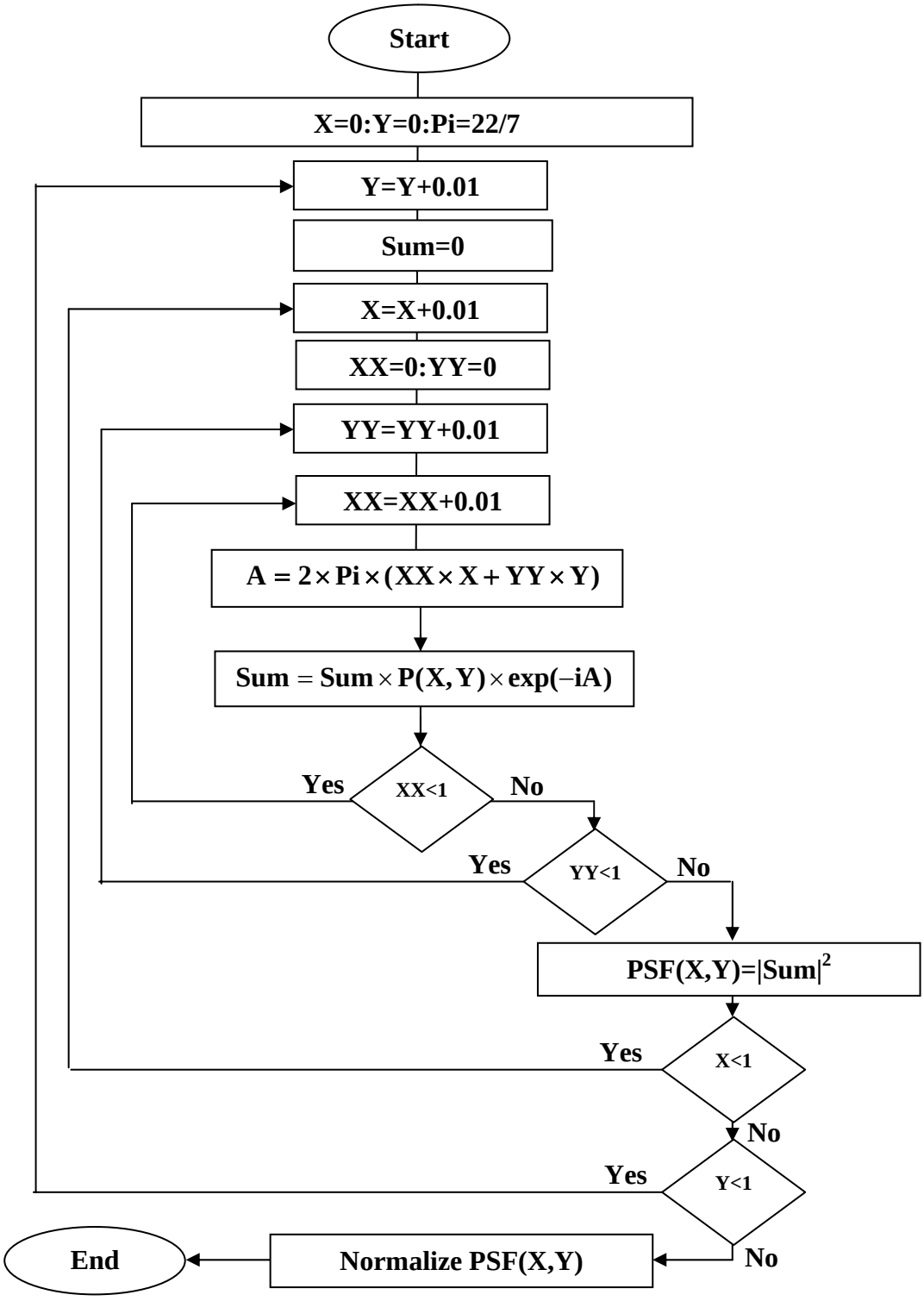

Figure 4.20: PSF flowchart of perfect and suggested OSD by Fourier transform method.

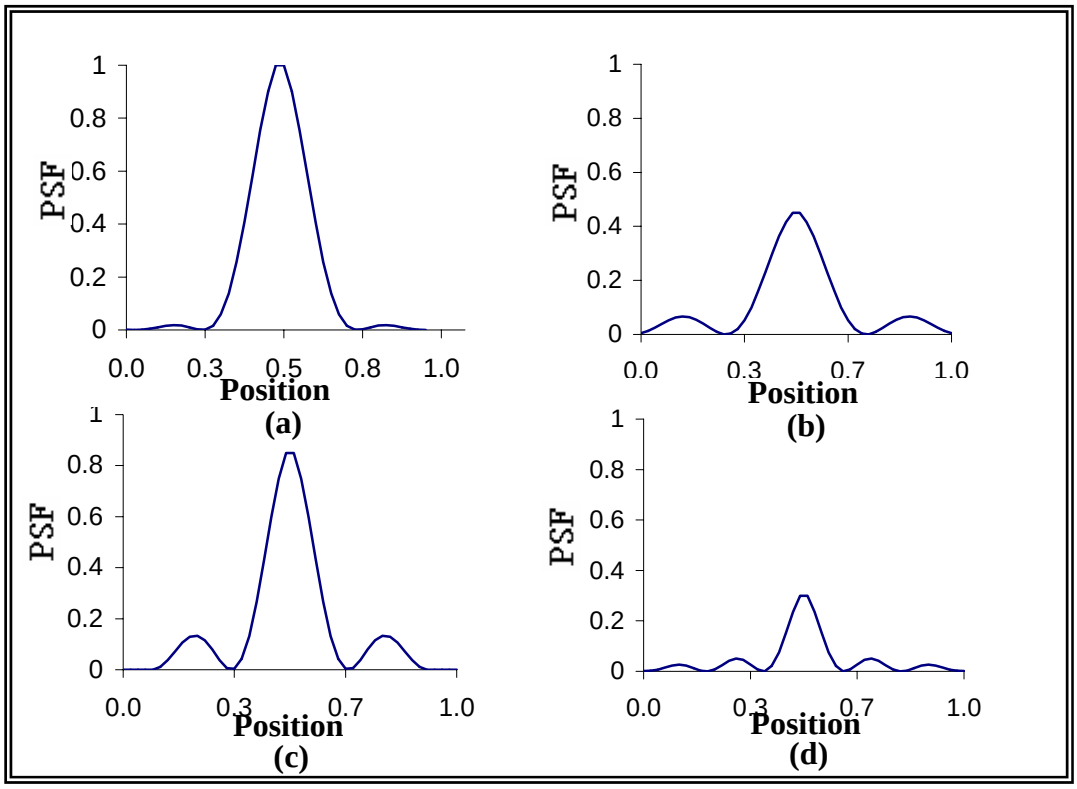

Figure 4.21: PSF shapes of the perfect and suggested design using the Fourier transform method by OID for the perfect and 3, 4, and 5 wavelengths.

Therefore, the suggested optical system disperses small percent of the energy carried by each ray because of the existence aberration of in the suggested system. Figure 4.22 shows the PSF shapes for the perfect and suggested system extracted by Zemax considered at the wavelengths of interest.

By comparing the shape of PSF of the suggested system extracted by OID with its corresponding shapes extracted by Zemax, one can notice that both of them are similar behaving since they have same behavior of the width of central peak and same number of the surrounding rings at each case of wavelength, which ensure the correct way of the calculations.

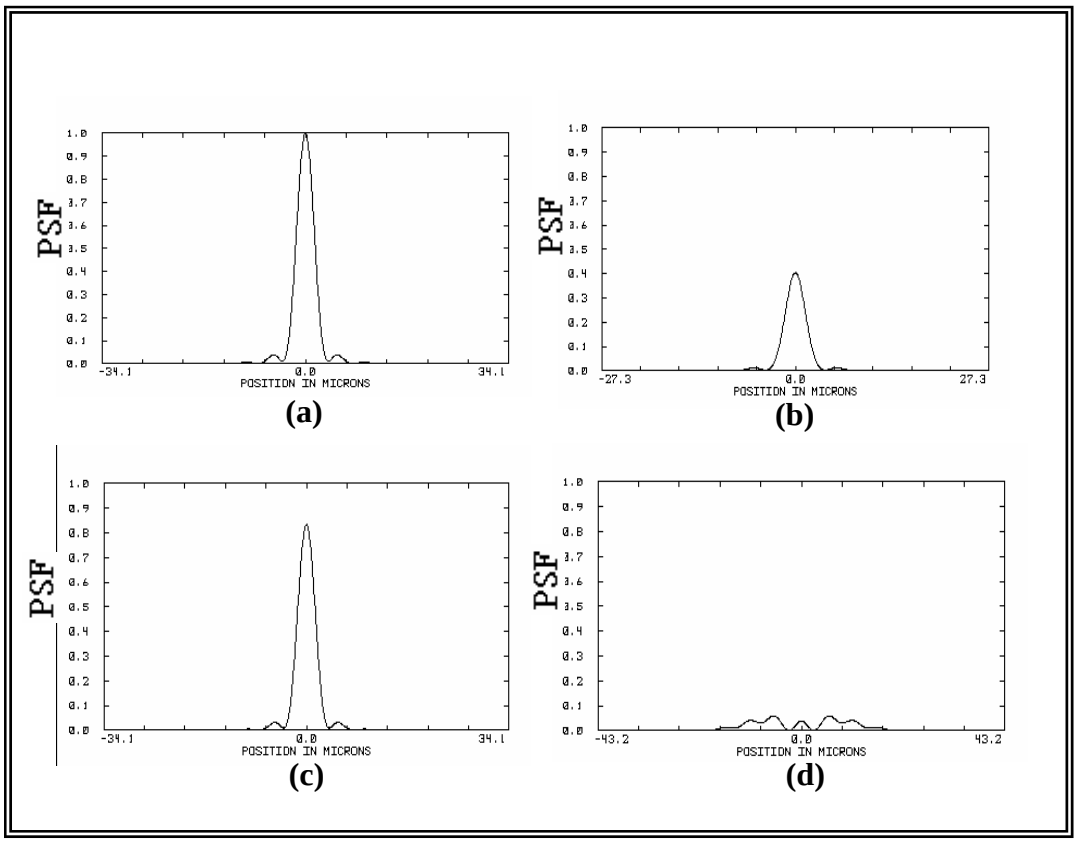

Figure 4.22: PSF shapes for the perfect and suggested OSD for different wavelengths extracted by Zemax for the perfect and 3, 4, and 5 wavelengths.

In general, the suggested system gave good PSF since it was very approach to the perfect PSF at the middle IR region, which indicate that the information of the image are conserved during the process of imaging.

4.5.2 MTF Computation

In order to determine the MTF, one must pass through OTF determination, because the MTF is the modulus of the resulting OTF. The OTF depends on the frequency of each point in the image.

MTF is second chosen parameter used to strengthen the decision of the PSF result. Because of the MTF represent the resolution of the image, it is important to compute this resolution accurately since the MTF is very sensitive for small amount of aberration in the optical system.

Practically, MTF computed by two different methods; the first depends on the mathematical relationship previously mentioned for the two cases of the perfect and usual, while the second based on the fact that state that the MTF is the modulus of the power spectrum of the PSF. In the following, a detailed explanation about each of them:

1. **Mathematical Method**

The perfect OTF is real for all spatial frequencies, which means that there is no phase shift, in which the OTF and MTF are identical. This is the basic concept by which equation (3.90) is driven, so it can be used to find the MTF for the perfect system.

In the existence of aberration, the usual OTF is a complex function consisting of the product of a real modulus (MTF) and a factor having an imaginary exponential term (PTF). The OTF can be calculated along the spatial frequency that expanded through the range from 0 into the cutoff frequency (f_c). Therefore, it should be determined the cutoff value which equal to $(1/\lambda(f/no)$ and then MTF can be taken as the modulus of the integral equation (3.93). The integral equation (3.93) can be written in the sum form:

$$OTF(f_s) = \sum_{y=0}^{1}\sum_{x=0}^{1} exp(-inkf_s V(x,y,f_s))$$

The flowchart for determining the MTF by OID software is shown in figure 4.23 and 4.24. Figure 4.25 shows the resulting MTF curve determined by OID software for the suggested OSD at the wavelengths of interest.

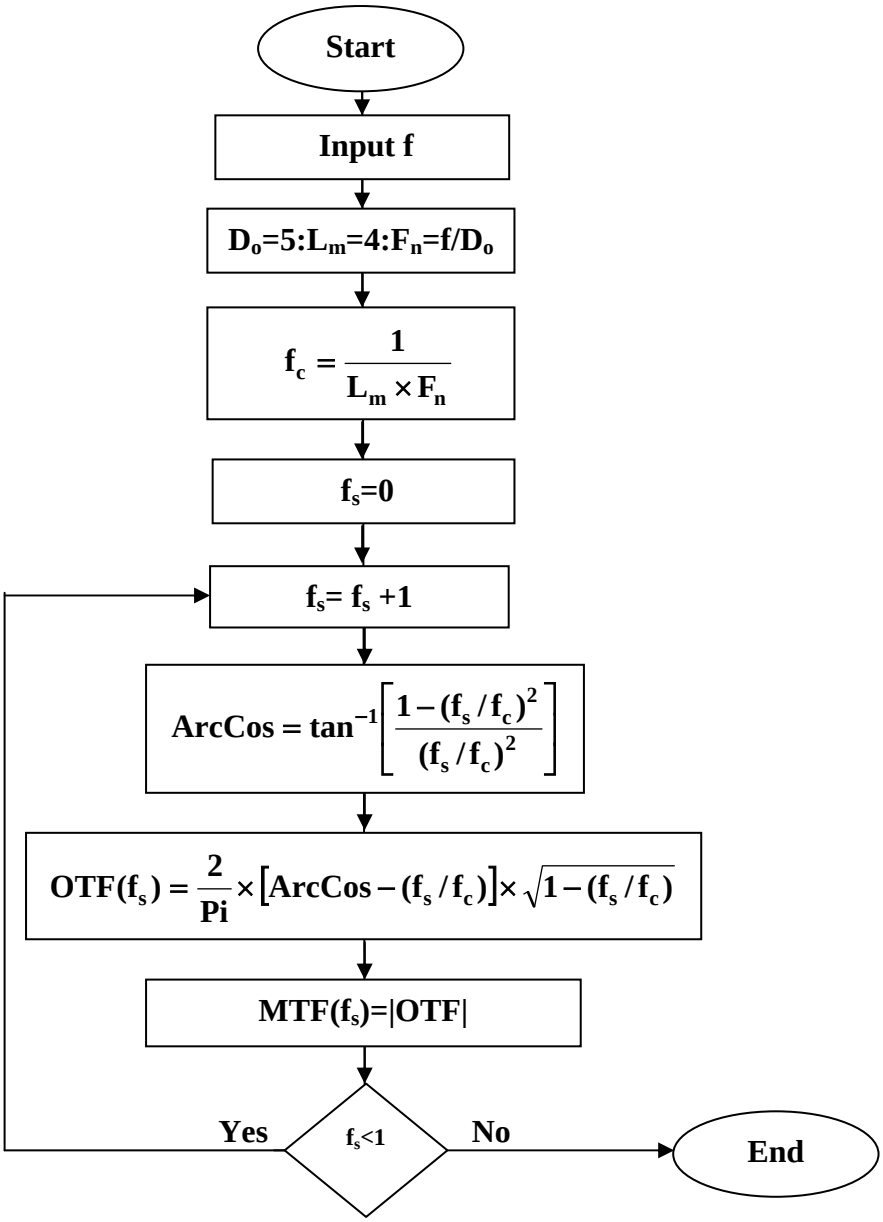

Figure 4.23: Perfect MTF flowchart of the mathematical method.

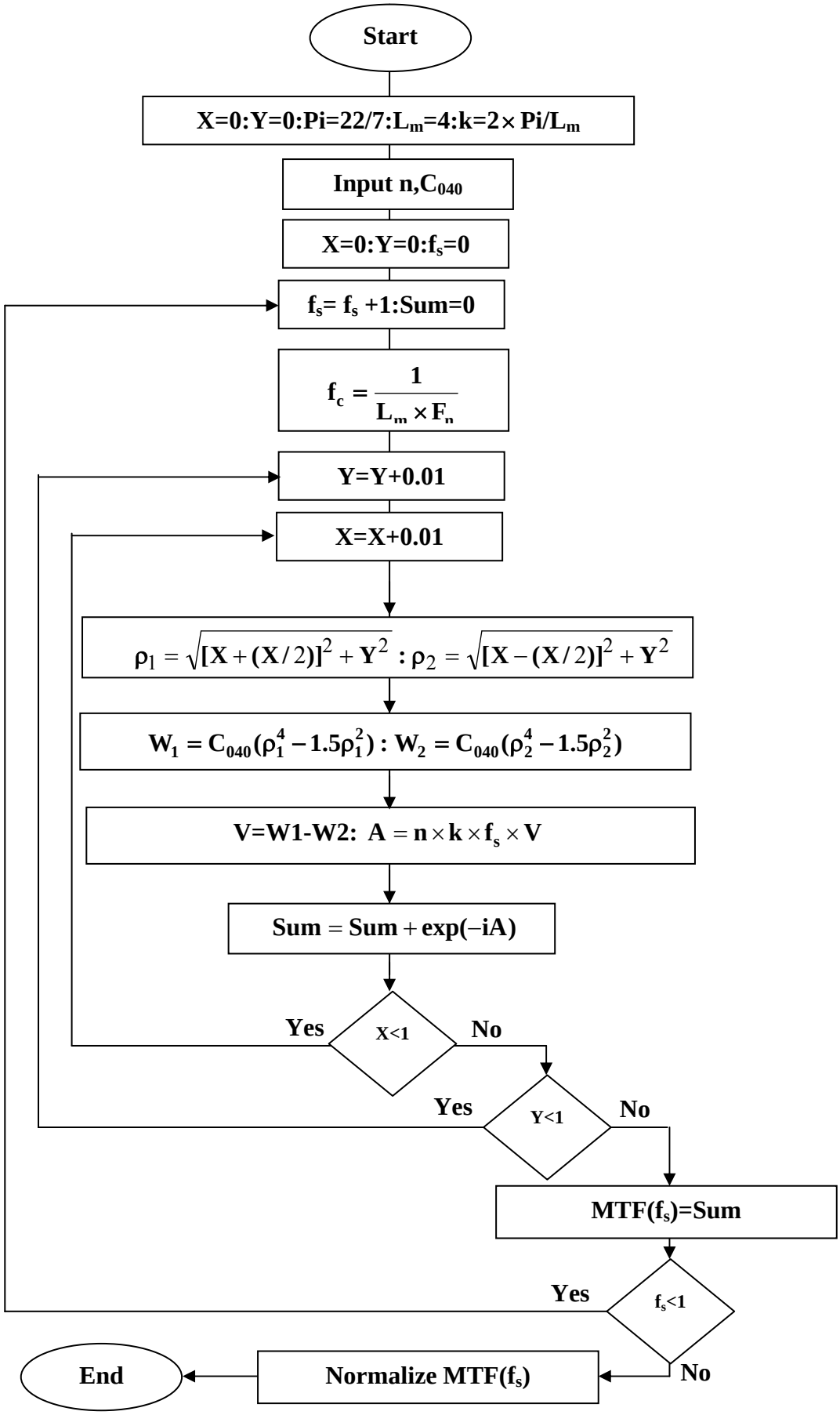

Figure 4.24: MTF flowchart of usual by mathematical method.

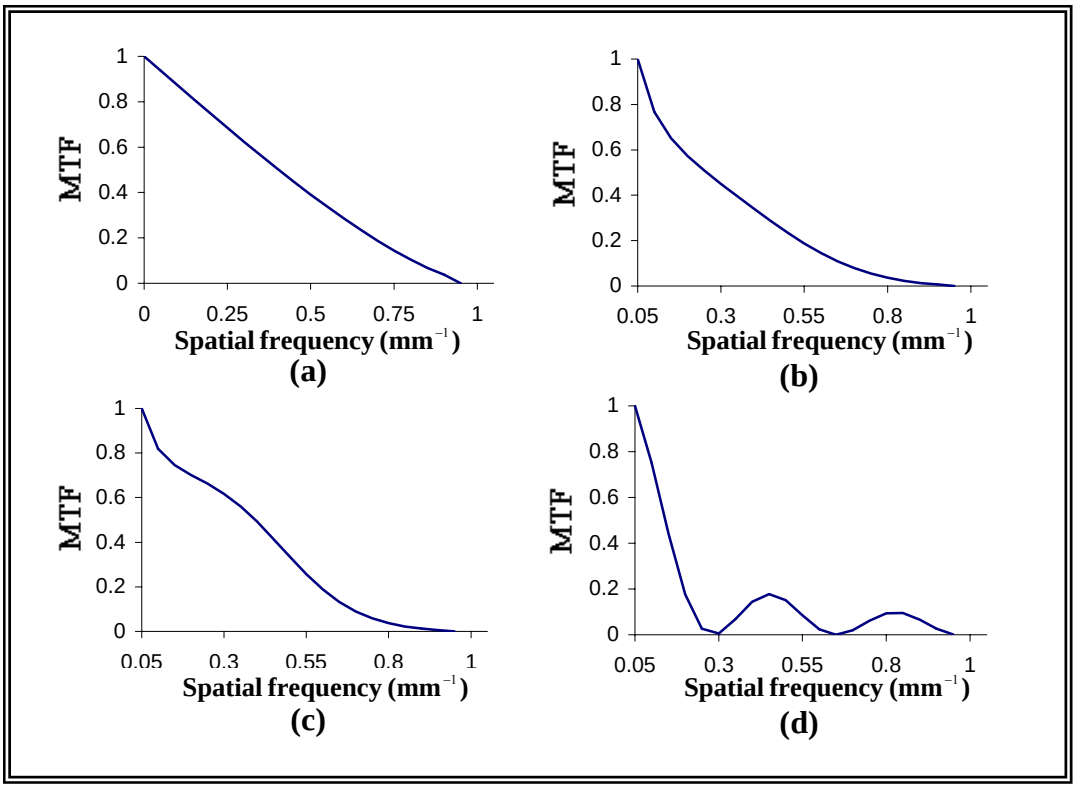

Figure 4.25: MTF curves for the perfect and suggested OSD by OID using the mathematical method for the perfect and 3, 4, and 5 wavelengths.

2. **Fourier Transform Method**

In this method, OTF can be derived from PSF which has been described as the image of an axial point object formed by diffraction limited system. The relation by which one can determine the perfect OTF is given by equation (3.94). Therefore, one can employs equation (3.94) to determine the behavior of MTF. That means the previously determined PSF enable to determine MTF using the common relationship that relates them given in equation (3.94). The perfect PSF give perfect MTF, while the usual PSF belong to the suggested design give usual MTF which describe the resolution of the image consisting in the suggested design. Figure 4.26 presents the flowchart of computing the MTF. Figures 4.27-a and 4.27-b, c, and d show the MTF curves for both cases of the perfect and suggested system. By comparing figure 4.27 with their correspondent

extracted by Zemax shown in figure 4.28, one can find that both of the MTF curves belong to the adopted methods have similar behaviors comparing with their correspondent curves extracted by Zemax. The similarity of MTF behaviors ensures the correct path of the computation and the safe application of the adopted method.

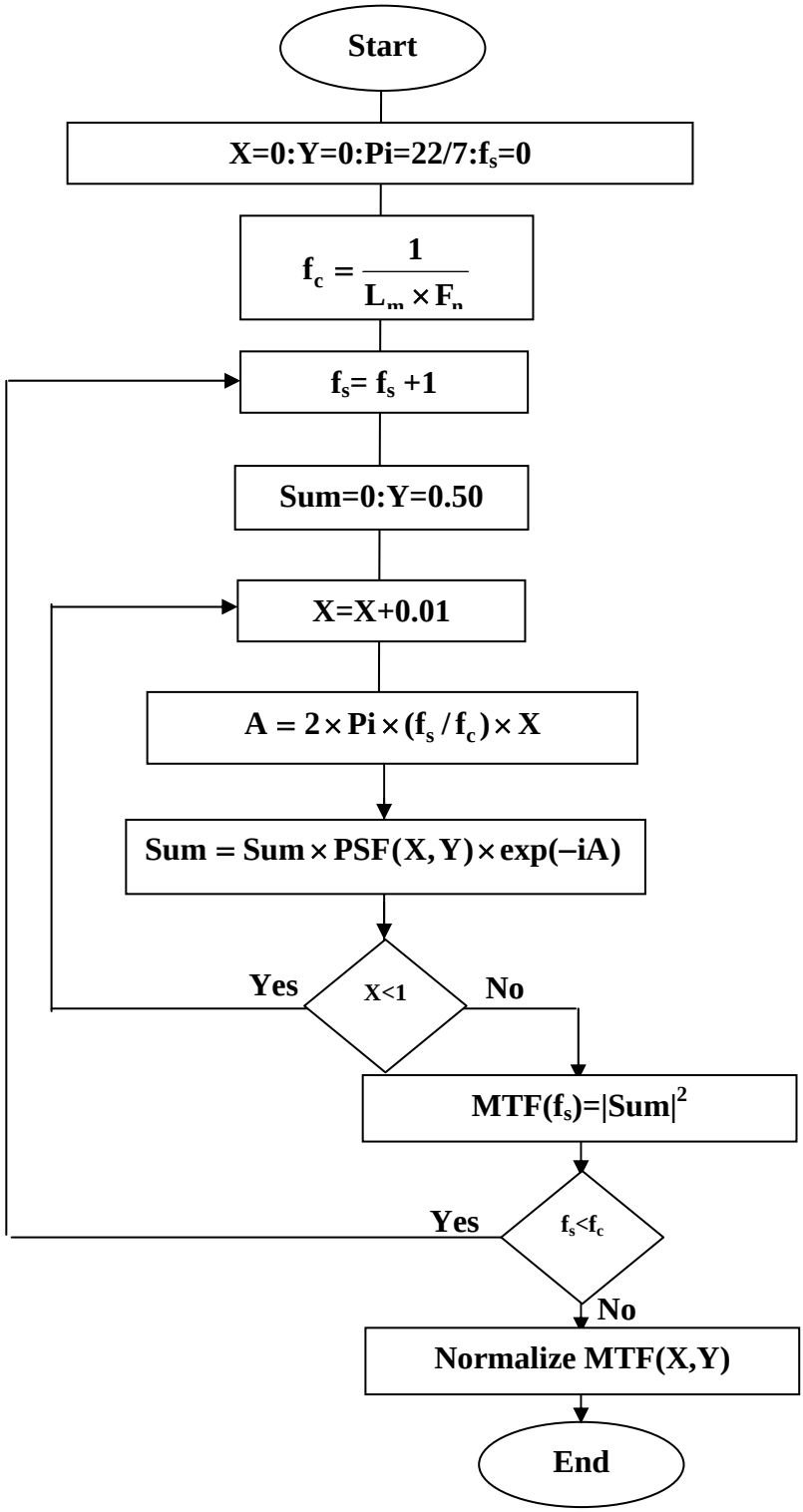

Figure 4.26: MTF flowchart of perfect and suggested OSD by Fourier transform method.

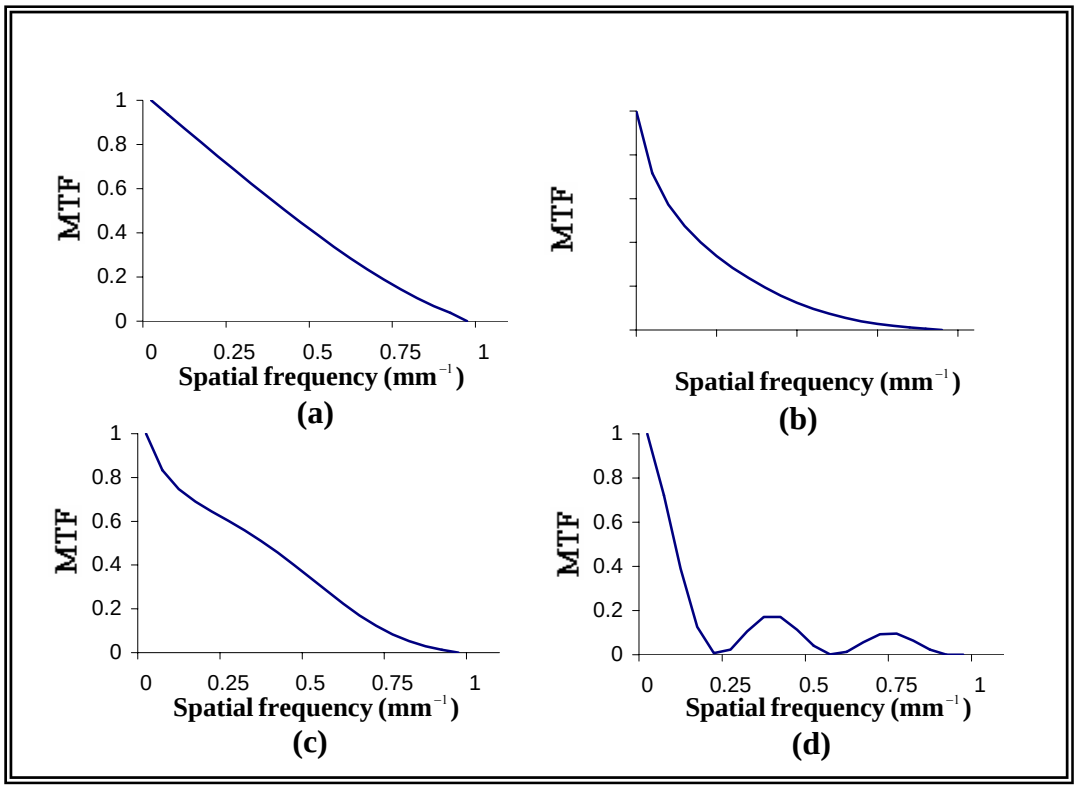

Figure 4.27: MTF curves for the perfect and suggested OSD by OID using Fourier transform method for the perfect and 3, 4, and 5 wavelengths.

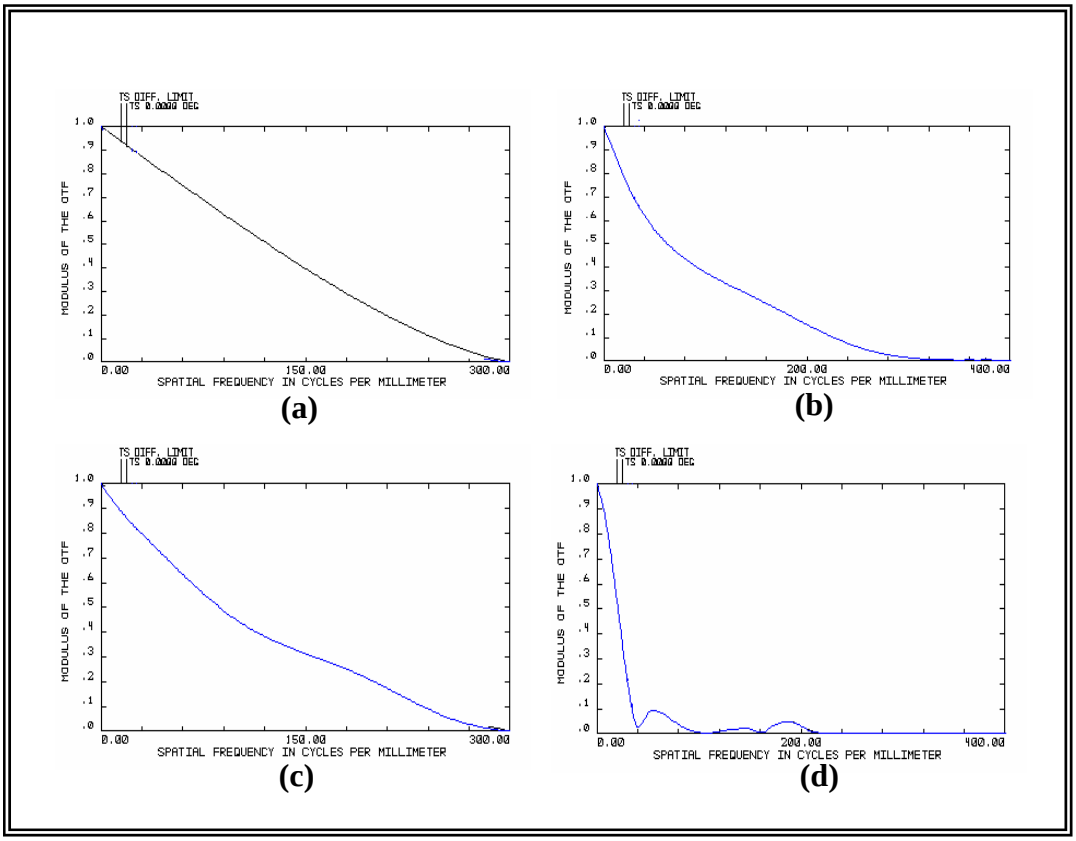

Figure 4.28: MTF curves for the perfect and suggested OSD extracted by Zemax for the perfect and 3, 4, and 5 wavelengths.

In order to stand for how much the suggested design is close to the perfect, one can compare the behavior of the usual MTF with the perfect one. It seen that the usual MTF includes greater decay due to the residual aberration in the optical system. The smooth behavior of the MTF curve refers to the uniformity of the energy distribution along the two dimensions of the image. In other words, it refers to the absence of the noise effect in the image along the allowed frequency. It should be remarked that at $\lambda = 4\mu m$ there is a middle protrusion in the MTF curve pushes it into outward. It thought that this protrusion that corresponding to the spread points of frequency 0.45 mm^{-1} is resulting from the residual aberration exist in the suggested system, while the more decay of the MTF curve is due to the defocusing exist in the suggested OSD.

In addition, the MTF does not match zero value unless the close approach to the amount of the cutoff frequency, which refer to include the information of high frequency band in the consisting image. The MTF plot show that the optical system operates as a low-pass filter with a specific cutoff frequency. Therefore, any quantity directly derived from the nonzero frequency range has significance for a more general MTF than the value of the perfect MTF. In other words, one can say that the suggested system receive all the allowed frequencies in between zero and cutoff frequency with their natural rates that approach to the perfect. This points to high resolution of the consisting image in the suggested OSD. High resulting resolution (i.e. good MTF) besides high resulting energy (i.e. good PSF) that characterize the consisting image ensure good quality of the image that appeared sharper features and higher contrast, and then refer to the good quality of the suggested OSD.

4.5.3 Spot Diagram Computation

The spot diagram is a parameter that describes the ability of the suggested system to be applied particularly. The smallest spot size is more accurate result since the position of the spot on the reticle refers to the position of the target with respect to the optical axis of the homing head. The spot diagram is determined by two methods; the first is based on the ray tracing with some geometrical processing according to proposed algorithm, while the second method is based on some mathematical equations mentioned previously. In the following more explanation about each of them;

1. **Ray Tracing Method**

This method concentrated in dividing the image into 100×100 segments (points), and there are 100×100 incident rays on the optical system where each ray illuminate the segment that the ray incident on it. Thus, the segment of image is either do not receipt any ray to be dark, or receipt ray or many rays to be illuminated. The amount of the illumination on each segment depends on the number of rays incident on it. The central bright spot consisting from the focused ray, while the surrounding rings resulting from few rays that do not focused due to the defocusing of aberration. Practically, this algorithm is applied on one dimension to describe only the rays included in the mardional plane above the optical axis (50 ray only), and then the two-dimensional image achieved by distributing the illumination curve along all the image, which equivalent to rotate the resulting one-dimensional curve about the center of the image by 360^{o} to fed the illumination of the skew rays as presents in flowchart of figure (4.29). This is done depending on the rotational symmetry that by which the image and aberration are characterized.

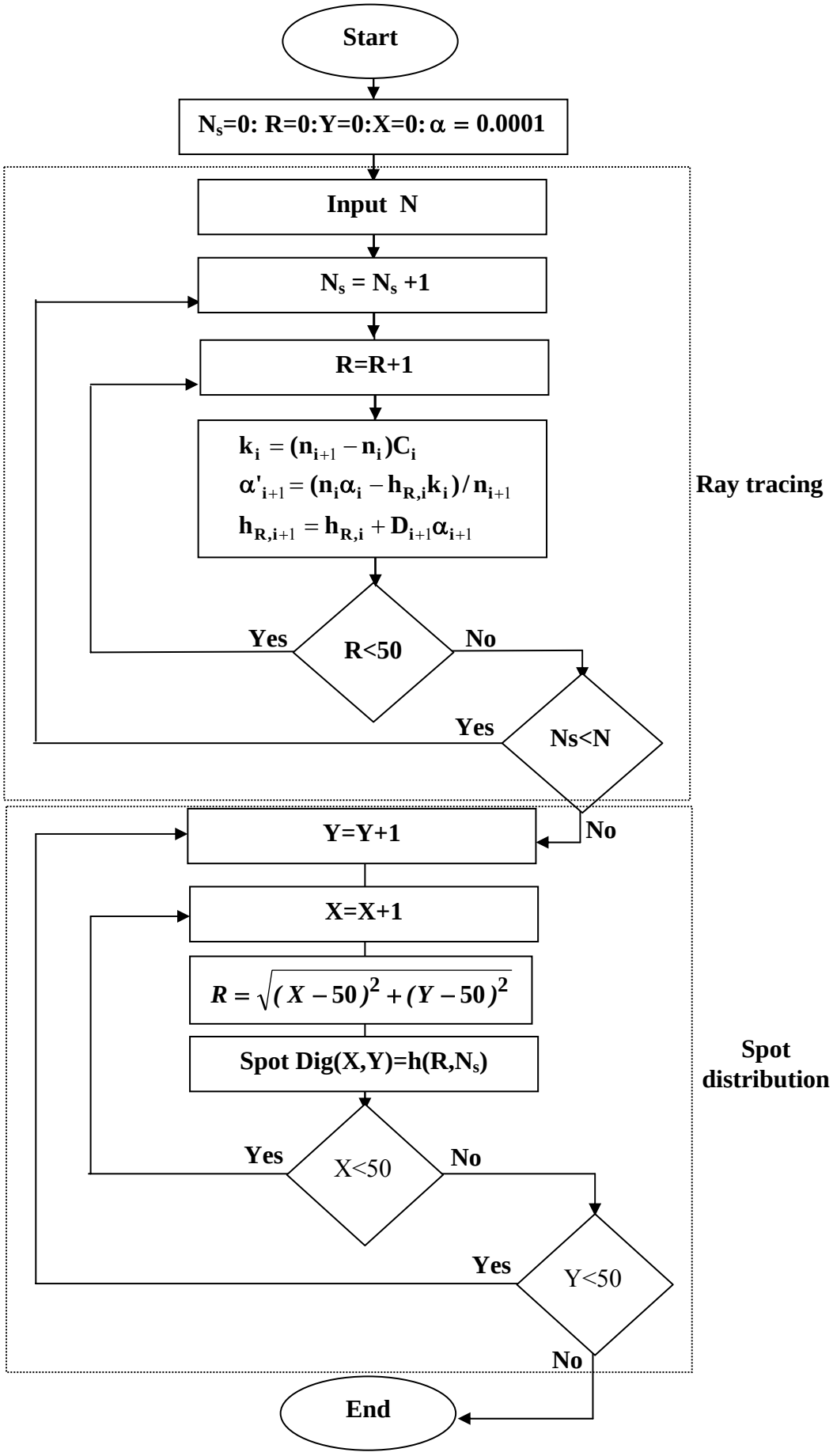

Figure 4.29: Flowchart of computing spot diagram by the ray tracing method.

The spot diagram belongs to the perfect OSD is computed by regarding the paraxial ray only and neglecting the marginal rays. Paraxial is the rays that far away from the optical axis by an amount do not exceed 0.1 from the diameter of aperture. At the paraxial limitation, there is one focus "paraxial focus" appear without rings else rings of diffraction, which make the image seems to be perfect. Figure 4.30 displays the spot diagram resulting for the both cases of the perfect and suggested OSD. It shown that the spot diagram belong to the suggested OSD characterized by some sharpness of imaging which can be avoided by producing a smoothness on the consisting image.

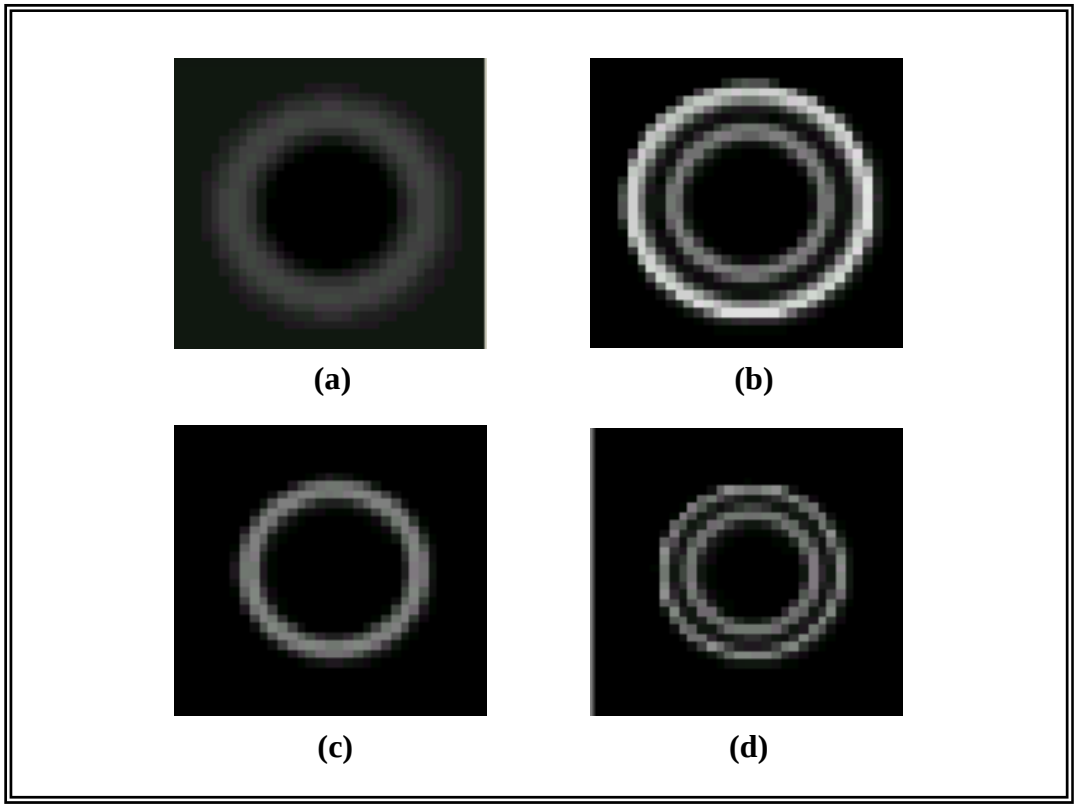

Figure 4.30 Spot diagrams for the perfect and suggested OSD by OID using the ray tracing method for the perfect and 3, 4, and 5 wavelengths.

2. **Convolution Method**

This method depends on the basic concept of distributing the thermal radiation received from the target, which assumed to be Gaussian. Thus, one can use the equation (3.60) to determine the energy distribution of the image after knowing the average rate of distributing the PSF of the image itself, i.e. the convolution of the PSF around the object function yield the final distribution of the image. The resulting spot diagram is shown in figure 4.31 for both cases of usual and perfect, and figure 4.32 presents the flowchart of computing the spot distribution by the convolution method. On the other hand, figure 4.33 displays the spot diagram of the suggested system computed by Zemax.

By comparing the correspondent shapes of figures 4.33 and 4.31, one can see that all of them are similar. In spit of some small differences related by width of the rings, the behaviors were similar which ensure the correct line of the calculations. It noticeable that the spot diagram determined by Zemax and OID are containing on a central black spot whereas the logic is pointing to existence a central white spot. This problem related by a physical phenomena in which the incident ray interfere with the reflected ray distractively, since the phase difference between them is π at the center of the image where the detector is in touch with the second surfaces of the last element in the optical system. Therefore, OID software contains the optical processing of this phenomena to be valued for the optical basis. Figure 4.34 shows the window specified by OID to display the PSF, MTF, and Spot diagram for the both cases of perfect and proposed OSD, it shown that there is an option by which one can chose the intended case and another one to determining the wavelength in use, and there is tagged check box to produce the distractively interference at the central spot.

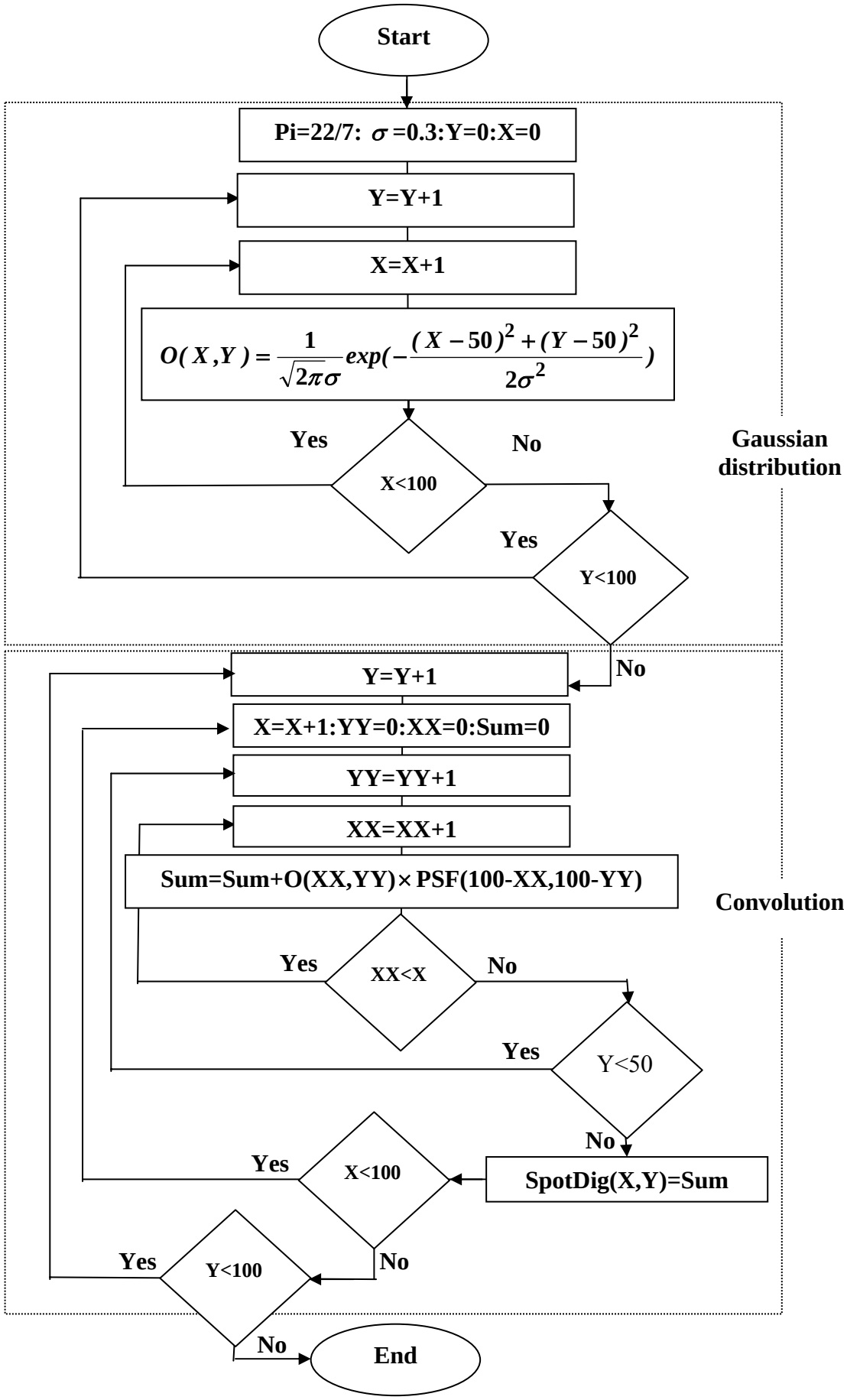

Figure 4.31: Flowchart of computing spot diagram by the convolution method.

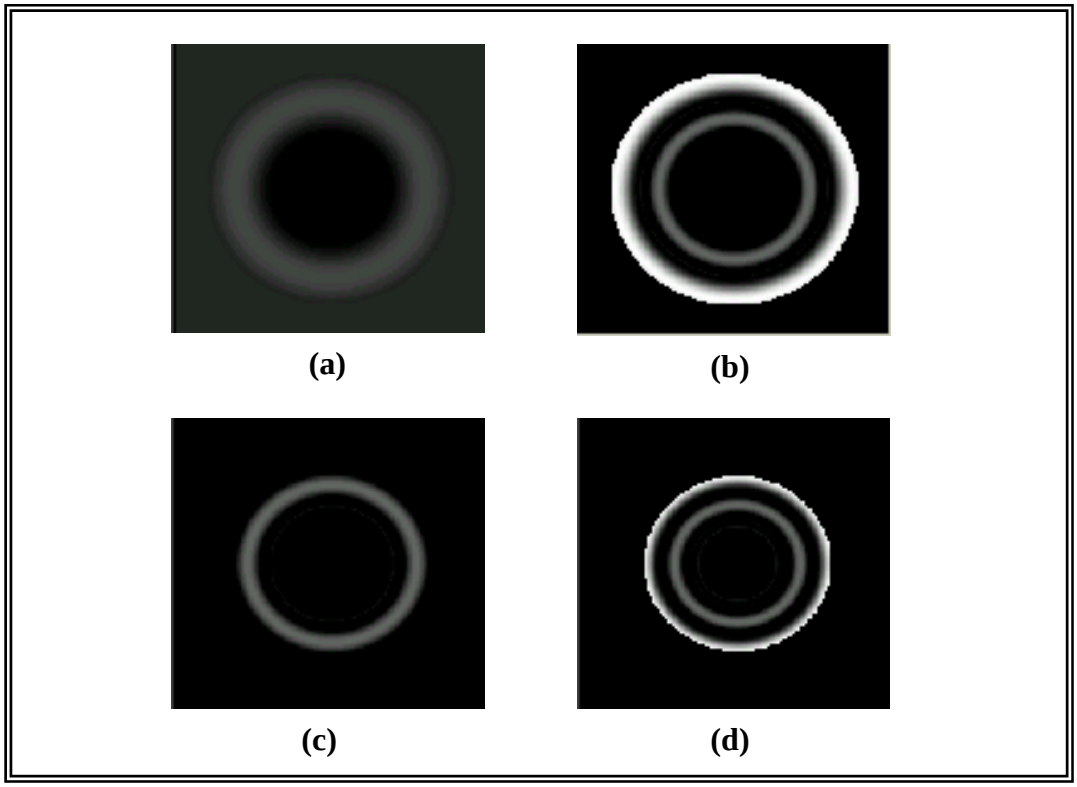

Figure 4.32 Spot diagrams for the perfect and suggested OSD by OID using the convolution method for the perfect and 3, 4, and 5 wavelengths.

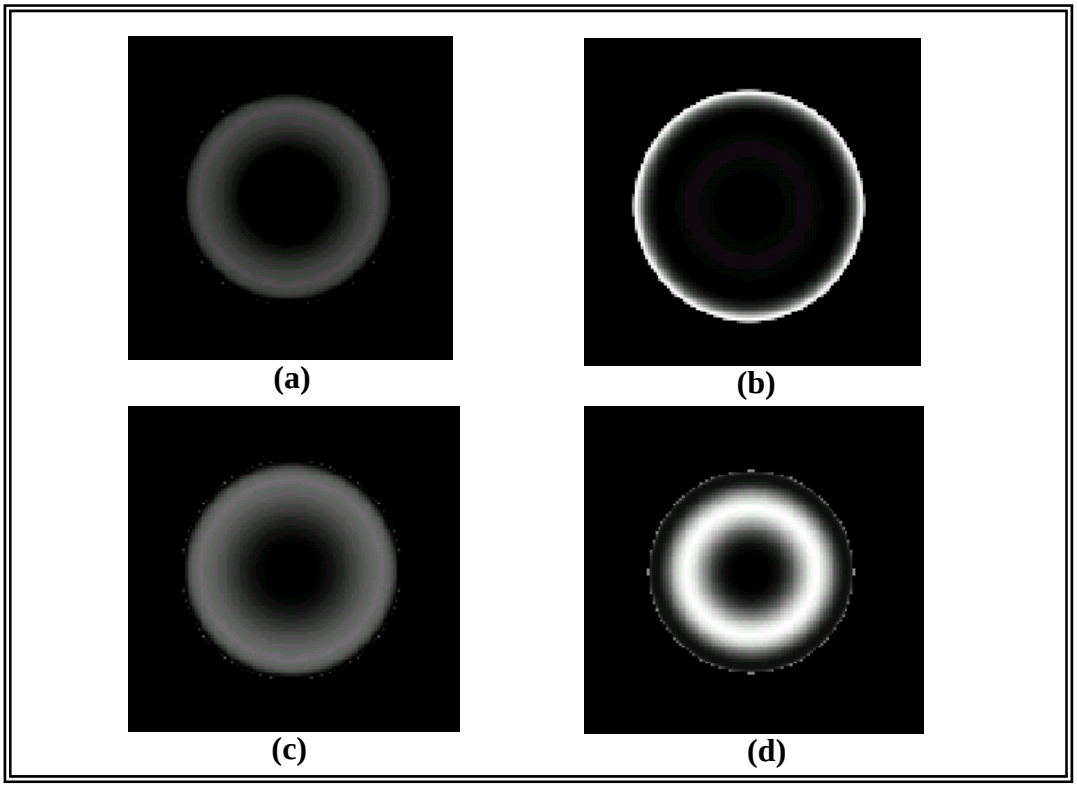

Figure 4.33 Spot diagrams for the perfect and suggested OSD by Zemax for the perfect and 3, 4, and 5 wavelengths.

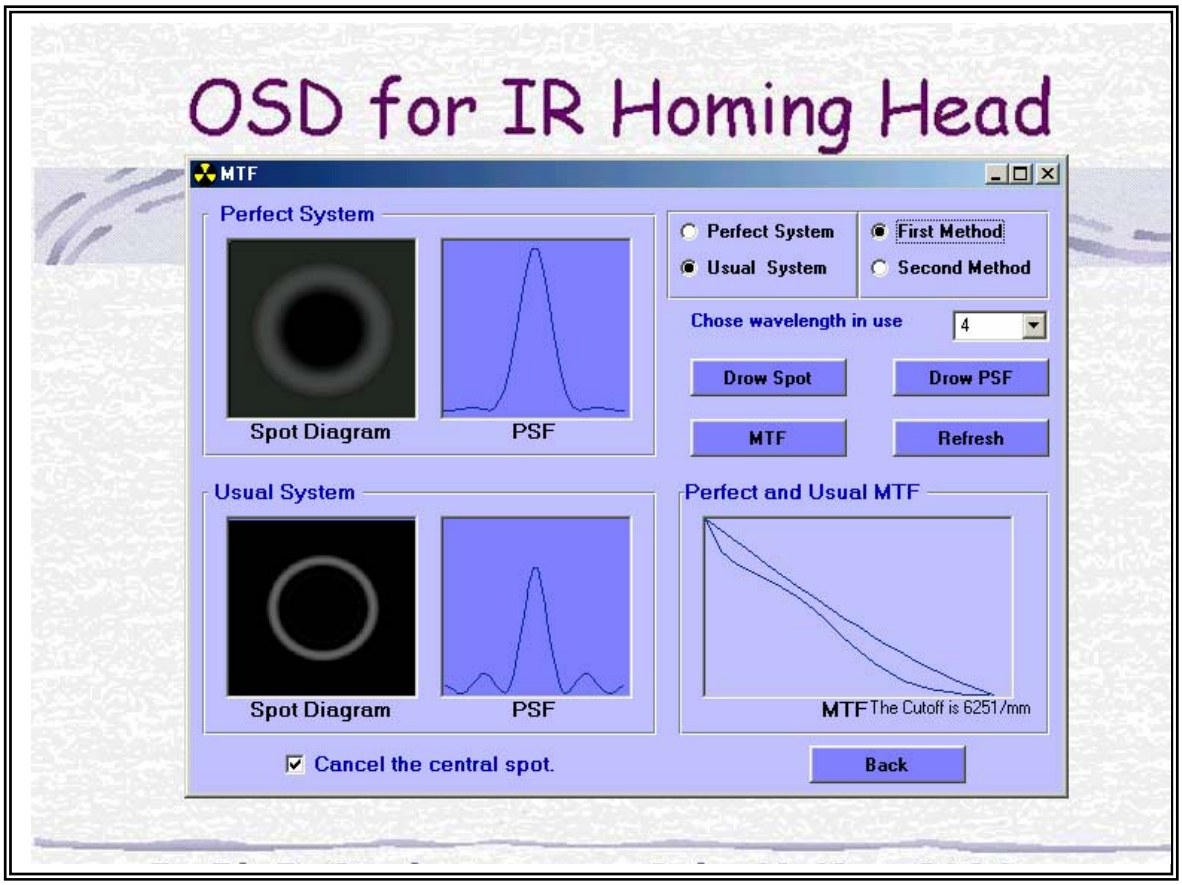

Figure 4.34 PSF, MTF, and Spot diagram window by OID software.

4.5.4 Spot Size Computation

The OID software specifies a window for calculating of the spot size shown in figure 4.35. The spot size window contains two tables are intended for the results of the system output which are mainly *f, A, Z,* Z_T ,and δ'. The computations are done at each optical element in the suggested OSD with regarding the wavelengths of interest, i.e. $3,4, and\ 5\mu m$.

The spot size is computed by two methods; the first method is based on the mathematical relationships mentioned previously, whereas the second based on the geometry of the ray tracing. Each of the two

tables in the spot window of OID are specified for the results of each method. In the following details explanation about each methods

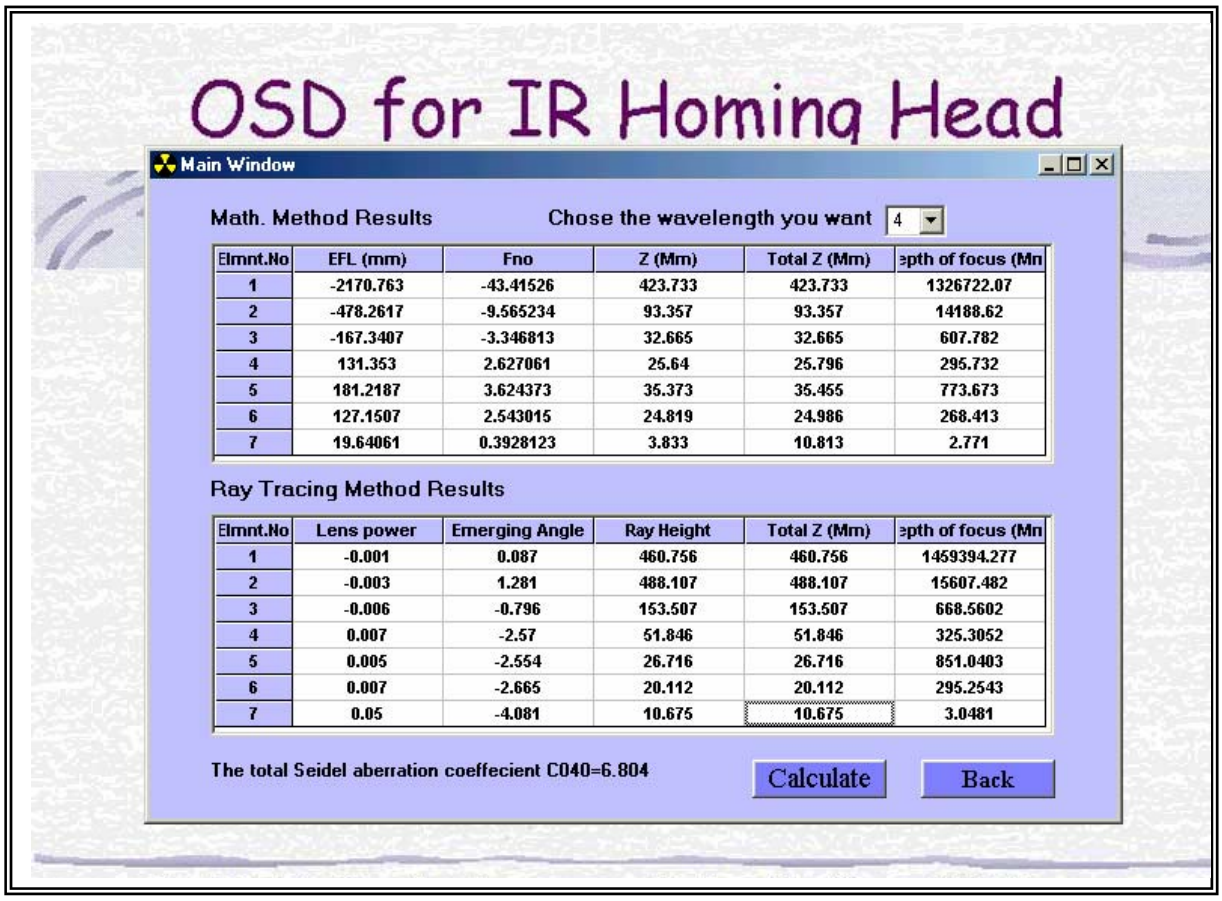

Elmnt.No	EFL (mm)	Fno	Z (Mm)	Total Z (Mm)	epth of focus (Mn
1	-2170.763	-43.41526	423.733	423.733	1326722.07
2	-478.2617	-9.565234	93.357	93.357	14188.62
3	-167.3407	-3.346813	32.665	32.665	607.782
4	131.353	2.627061	25.64	25.796	295.732
5	181.2187	3.624373	35.373	35.455	773.673
6	127.1507	2.543015	24.819	24.986	268.413
7	19.64061	0.3928123	3.833	10.813	2.771

Elmnt.No	Lens power	Emerging Angle	Ray Height	Total Z (Mm)	epth of focus (Mn
1	-0.001	0.087	460.756	460.756	1459394.277
2	-0.003	1.281	488.107	488.107	15607.482
3	-0.006	-0.796	153.507	153.507	668.5602
4	0.007	-2.57	51.846	51.846	325.3052
5	0.005	-2.554	26.716	26.716	851.0403
6	0.007	-2.665	20.112	20.112	295.2543
7	0.05	-4.081	10.675	10.675	3.0481

Figure 4.35 Total spot size window by OID software.

1.**Mathematical Method**

In this method, the effective focal length is computed depending on the algorithm in flowchart of figure 4.17. Other arguments (i.e. *A*, *Z*, Z_T, and δ') are computed depending on equations (3.77), (3.74), (3.3.76), and (3.84) respectively. Figure 4.36 shows the flowchart used to compute the spot size and its related parameters displaced in the interface of spot size window of OID. Tables 4.3, 4.4, and 4.5 include the results of spot size and its related parameters for the three different wavelengths, namely 3, 4, and 5 μm. Figure 4.37 shows the behavior of the spot size with

respect to the variation of the wavelength considered for each element in the suggested OSD.

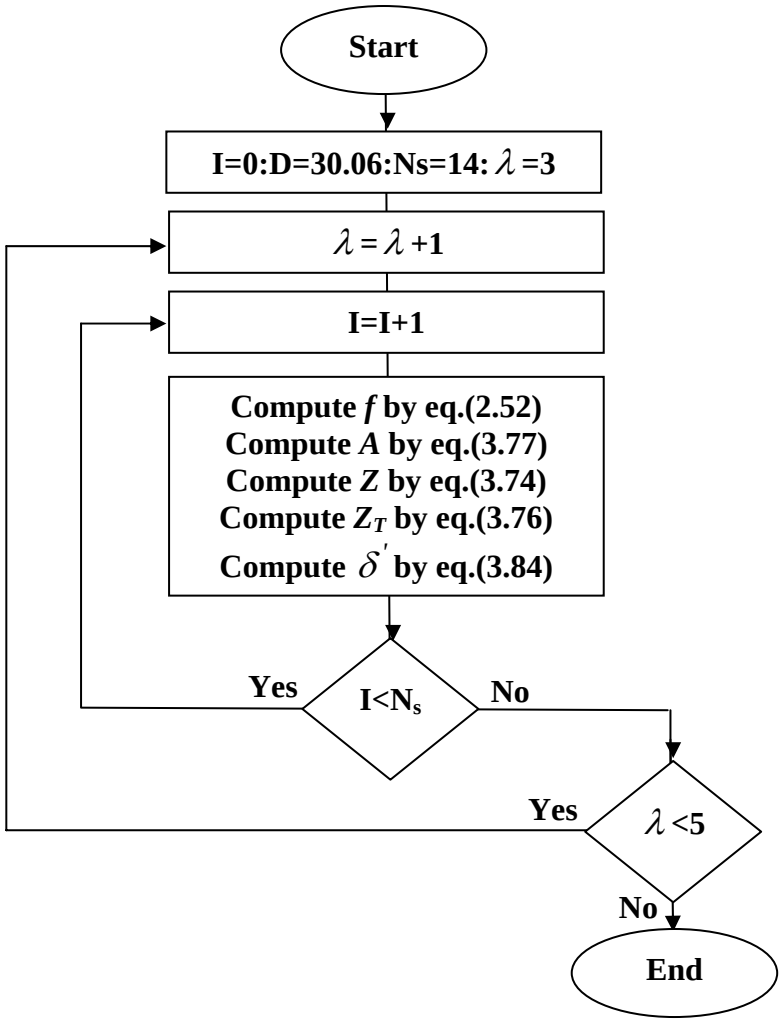

Figure 4.36: Flowchart of computing spot size by the mathematical method.

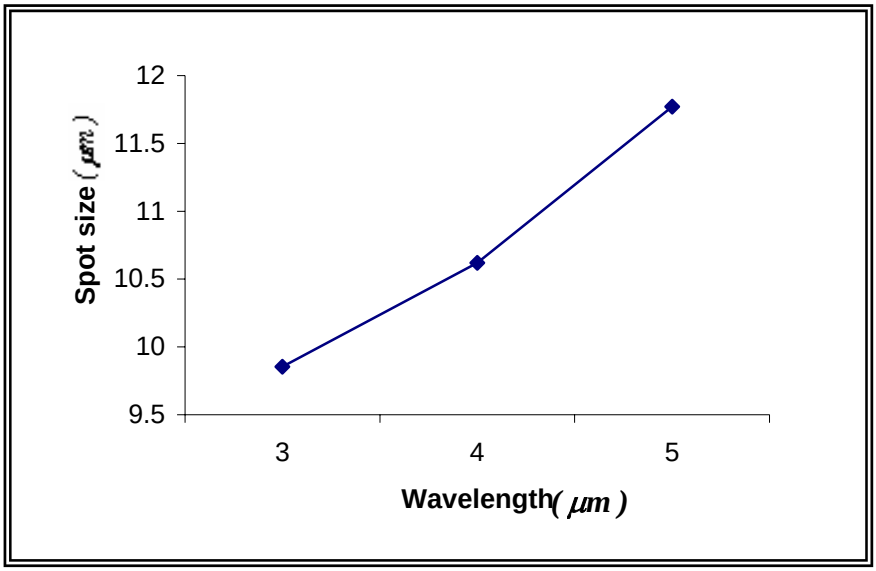

Figure 4.37:Spot size versus wavelength using the mathematical method.

Table 4.3: Total spot size and its related parameters at λ=3 μm

N_e	f (mm)	f/no	Z (μm)	Z_{total} (μm)	δ' (μm)
1	-2139.6	-42.8	313.2	313.2	952670.3
2	-474.1	-9.5	69.4	69.5	10363.6
3	-166.1	-3.3	24.3	24.3	445.5
4	131.9	2.6	19.3	19.4	224.8
5	181.9	3.6	26.6	26.7	587.3
6	127.4	2.5	18.6	18.8	203.3
7	19.6	0.3	2.8	9.8	2.5

Table 4.4: Total spot size and its related parameters at λ=4 μm

N_e	f (mm)	f/no	Z (μm)	Z_{total} (μm)	δ' (μm)
1	-2170	-43.4	423.7	423.7	132672.2
2	-478.2	-9.5	93.3	93.3	14188.6
3	-167.3	-3.3	32.6	32.6	607.7
4	131.3	2.6	25.6	25.7	295.7
5	181.2	3.6	35.3	35.4	773.6
6	127.1	2.5	24.8	24.9	260.4
7	19.6	0.3	3.8	10.8	2.77

Table 4.5: Total spot size and its related parameters at λ=5 μm

N_e	f (mm)	f/no	Z (μm)	Z_{total} (μm)	δ' (μm)
1	-2202.1	-44.1	537.3	537.3	173140.7
2	-482.4	-9.6	117.7	117.7	18205.8
3	-168.6	-3.3	41.4	41.1	770.1
4	130.8	2.6	31.9	32.1	364.8
5	180.5	3.6	44.1	44.1	955.7
6	126.8	2.5	30.9	31.1	332.4
7	19.6	0.39	4.7	11.7	3.01

2- Ray Tracing Method

This method assumes that the spot size is equal to the distance between the optical axis and most distant off-axis ray with respect to the optical axis. The fifty rays incident on the image in between the optical axis and the rim of the dome are tracing until the last surface in the suggested OSD. The height and the emerging angle determined by the ray tracing helps to compute the spot size and its related parameters. By scanning rays incident on the image, the spot size is equal to twice the height of the last distant off-axis ray from the optical axis multiplied by the diameter of the dome. The multiplication by the diameter is because of the rays are tracing through a normalized diameter of aperture, which make the determined height of the ray is normalized too, and it represents the percentage of the way between the ray and the optical axis. Therefore, the backing into actual measurements requires multiplying the height of the chosen ray by the diameter of the dome. Figure 4.38 presents the flowchart of the ray tracing method to compute the spot size at different wavelengths of interest, and table 4.6 shows the resulting spot size as a function of wavelength.

Table 4.6: Total spot at λ of 3, 4, and 5 μm

N_e	Angle	Z_3 (μm)	Angle	Z_4 (μm)	Angle	Z_5 (μm)
1	0.08	461.4	0.08	460.7	0.08	460.1
2	1.28	488.4	1.28	488.1	1.28	487.7
3	-0.82	153.7	-0.79	153.5	-0.77	153.2
4	-2.52	49.7	-2.57	51.8	-2.61	53.9
5	-2.51	25.1	-2.55	26.7	-2.59	28.3
6	-2.61	18.6	-2.66	20.1	-2.71	21.6
7	-3.93	9.4	-4.08	10.6	-4.22	11.9

It should be mentioned that this method require input three refractive indices of each optical material correspondent to the three wavelengths of interest 3, 4, and 5 μm, this make some differences between the spot size of different wavelength to be more accurate.

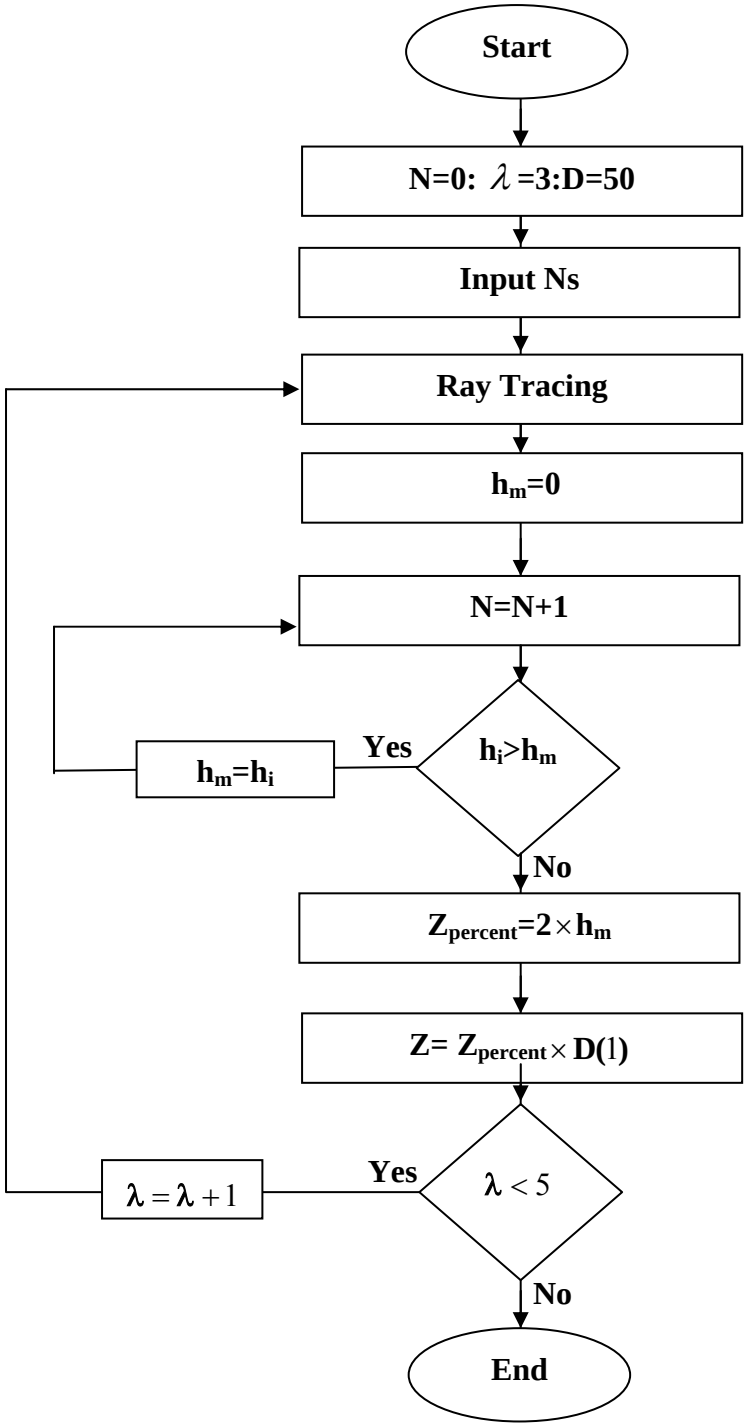

Figure 4.38: Flowchart of computing spot size by the ray tracing method.